SnRK1-triggered switch of bZIP63 dimerization mediates the low-energy response in plants

Andrea Mair[1], Lorenzo Pedrotti[2], Bernhard Wurzinger[1], Dorothea Anrather[3], Andrea Simeunovic[1], Christoph Weiste[2], Concetta Valerio[4], Katrin Dietrich[2], Tobias Kirchler[5], Thomas Nägele[1], Jesús Vicente Carbajosa[6], Johannes Hanson[7,8], Elena Baena-González[4], Christina Chaban[5], Wolfram Weckwerth[1], Wolfgang Dröge-Laser[2], and Markus Teige[1,9*]

[1] Department of Ecogenomics and Systems Biology, University of Vienna, Vienna, Austria

[2] Julius-von-Sachs-Institute, Pharmaceutical Biology, University of Würzburg, Würzburg, Germany

[3] Mass Spectrometry Facility, Max F. Perutz Laboratories, University of Vienna, Vienna, Austria

[4] Instituto Gulbenkian de Ciência, Oeiras, Portugal

[5] Department of Plant Physiology, Center for Plant Molecular Biology, University of Tübingen, Tübingen, Germany

[6] Centro de Biotecnología y Genómica de Plantas, Universidad Politécnica de Madrid, Madrid, Spain

[7] Department of Molecular Plant Physiology, Utrecht University, Utrecht, The Netherlands.

[8] Department of Plant Physiology, Umea Plant Science Center, University of Umea, Umea, Sweden

[9] Department of Applied Genetics and Cell Biology, University of Natural Resources and Life Sciences, Vienna, Austria

* Contact Information:

markus.teige@univie.ac.at

Competing interests:

The authors declare that no competing interests exist.

Abstract

Metabolic adjustment to changing environmental conditions, particularly balancing of growth and defense responses, is crucial for all organisms to survive. The evolutionary conserved AMPK/Snf1/SnRK1 kinases are well-known metabolic master regulators in the low-energy response in animals, yeast and plants. They act at two different levels: by modulating the activity of key metabolic enzymes, and by massive transcriptional reprogramming. While the first part is well established, the latter function is only partially understood in animals and not at all in plants. Here we identified the Arabidopsis transcription factor bZIP63 as key regulator of the starvation response and direct target of the SnRK1 kinase. Phosphorylation of bZIP63 by SnRK1 changed its dimerization preference, thereby affecting target gene expression and ultimately primary metabolism. A *bzip63* knock-out mutant exhibited starvation-related phenotypes, which could be functionally complemented by wild type bZIP63, but not by a version harboring point mutations in the identified SnRK1 target sites.

Introduction

Flexibility in the regulation of gene expression is crucial for all organisms to adjust their metabolism to changing growth conditions. Particularly under stress, available energy resources need to be balanced between defense and growth. The SUCROSE NON-FERMENTING RELATED KINASE 1 (SnRK1) in plants and its orthologs, the sucrose-non-fermenting 1 (Snf1) kinase in yeast and the AMP-dependent protein kinase (AMPK) in mammals, are well-known and crucial master regulators of energy homeostasis. SnRK1 is involved in the regulation of plant metabolism, development, and stress response (Baena-Gonzalez and Sheen, 2008; Polge and Thomas, 2007), Snf1 is required for the switch from fermentative to oxidative metabolism in the absence of glucose (Hedbacker and Carlson, 2009), and AMPK regulates glucose, lipid, and protein metabolism, mitochondrial biogenesis, and feeding behavior in animals (Hardie et al., 2012). They are generally activated under energy starvation conditions and trigger metabolic reprograming to slow down energy-consuming processes and turn on pathways for alternative energy production in order to survive the stress conditions (Hardie 2007, Tome et al., 2014). This happens, in two ways: by direct phosphorylation and modulation of the activity of key enzymes in nitrogen, carbon, or fatty acid metabolism (Kulma et al., 2004; Sugden et al., 1999; Harthill et al., 2006), and by massive transcriptional reprogramming (Baena-Gonzalez and Sheen, 2008; McGee and Hargreaves, 2008; Polge and Thomas, 2007). Especially in plants, the latter aspect, the regulation of transcription, is still poorly understood. In Arabidopsis protoplasts, transient overexpression of AKIN10, a catalytic subunit of the SnRK1 complex, resulted in a transcriptional profile reminiscent of various starvation conditions and led to the identification of 1021 putative SnRK1 target genes (Baena-Gonzalez et al., 2007). However, the transcription factors mediating the transcriptional response of SnRK1 to energy starvation are still unknown. Based on reporter gene activation assays in protoplasts (Baena-Gonzalez et al., 2007) and modelling of microarray data (Usadel et al., 2008), some members of the C/S1 group of basic leucine zipper (bZIP) transcription factors (TFs) – foremost bZIP11 and bZIP1 from the S1 group - were

speculated to be involved in this process. Yet, a direct regulation of these bZIPs by SnRK1 has never been shown.

bZIP proteins form a large and highly conserved group of eukaryotic TFs. They bind the DNA as dimers and are characterized by a basic region for specific DNA binding and a leucine zipper for dimerization (Deppmann et al., 2006; Reinke et al., 2013). They are involved in a multitude of cellular processes, including cell proliferation and differentiation, metabolism, stress response, and apoptosis (Jakoby et al., 2002; Mayr and Montminy, 2001; Motohashi et al., 2002; Rodrigues-Pousada et al., 2010; Tsukada et al., 2011). The diversity and flexibility of transcriptional regulation by bZIP TFs can at least partially be attributed to their potential to form variable dimer combinations, which bind to different consensus target sites (Deppmann et al., 2006; Tsukada et al., 2011). While the leucine zipper determines the possible dimer combinations (Deppmann et al., 2006; Reinke et al., 2013), the actual in vivo dimer composition is further influenced by factors such as protein availability, binding of regulatory proteins, or post-translational modifications (Kim et al., 2007; Lee et al., 2010; Schuetze et al., 2008). Since the initial discovery that the mammalian bZIP cAMP response element binding protein (CREB) is regulated by reversible phosphorylation, many bZIP TFs were reported to be phosphorylated (Holmberg et al., 2002; Schuetze et al., 2008; Tsukada et al., 2011). However, particularly in plants, the functional consequences of these phosphorylation events often remained unclear. For example, it has been known for several years that abscisic acid (ABA)-dependent phosphorylation of some ABA-responsive element binding proteins (AREBs) by SnRK2 kinases increases their transcriptional activity (Furihata et al., 2006), yet the underlying mechanism of this activation is still unknown. It is also surprising that, while many examples for phosphorylation-dependent regulation of bZIP activity, DNA-binding, subcellular localization, stability, and interaction with regulatory proteins are known (Schuetze et al., 2008; Tsukada et al., 2011), reports on the regulation of dimerization are scarce. So far, only three publications (Guo et al., 2010; Kim et al., 2007; Lee et al., 2010) showed compelling evidence for phosphorylation-dependent changes in bZIP

dimerization in animals. Still, even in these cases it is often not entirely clear whether bZIP phosphorylation affects dimerization directly or indirectly by enhancing DNA binding.

bZIP63 is a member of the C-group of Arabidopsis bZIPs, which was proposed to play a role in energy metabolism, seed maturation, and germination under osmotic stress (Correa et al., 2008; Jakoby et al., 2002; Veerabagu et al., 2014). Its transcriptional profile indicates that bZIP63 could be involved in the (energy) starvation response, as transcription and mRNA stability are repressed by sugars and ABA and mRNA levels increase in the night and even more during extended night treatments (Kunz et al., 2014; Matiolli et al., 2011). A small set of potential target genes for bZIP63 has been identified, including genes involved in amino acid metabolism (*ASN1*/*DIN6* = ASPARAGINE SYNTHETASE 1, *ProDH* = PROLINE DEHYDROGENASE), energy starvation response (*DIN10* = RAFFINOSE SYNTHASE 6), and senescence (*SEN1* = SENESCENCE 1) (Baena-Gonzalez et al., 2007; Dietrich et al., 2011; Matiolli et al., 2011; Veerabagu et al., 2014). The C-group bZIPs form a dimerization network with the S1-group in plants, in which bZIP63 can interact with all members (Ehlert et al., 2006; Kang et al., 2010). Three of its dimerization partners from the S1-group – bZIP1, bZIP11, and bZIP53 – were shown to be important metabolic regulators, especially under energy starvation conditions, and to regulate the expression of *ASN1* and *ProDH* as well (Dietrich et al., 2011; Hanson et al., 2008; Ma et al., 2011). Furthermore, bZIP1 was recently confirmed as a transcriptional master regulator of the rapid response to nutrient signals controlling mainly genes involved in amino acid metabolism and cell death/phosphorus metabolism as primary targets (Para et al., 2014). In that study the authors also speculate about a posttranslational modification of bZIP1 or its binding partners.

Here we show that bZIP63 is an important metabolic regulator, especially under stress/starvation conditions, and that bZIP63 is phosphorylated at multiple sites in vivo in a sugar and energy-dependent manner. In an unbiased approach, we identified SnRK1 as one of the kinases responsible for bZIP63 phosphorylation and found that it targets three highly conserved serine residues in the N- and C-terminus of bZIP63. Moreover, we demonstrate that the phosphorylation of these sites is crucial for bZIP63's dimerization and activity in planta and propose a molecular model for a

phosphorylation-triggered switch of bZIP63 dimerization partners, which ultimately regulates metabolic reprogramming.

Results

bZIP63 controls dark-induced senescence and primary metabolism

To better understand the role of bZIP63 in the plant we first tested whether bZIP63 has a similar phenotype as its dimerization partners bZIP1 and bZIP11. Prolonged darkness was shown to induce increased chlorophyll loss in plants overexpressing bZIP1 (Dietrich et al., 2011). Therefore, we incubated a bZIP63 knock-out (ko), two independent overexpressor (ox) lines (Figure 1 – figure supplement 1), and their respective wild types (wt) in the dark and determined the percentage of the green leaf area as a measure for chlorophyll content (Figure 1; Figure 1 – figure supplement 2A). This method was preferred over direct chlorophyll measurements (Figure 1 – figure supplement 2B) as it is not affected by the water loss in senescing leaves. While no differences were observed before dark treatment, significant differences were visible after 9 days in darkness (Figure1 - figure supplement 2C-E). Similar to the bZIP1 ox, the bZIP63 ox lines (ox#2 and ox#3) had a significantly higher percentage of yellow leaf area than the wt. In contrast, *bzip63* plants displayed a stay-green phenotype (Figure 1A and 1B; Figure1 - figure supplement 2F). RT-qPCRs of different senescence marker genes confirmed that the phenotype is due to dark-induced and not to natural senescence (Figure 1 – figure supplement 3). Transcriptional responses in dark-induced senescence show clear similarities to starvation-induced senescence in cell suspension culture, which likely results from carbon depletion in both systems (Buchanan-Wollaston et al., 2005). We therefore tested whether addition of sugar could rescue this phenotype by performing the dark-induced senescence experiment with seedlings grown on agar plates with and without addition of sugar. Indeed, we found that the phenotype could be rescued by the addition of glucose (Figure 1C and 1D – figure supplement 4), supporting the suggested role of bZIP63 in energy/carbon starvation response.

The notion that several hetero-dimerization partners of bZIP63, including bZIP1 and bZIP11, are important metabolic regulators under starvation conditions (Dietrich et al., 2011; Ma et al., 2011) prompted us to perform an unbiased metabolomics analysis of *bzip63* and ox#3 plants and their respective wt lines. Leaves of five week-old plants were harvested after 6h of light and extended night and analyzed for changes in the primary carbon and nitrogen metabolism using gas chromatography coupled to mass spectrometry (Figure 2; Figure 2 – figure supplement 1 and source data 1). Intriguingly, almost all amino acid levels were increased in the bZIP63 ko and decreased in the ox plants. This effect was even more pronounced after the extended night treatment. The biggest differences were observed for proline and the entire glutamate family. This accumulation of amino acids, particularly of proline, is striking in view of the observed senescence phenotype as it has been suggested that proline serves as an alternative energy source, especially under low carbon conditions (Szabados and Savouré, 2010; Szal and Podgórska, 2012).

bZIP63 is phosphorylated at multiple sites in an energy-dependent manner

Kirchler et al. (2010) showed that bZIP63 can be phosphorylated in vitro by crude Arabidopsis extracts. To test whether bZIP63 is also phosphorylated in vivo, we treated total leaf protein extracts of ox#3 plants, expressing GFP-tagged bZIP63, with lambda protein phosphatase (λPP) and separated treated and untreated extracts on 2D gels by isoelectric focusing (IEF) in the first, and SDS-PAGE in the second dimension (Figure 3A). λPP treatment induced a clear shift of bZIP63 towards the basic region of the IEF strip, thus indicating dephosphorylation of the protein.

As bZIP63 expression is strongly regulated by the day/night cycle and by sugars (Kunz et al., 2014; Matiolli et al., 2011), we investigated its phosphorylation status under these conditions, applying the Phos-tag technique to enhance phosphorylation-induced mobility shifts in 1D SDS-PAGE (Kinoshita et al., 2006). Comparison of protein extracts from seedling cultures after 6h extended night in the presence or absence of sucrose or leaves harvested after 6h of light or extended night revealed strong differences in the phosphorylation patterns of bZIP63 (Figure 3B; Figure 3 - figure supplement

1). Compared to the recombinantly expressed (not phosphorylated) bZIP63-YFP, the majority of plant-expressed bZIP63-GFP appeared in several slower migrating forms, thus indicating multiple and differentially phosphorylated forms. In total, we were able to distinguish eight different forms on the Phos-tag gels, depending on the conditions (Figure 3B; Figure 3 – supplement 1). However, it is important to note, that not every phosphorylation event results in an equal shift as can be seen in Figure 6 – figure supplement 2. In the light, two strong bands were visible, possibly reflecting the two spots on the 2D gel (Figure 3B, labelled as band 6 and band 7, respectively). Under extended night conditions, an additional band appeared (labelled as band 8), indicating increased phosphorylation of bZIP63. Notably, the ratio of the most phosphorylated form of bZIP63 (band 8) to the two less phosphorylated forms (band 6 and 7) was different between the ox (ox#3) and a genomic complementation line of *bzip63* (GY11, detailed description follows later in the text and in Figure 6). In the genomic complementation line, the most phosphorylated form of bZIP63 was the strongest band under extended night conditions, which might be a result of the different bZIP63 amounts in relation to the endogenous kinase(s), and likely better reflects the phosphorylation state of the endogenous protein. Interestingly, in seedlings grown in liquid culture, the extended night-triggered phosphorylation of bZIP63 could be abolished by the addition of 1% of sucrose (Figure 3B). In fact, phosphorylation was even lower here than in the light. These data indicate that bZIP63 has a basal level of phosphorylation in the plant and undergoes hyper-phosphorylation under starvation conditions. In contrast, addition of external sugars leads to a reduced phosphorylation status of bZIP63.

In order to identify the in vivo phosphorylated residues, bZIP63-GFP was immunoprecipitated from total leaf extracts using bead-coupled anti-GFP antibodies, subjected to proteolytic digest and analyzed by liquid chromatography coupled to tandem mass spectrometry (LC-MS/MS) (Figure 3C). To achieve maximum sequence coverage of the protein we combined proteolytic digests from four proteolytic enzymes (trypsin, chymotrypsin, LysC, and subtilisin). This approach resulted in a total sequence coverage of 93.6% and the identification of several phospho-peptides, indicating that

bZIP63 is phosphorylated at up to seven serines (S29, S59, S102, S160, S261, S294, and S300) in vivo (Figure 3C; Figure 3 – figure supplement 2). Two of these sites – S29 and S300 – were also found in a recent phospho-proteomics study (Umezawa et al., 2013). Notably, only three of the seven sites – S29, S294, and S300 – were found by tryptic protein digest, underpinning the advantage of alternative proteolytic digests for phospho-peptide identification in targeted proteomics.

SnRK1, CDPKs and CKII are potential upstream kinases of bZIP63

To identify potential upstream kinases of bZIP63, we performed in-gel kinase assays with plant protein extracts from roots of hydroponically grown Arabidopsis plants or root cell culture using recombinantly expressed bZIP63 as substrate. Root material was chosen because in leaf extracts the large amount of Ribulose-1,5-bisphosphate carboxylase/oxygenase (RuBisCO) interfered with some of the kinase signals and poses a considerable problem during MS-based protein identification. Three strong bands of about 40, 50, and 55kDa, respectively, were visible on the autoradiogram (Figure 4A), indicating that at least three kinases can phosphorylate bZIP63 in vitro. These bands were not visible on a gel without substrate, excluding the possibility that they originate from kinase auto-phosphorylation (Figure 4 – figure supplement 1). To reduce the sample complexity and to enrich low abundant bZIP63-binding proteins before kinase identification, we affinity purified plant protein extracts on immobilized bZIP63. The eluted fractions were tested in an in-gel kinase assay for kinase activity towards bZIP63 and loaded on a normal SDS-PAGE gel without substrate for kinase identification. Bands corresponding in molecular weight (MW) to the signal from the in-gel kinase assay were excised from the gel, digested with trypsin and analyzed by LC-MS/MS (Figure 4B and 4C). In total, 27 protein kinases and kinase complex subunits were identified in four independent experiments (Figure 4 – figure supplement 2; Figure 4 – source data 1). From those, proteins which did not match the expected MW or for which it had been shown experimentally that they are not localized in the nucleus were excluded. Only proteins which were identified in more than one sample with at least one proteotypic peptide were considered to be high confidence candidates, resulting in

six protein kinases and two kinase regulatory subunits (Figure 4C; Figure 4 – figure supplement 2; Figure 4 – source data 1). We identified the two main catalytic subunits of SnRK1, AKIN10 and AKIN11, as well as the regulatory subunit SNF4. Several members of the calcium dependent protein kinase (CDPK) family were found, but only CPK3 was identified with high confidence. In addition, two catalytic (CKA1 and CKA2) and one regulatory subunit (CKB1) of casein kinase II (CKII) were found, as well as Casein kinase like 2 (CKL2). The SnRK1 kinases, CDPKs, and CKL2, correspond in MW to the two upper bands, while the lower band corresponds to the CKII kinase subunits. As SnRK1 was previously reported to enhance the activity of several C/S1 group bZIPs (Baena-Gonzalez et al., 2007) and was suggested to be activated under energy starvation conditions (Baena-Gonzalez and Sheen, 2008) – which could explain the observed hyper-phosphorylation of bZIP63 in extended night – we focused our further analysis on AKIN10 and AKIN11.

The SnRK1 kinase AKIN10 interacts with and phosphorylates bZIP63 in vivo

To confirm that AKIN10 and AKIN11 phosphorylate bZIP63, we first performed an in-gel kinase assay with protein extracts of wt and *akin10* seedlings in the presence of EGTA, to reduce the signal from CDPKs of the same MW (Figure 5A). In both root and leaf extracts of *akin10* plants one band at the expected MW of AKIN10 nearly disappeared (see Figure 5 – figure supplement 1-3 for characterization of the *akin10* line). As AKIN11 has approximately the same MW as AKIN10, the remaining signal likely originates from AKIN11. In vitro kinase assays, with equal amounts of both kinases, showed that both kinases can phosphorylate bZIP63. However, AKIN10 phosphorylates bZIP63 much stronger than AKIN11 does (Figure 5B). Addition of the SnRK1 upstream kinase SnAK2 increased the activity of AKIN10 and AKIN11 about seven-fold (see also Crozet et al., 2010), but had no effect on the ratio between the signal intensities (Figure 5 – figure supplement 4). In vivo interaction assays with the identified SnRK1 complex subunits supported the findings of the kinase assays. In both yeast two-hybrid (Y2H) (Figure 5C) and bimolecular fluorescence complementation (BiFC) assays (Figure 5D) AKIN10 and the regulatory subunit SNF4 interacted strongly with bZIP63, to

247 a comparable level as measured for the bZIP63 homo-dimer, which was used as positive control
248 (Walter et al., 2004). In contrast, AKIN11 and the two regulatory subunits AKINβ1 and AKINβ2
249 showed almost no interaction with bZIP63 (Figure 5C and 5D; Figure 5 – figure supplement 5).
250 However, it has to be considered that AKIN10 and AKIN11 are part of a trimeric complex including
251 SNF4 (Emanuelle et al., 2015), which is neglected in these two assays. It is therefore still possible that
252 AKIN11 interacts indirectly with bZIP63 via the regulatory subunit of the SnRK1 complex and plays a
253 minor role in bZIP63 phosphorylation in the plant.
254 To verify that SnRK1 plays an important role in the in the in vivo phosphorylation of bZIP63 we
255 compared the phosphorylation state of bZIP63 in plants overexpressing bZIP63-GFP or -YFP in the wt
256 and *akin10* background, respectively. As SnRK1 has been suggested to act as a major regulator in the
257 energy deprivation response, we again compared leaf protein extracts after 6h light and extended
258 night and found that the hyper-phosphorylated form (band 8) of bZIP63, observed in the wt in
259 extended night, was much weaker in the *akin10* background (Figure 5E). The same effect was
260 observed in seedling cultures after 6h of extended night (Figure 5– figure supplement 6). To see
261 whether the weak phosphorylation remaining in the *akin10* mutant would be further reduced in an
262 *akin10/11* double mutant, we employed virus-induced gene silencing (VIGS) to knock down AKIN10
263 and AKIN11 in a genomic *bzip63* complementation line (GY9). Resulting plants showed strongly
264 reduced growth and accumulation of anthocyanins (Figure 5 – figure supplement 7), as previously
265 described in Baena-Gonzalez et al. (2007). Like in the *akin10* line, there was no difference in bZIP63
266 phosphorylation between *akin10/11* and control plants in light, but the hyper-phosphorylated form
267 of bZIP63 (band 8) in the extended night was now almost completely gone (Figure 5E). This shows
268 clearly, that AKIN10 and - to a lower extent - AKIN11 are the major kinases responsible for bZIP63
269 hyper-phosphorylation under starvation conditions.
270 Additional evidence for in vivo phosphorylation of bZIP63 by SnRK1 emerges from a recent
271 phosphoproteomics study in which one of the in vivo phosphorylation sites in bZIP63 (S300) was

found to be more abundant in an AKIN10 ox line and less abundant in the ko line after extended night treatment, respectively (Nukarinen et al., submitted).

AKIN10 phosphorylates three conserved and functionally important serine residues in bZIP63

Next, to elucidate which of the seven in vivo phosphorylation sites can be phosphorylated by AKIN10, we performed in vitro kinase assays using the wt version of bZIP63 and different serine to alanine (S/A) mutants as substrates (Figure 6A; Figure 6 – figure supplement 1 and 2). Differences in phosphorylation were observed for proteins with mutations in S29, S294, and S300. In detail, the signal from S29A was strongly decreased in full length bZIP63 and completely gone in the N-terminal peptides that appeared as lower MW degradation products in these assays. The S300A mutation led to an even stronger decrease of the signal, comparable to the S294/300A double mutant. Even though the S294A single mutant showed a similar signal as the wt, all three serines had to be mutated to completely abolish phosphorylation, suggesting that all of them are in vitro targets for AKIN10, with S294 being the weakest. Importantly, all three sites match the SnRK1 consensus sequence (Huang and Huber, 2001) (Figure 6B).

A comparison of Arabidopsis bZIP63 with orthologs from eight other plant species, ranging from mosses to higher plants, showed that the three putative AKIN10 target sites are highly conserved throughout evolution (Figure 6B; Figure 6 – figure supplement 3 and source data 1). As the origin of SnRK1 dates back even further, to the common ancestor of plants and animals (Bayer et al., 2014), it is likely that phosphorylation of bZIP63 by AKIN10 poses an ancient and important regulatory mechanism. We therefore set out to test the functional relevance of AKIN10-mediated phosphorylation of bZIP63. To this end, we tested the transcriptional activity of bZIP63 in protoplast-based promoter activation assays using the *ASN1* or *ProDH* promoter fused to the beta galactosidase (GUS) reporter (Figures 6C; Figure 6 – figure supplement 4). In both cases, co-transformation of wt bZIP63 and AKIN10 strongly induced reporter gene expression, while transformation of bZIP63 alone was not sufficient for significant induction. Transformation of AKIN10 alone also led to a weak

induction of the reporters, which could be explained by the action of endogenous bZIPs. Mutation of S29 or all three AKIN10 target sites on bZIP63 to alanine reduced the reporter activation almost to background level. In contrast, mutation of the two C-terminal serines, S294 and S300, had only a weak negative effect on *ASN1* and no significant effect on *ProDH* activation. Taken together, our data suggest that AKIN10 phosphorylates bZIP63 at up to three conserved sites, namely S29, S294, and S300 and phosphorylation by AKIN10, especially at S29, is crucial for bZIP63 TF activity.

The AKIN10 target sites play an important role for bZIP63 function in planta

To determine the impact of bZIP63 phosphorylation in planta, we transformed the *bzip63* mutant with genomic constructs of bZIP63 containing either the wt sequence (GY lines), or a S/A mutation of S29, S294, and S300, respectively (GAY lines) with a C-terminal YFP tag (Figure 7A; Figure 7 – figure supplement 1 A-C). The wt construct showed strong phosphorylation in the light (bands 6 and 7) and an even stronger phosphorylation in extended night (band 8), as well as reduced phosphorylation in the presence of sucrose (bands 1, 2, and 4) (Figure 7B; Figure 7 – figure supplement 1D). In contrast, the S/A construct showed only weak phosphorylation (only bands 1 and 3 visible) and most importantly no difference between all tested conditions. This indicates that S29, S294 and S300 are the major in vivo phosphorylation sites on bZIP63, which are also responsible for the observed condition-dependent shift in bZIP63 phosphorylation.

Next, we tested whether complementation of the observed *bzip63* phenotypes depends on the bZIP63 phosphorylation status, using two independent GY and GAY lines. The dark-induced senescence phenotype of *bzip63* was complemented in the GY lines, but not in the GAY lines (Figure 7C and D; Figure 7 – figure supplement 2). After 9 days in darkness, the ko and GAY lines showed visibly less chlorosis and had a higher percentage of green leaf area as compared to the wt and GY lines. Metabolite profiling of leaves harvested after 6h of light also revealed marked differences between the GY and GAY lines (Figures 7E and F; Figure 7 – source data 1). The metabolite profile of the GAY lines was similar to that of *bzip63* plants. In contrast, in the GY lines the metabolic changes

between mutant and wt were mostly weaker than in *bzip63* or even resembled those observed for ox#3 (Figure 7E). In a principal component analysis the GAY lines grouped together with *bzip63*, while the GY lines were closer to the two wt lines and the ox (Figure 7F).

To test the effect of the S/A mutation on the expression of bZIP63 target genes, we performed RT-qPCR of *ASN1*, *DIN10,* and *ProDH* (Figure 7G) - three suggested AKIN10 target genes (Baena-Gonzalez et al., 2007). The expression of all three genes increased steadily during a 4h extended night treatment, but the increase was delayed in the *bzip63* mutant as compared to the wt. At the 4h time point we could observe a clear difference between wt and ko. We therefore chose this time point to quantify *ASN1*, *DIN10*, and *ProDH* transcripts in one GY and GAY line. As expected, the GY line had the same or even more transcript than the wt for all three genes, while the GAY line had significantly lower expression levels, similar to *bzip63*.

In summary, expression of wt bZIP63 but not of the S/A mutant - which cannot be phosphorylated by AKIN10 - in the *bzip63* background led to complementation of the *bzip63* phenotypes. Together, these experiments demonstrate that phosphorylation of bZIP63 at the AKIN10 target sites is essential for the function of bZIP63 in the plant.

AKIN10-mediated phosphorylation affects bZIP63 dimerization

Our findings show that bZIP63 phosphorylation, at residues distant from the central bZIP domain, strongly regulates its activity. As we did not observe any changes in localization in the bZIP63 mutants and also no change in DNA-binding activity (of the bZIP63 homodimer) towards a C-box motif (GACGTC) as canonical bZIP target site (data not shown), we suspected that the observed effect on transcription would be due to changes in dimerization preferences of bZIP63. Therefore, we tested the effect of AKIN10-mediated phosphorylation on bZIP63 homo- and hetero-dimerization with bZIP1 and bZIP11. Both bZIP1 and bZIP11 are metabolic regulators and mediate transcription of *ASN1* and *ProDH* (Dietrich et al., 2011; Hanson et al., 2008). In protoplast two-hybrid (P2H) assays, the addition of exogenous AKIN10 resulted in a clear enhancement of dimerization in all cases -

homo-dimerization as well as hetero-dimerization with bZIP1 and bZIP11 (Figure 8A; Figure 8 – figure supplement 1A). Note, that the very strong effect observed with bZIP11 in these assays is misleading because bZIP11 is a much stronger activator of transcription as compared to bZIP1 and 63 (see also discussion). From that we concluded that the phosphorylation of bZIP63 by AKIN10 is required for dimerization and set out to test the effect of S/A mutations of the AKIN10 target sites on bZIP63 homo- and hetero-dimerization with bZIP11 where we had observed the strongest effect before (Figure 8B; Figure 8 – figure supplement 1B). In both cases, the signal was reduced to about 30-40% of the signal obtained from dimerization with wt bZIP63 when S29 or all three serines were mutated to alanine. Mutation of one or two of the C-terminal sites decreased bZIP63 homo-dimerization weakly but had no visible effect on bZIP63-11 dimerization, indicating that these sites play, at most, a minor role in regulation of dimer formation.

To exclude the possibility that the observed effects on dimerization are due to phosphorylation of the hetero-dimerization partner rather than bZIP63 itself, we tested whether AKIN10 is able to phosphorylate any of the S1 group bZIPs. To increase the phosphorylation efficiency of AKIN10 we included SnAK2 in the reactions. In contrast to bZIP63, none of the S1 group bZIPs were phosphorylated by AKIN10 (Figure 8C; Figure 8 – figure supplement 2). Together, these data indicate that AKIN10-mediated phosphorylation of bZIP63 – especially at S29 – strongly enhances its ability to form homo- as well as hetero-dimers.

To further substantiate the relevance of S29 phosphorylation in vivo, we compared the phosphorylation patterns of the S29/S294/S300 mutant with a S294/S300 mutant in the light and after extended night treatments in the genomic complementation lines (Figure 8D). Compared to the triple mutant, that did not show any change in the phosphorylation pattern in response to starvation, bZIP63 phosphorylation was clearly increased in the S294/S300 double mutant in the extended night. As S29 is the only AKIN10 target site left in this version, it must indeed be S29 that is phosphorylated by AKIN10 under starvation conditions.

As we saw that AKIN10-dependent phosphorylation promotes dimerization of bZIP63 with all tested partners we wanted to analyze whether phosphorylation has an effect on the dimerization partner preference. Because protoplast two-hybrid assays only allow to analyze the effect of AKIN10 on a single dimer we set up a multicolor BiFC approach (Waadt et al., 2008) in N. tabacum leaves with bZIP1 and 11 as alternative interaction partners for bZIP63. For this, we expressed all three bZIPs (1, 11, and 63) from the same plasmid and co-transformed AKIN10 (Figure 9A). bZIP11 was fused to CFP_N, bZIP1 to $VENUS_N$, and bZIP63 to CFP_C. Accordingly, the bZIP63-11 hetero-dimer generates a blue (cyan) signal and the bZIP63-1 hetero-dimer a yellow signal, whereas the bZIP63 homo-dimer cannot be detected. To compare the dimerization preference of phosphorylated and non-phosphorylated bZIP63 we used wt and a S29/294/300A mutant of bZIP63. Quantification of the ratio of the VENUS/CFP signal in more than 100 nuclei clearly showed a shift towards the VENUS emission when wt bZIP63 was compared to the S/A mutant. This demonstrates that phosphorylation by AKIN10 triggers the preferential formation of bZIP63-1 over bZIP63-11 dimers in a competitive in vivo assay.

Discussion

bZIP63 is an important metabolic regulator in the starvation response

Here we show that bZIP63 plays an important role in the energy starvation response and metabolic regulation. This is in accordance with the sugar/energy-dependent expression of bZIP63 (Kunz et al., 2014; Matiolli et al., 2011), as well as with the fact that several of its proposed target genes are involved in the low-energy response and metabolism (Matiolli et al., 2011; Veerabagu et al., 2014). Furthermore, three members of the S1-group of plant bZIPs – hetero-dimerization partners of bZIP63 (Ehlert et al., 2006; Kang et al., 2010) – have also been linked to energy starvation response and metabolism. Inducible bZIP11 ox lines exhibit a severe dwarf phenotype (Hanson et al., 2008) and a

401 metabolic profile resembling that of carbon starved plants (Ma et al., 2011), while overexpression of
402 bZIP1 and bZIP53 results in enhanced dark-induced senescence and reduced levels of proline and
403 branched-chain amino acids (Dietrich et al., 2011).
404 Similar to the bZIP1 ox, bZIP63 ox plants showed increased chlorosis after 9 days of darkness, while
405 the bZIP63 ko displayed a clear stay-green phenotype under these conditions. In contrast, neither the
406 single, nor the double ko of bZIP1 and 53 showed reduced dark-induced senescence (Dietrich et al.,
407 2011). This suggests that other bZIPs can take over the function of bZIP1 - in starvation-induced leaf
408 yellowing, while bZIP63 plays a more unique role.
409 Looking at primary metabolism, we found that misregulation of bZIP63 expression has a strong
410 effect, especially on amino acids, which was further enhanced under starvation conditions. In line
411 with the finding that bZIP63 is a positive regulator of *ProDH* and *ASN1* (Matiolli et al., 2011;
412 Veerabagu et al., 2014, and this work: Figures 6C and 7G) and the changes in proline levels in *bZIP63*
413 mutants reported by Veerabagu et al. (2014), we measured the strongest differences in proline and
414 the entire glutamate family as well as in aspartate and asparagine levels in the bZIP63 ko and ox.
415 Notably, there is a strong correlation between the amino acid profiles of the bZIP63 and the bZIP1 ox
416 lines (Dietrich et al., 2011). A similar accumulation of amino acids during dark-induced senescence
417 has frequently been observed and was attributed to enhanced protein degradation (reviewed in
418 Araújo et al., 2011). Particularly under low carbon conditions or during senescence, alternative
419 energy sources need to be used in plant cells, and the important role of proline and branched-chain
420 amino acids in this process has been highlighted in a number of studies (reviewed in: Szabados and
421 Savouré, 2010; Szal and Podgórska, 2012). Thus also the altered amino acid levels could contribute to
422 the observed dark-induced senescence phenotype of the bZIP63 mutants.
423
424 **bZIP63 function is regulated by SnRK1-dependent phosphorylation**
425 We found that bZIP63 is highly phosphorylated in Arabidopsis. By applying different proteolytic
426 digests we were able to identify seven in vivo phosphorylated serine residues, distributed all over the

protein. While exogenous sucrose decreased the global phosphorylation level of bZIP63, extended night treatment further increased its phosphorylation, thus supporting the idea that bZIP63 plays a role in energy signaling. Moreover, we found that the SnRK1 kinase AKIN10, which was proposed to be a central regulator of transcription in starvation response (Baena-Gonzalez and Sheen, 2008), is the major kinase responsible for the starvation-induced hyper-phosphorylation of bZIP63. Therefore, bZIP63 presents the first TF acting as direct target of SnRK1 in the transcriptional energy deprivation response. In vitro, AKIN10 phosphorylated three highly conserved and functionally important residues in the N- and C-terminus of bZIP63 - S29, S294, and S300, respectively. Reporter activation assays in protoplasts revealed that these sites – especially S29 - are essential for AKIN10-dependent induction of *ASN1* and *ProDH* by bZIP63. Remarkably, the phosphorylation patterns of different bZIP63 mutants on Phos-tag gels pointed towards S29 as the main target site for AKIN10 under extended night conditions. The importance of bZIP63 phosphorylation at the SnRK1 target sites for its in planta function was further underlined by complementation of the *bzip63* mutant with genomic bZIP63 constructs. Wt, but not a S29/S294/S300A mutant of bZIP63, could complement the metabolic and senescence phenotypes. Likewise, also the strong delay in extended night-triggered induction of *ASN1*, *DIN10*, and *ProDH* in *bzip63* plants was complemented with wt bZIP63, but not the (triple) S/A mutant. The relatively small difference in *ProDH* expression in plants, as compared to the protoplast assay, is probably due to redundancy within the C/S1 group bZIPs, as it was shown by Dietrich et al. (2011), that only ko of multiple members of the C/S1 group leads to a strong reduction in *ProDH* and *ASN1* expression.

Since the discovery that AKIN10 can activate several members of the C/S1 network (Baena-Gonzalez et al., 2007), it has been speculated (Baena-Gonzalez and Sheen, 2008; Usadel et al., 2008), but never shown experimentally, that they are downstream targets of SnRK1. Our data provide compelling evidence that bZIP63, but none of the S1 group bZIPs, is a bona fide in vivo target of SnRK1 in low-energy signaling.

Phosphorylation of bZIP63 alters its dimerization preferences

Differential dimerization is a well-known mechanism for changing the target recognition site, and thereby the target genes of bZIP TFs (Tsukada et al., 2011). For the S1-group bZIP1 is has been shown that dimerization with C-group bZIP10 or bZIP63 affects its in vitro binding to ACGT-based motifs differently (Kang et al., 2010). The notion that different C/S1 dimers have different target genes is further supported by a recent transcriptomics study in protoplasts. Overexpression of four C/S1 group bZIPs (bZIP1, bZIP10, bZIP11, and bZIP63), individually or in combination of two, revealed overlapping but distinct gene expression patterns (Ma, 2012). This means, that although they regulate a core set of common genes, such as *ASN1* and *ProDH* (Baena-Gonzalez et al., 2007; Dietrich et al., 2011; Ma et al., 2011), different dimers also have distinct functions, and switching of dimerization partners can have a considerable impact on gene expression.

Our data indicate that dimerization and activity of bZIP63 strongly depend on its phosphorylation status. In general, the dimerization of bZIP63 with bZIP1, bZIP11, and bZIP63, was boosted by AKIN10-mediated phosphorylation. Like in the promoter activation assays, the main influence on dimerization came from S29 phosphorylation, while phosphorylation of S294 and S300 showed a mild effect at most. Incidentally, this enhanced dimerization with bZIP63 would explain why AKIN10 was found to activate the S1 group bZIPs (bZIP1, 2, 11, and 53) in protoplast assays (Baena-Gonzalez et al., 2007), although they do not present direct targets of AKIN10.

At first sight, the phosphorylation triggered boost of dimerization seemed to be strongest for hetero-dimerization with bZIP11. However, it has to be considered that bZIP11 is a very strong activator of transcription as it harbors an activation domain (Ehlert et al., 2006) and was recently also shown to recruit the histone acetylation machinery (Weiste and Dröge-Laser, 2014). The same is not the case for bZIP1 and bZIP63. As the readout of the protoplast two-hybrid interaction assay is transcription-based it is therefore not possible to quantitatively compare the effect of phosphorylation on the formation of different dimers and to draw conclusions about the in vivo dimerization preference. Therefore we used a multi-color BiFC assay with bZIP1 and bZIP11 as alternative partners for bZIP63

to test the effect of bZIP63 phosphorylation by AKIN10 on its dimerization preference. The three bZIPs were co-expressed with AKIN10 in N. tabacum leaves and the formation of bZIP63-1 and bZIP63-11 dimers was quantified. Comparison of wt and S/A mutated bZIP63 revealed that, phosphorylation of bZIP63 shifts the dimerization preference from bZIP11 towards bZIP1. This trend fits well to the observation that both TFs are strongly upregulated in the night and extended night, while bZIP11 is downregulated under these conditions (see Figure 5 – figure supplement 3). Furthermore, increased expression of bZIP63 and bZIP1 under conditions when bZIP63 is phosphorylated might further enhance the observed shift in the dimerization towards bZIP63-1 dimers.

Based on the data presented in this study, we propose a simplified model for the regulation of bZIP63 dimerization by AKIN10 (Figure 8B). When bZIP63 is not phosphorylated, its capacity to dimerize with other bZIPs is rather low. Under starvation conditions, bZIP63 is phosphorylated at S29 by AKIN10, favoring the formation of bZIP63 homo- and specific hetero-dimers, particularly of bZIP63-1 dimers. This ultimately results in the induction of a different set of target genes and thereby mediates the transcriptional reprogramming of metabolism. However, it is clear that in the plant additional factors like bZIP expression, stability and interaction with other components add more complexity to the situation.

Surprisingly, to date only a small number of papers have reported an influence of phosphorylation on bZIP dimerization (Guo et al., 2010; Kim et al., 2007; Lee et al., 2010). Moreover, to our knowledge this is the first time that phosphorylation outside the bZIP domain was shown to affect dimerization with different partners in a distinct way. While there are numerous reports on phosphorylation-mediated changes in bZIP activity in animals, plants, and yeast, in many cases the underlying mechanism is still unknown. We therefore believe that this novel mechanism of phosphorylation-triggered switch of bZIP dimerization partners could play a substantial role in the regulation of bZIP TF activity in all higher organisms, and should be further addressed in future studies.

Experimental Procedures:

Plant lines

The lines ox#2 and ox#3 are bZIP63 overexpressor lines in the Col-0 background, expressing bZIP63.2 with a C-terminal GFP tag under the control of the 35S promoter. Generation of these plant lines was previously described in Veerabgu et al. (2014). Overexpression was confirmed by RT-qPCR of *bZIP63* mRNA (Figure 1 – figure supplement 1B and 1C).

The bZIP63 knock-out line (*bzip63*) in the Ws-2 ecotype is a T-DNA insertion line. Pool number CSJ1 (NASC ID: N700001) from the Arabidopsis Knockout Facility (AKF) (Sussman et al., 2000) was screened for a T-DNA insertion in *bZIP63* and homozygous plants were selected using Kanamycin. Sequencing of the flanking regions revealed that the T-DNA is inserted in the first exon at position 76 (Figure 1 – figure supplement 1A). The knock-out was confirmed by PCR and RT-qPCR of *bZIP63* (Figure 1 – figure supplement 1B-D). The same line was used by Veerabgu et al (2014).

For the complementation lines (GY9 + GY11 = wt, GAY4 + GAY14 = S29/294/300A, S294/300A), a genomic fragment containing *bZIP63* and 2kb of upstream sequence was obtained by PCR on Col-0 genomic DNA and ligated into pCRBlunt (Invitrogen, Austria). For the S/A constructs, first S294 and S300 were mutated to alanine by mutagenesis PCR and the plasmid was subsequently used to mutate S29 to alanine (see table for primers). Correct sequences were confirmed by restriction digests and sequencing. The genomic fragments were then cloned KpnI/NotI into modified pBIN19, containing a BASTA resistance for plant selection and a C-terminal YFP tag, before transformation into the Agrobacterium tumefaciens strain GV3101 (pMP90). Homozygous *bzip63* plants were transformed with the floral dip method and selected for positive transformation events by spraying seedlings with 200mg/l BASTA solution (Bayer, Germany). Transgene expression in GY and GAY lines was tested using RT-qPCR, western blots with an antibody against GFP, and epifluorescence microscopy (Figure 7 – figure supplement 1A-C). The S294/300A shown in Figure 8D was at the time of submission still heterozygous and in the T2 generation. Therefore, expression of the transgene

was checked by epifluorescence microscopy (not shown), but no quantification by RT-qPCR or western blotting was done.

The *AKIN10* knock-out line (*akin10*, GABI_579E09) in the Col-0 ecotype is a T-DNA insertion line from the GABI KAT collection (Kleinboelting et al., 2012). For this line two T-DNA insertions were suggested, one in *AKIN10* and another one in *IMS2* (2-ISOPROPYLMALATE SYNTHASE 2, At5g23020). The insertion in *AKIN10* in front of the last exon was confirmed by PCR, but the second insertion in *IMS2* could not be detected and was thus assumed not to be present (Figure 5 – figure supplement 1A-C). The knock-out of *AKIN10* was further confirmed by RT-qPCR and western blotting, respectively. No significant amount of transcript or protein could be detected (Figure 5 – figure supplement 1D and 1E). The *akin10* line was further tested for obvious growth and developmental phenotypes by comparing leaf number, fresh and dry weight, water content, and flowering time in soil-grown wt and mutant. Only a slight delay in flowering was observed (Figure 5 – figure supplement 2A and 2B). Expression of selected AKIN10 target genes after 6h of light or extended night was tested by RT-qPCR. Some genes showed a slight, but not dramatic reduction in expression (Figure 5 – figure supplement 2C).

For the line expressing bZIP63-GFP in *akin10*, *bZIP63.2* was amplified from Col-0 cDNA (see table for primers) and cloned ApaI/NotI into modified pBIN19 containing the UBI10 promoter, a BASTA resistance for plant selection, and a C-terminal YFP tag. Homozygous *akin10* plants were transformed and selected like the GY and GAY lines.

Plant growth

Arabidopsis seeds were surface sterilized with chlorine gas before sowing on soil or growth medium and then vernalized at 4°C for two days. Plants were grown in a growth chamber in a 12h light/12h dark regime with day temperatures between 20 and 22°C and night temperatures between 18 and 20°C and a light intensity of 60 – 150 µmol/m^2s unless specified otherwise. Plants grown under short or long day conditions were cultivated with 8h or 16h of light per day, respectively. The soil mixture

consisted of 4 parts Huminsubstrat N3 (Neuhaus, Germany), 1 part perlite (Gramoflor, Germany), and the fertilizer Osmocote (Substral/Scotts, Germany) according to manufacturer's instructions. For hydroponic cultures, plants were grown with their roots in light-tight box filled with liquid ½ Hoagland medium (2mM $Ca(NO_3)_2$, 0.25mM K_3PO_4, 3mM KNO_3, 1mM $MgSO_2$, 45µM NaFeIII EDTA, 5µM H_3BO_3, 1µM $MnCl_2$, 0.15µM $ZnSO_4$, 0.1µM $CuSO_4$, 7nM MoO_3, 4.5nM $Co(NO_3)$). Seedling cultures in liquid medium were grown in ½ Gamborg medium (Duchefa, Harlem, The Netherlands) with or without 0.5% sucrose and the medium was exchanged after 7 days. Seedlings on plates were grown on ½ MS (Duchefa, Harlem, The Netherlands) with 0.7g/l plant agar (Duchefa, Harlem, The Netherlands) and a pH of 5.8. The root cell suspension culture was grown in MS medium containing 30g/l sucrose and 2.5µM 2,4D at 22°C in the dark under constant shaking. The medium was exchanged every seven days by transferring ⅛ to ½ of the culture to a fresh flask and addition of fresh medium.

Dark-induced senescence

4.5 week-old soil-grown plants were incubated in the dark - in a box with tubes allowing for gas exchange - for 9 days. Before and after incubation the true leaves of 4-8 representative plants were harvested, stuck on white paper with double sided tape, scanned with a flatbed scanner without color correction at a resolution of 600dpi, and saved as TIFF files. Images were then imported in ImageJ (FIJI) (Schindelin et al., 2012) and the total and green leaf area of each leaf were quantified using the built-in threshold and color threshold function, respectively. The green leaf area in % was then calculated by dividing the green area of a leaf or the whole plant by the respective total area.
See Figure 1 – source data 1 for the ImageJ macro for semi-automatic image processing. A scheme of this method can be found in Figure 1 – figure supplement 2A. Alternatively, chlorophyll content was determined according to Porra et al (1989). Total rosettes or seedlings were weighed and frozen in liquid nitrogen. Rosettes were crushed crudely with a spatula to increase extraction efficiency. Chlorophyll was extracted by adding 1-5ml of a mixture of 80% Acetone and 20% 12.5mM Hepes

KOH pH 8.2 and incubation in the dark for at least 12h. Absorbance at 646.6nm, 663.6nm, and 750nm was measured in a quartz cuvette and the chlorophyll content in µg chlorophyll/mg fresh weight was determined as follows: (12.5*(A663.6 – A750) – 2.55*(A646.6 – A750) + 20.31*(A646.6 – A750) – 4.91 (A663.5 – A750))/FW. For sugar rescue assays seeds were germinated on ½ MS agar plates containing 0.5% sucrose and grown in a 12h light/12h dark cycle for 12 days before transfer to ½ MS agar plates containing 0% or 2% glucose. After 6 additional days seedlings were either harvested or put in a dark box for 7 days. The chlorophyll content in µg/mg FW of individual seedlings was determined as described above.

Metabolic profiling

Metabolites were extracted from leaves of 5 week-old plants, derivatized and measured as described in Naegele et al. (2014) with minor variations. Approximately 80mg frozen and ground plant material were extracted with 1ml -20°C cold MeOH:chloroform:H_2O (2.5:1:0.5) by mixing and incubation on ice. The supernatant after centrifugation was mixed with 400 – 500µl H_2O and centrifuged. For the experiment shown in Figure 1 (1) the polar phase was split into 2 aliquots, spiked with 1µg C13 labeled Sorbitol (Campro Scientific, Berlin, Germany) and dried. For the experiment shown in Figure 6 (6) the polar phase was not split and 2µg of Sorbitol were added. For derivatization, metabolites were first dissolved in 10µl (1) or 30µl (6) pyridine containing 40mg/ml methoxyamine hydrochloride by 90min incubation at 30°C. Then, 40µl (1) or 120µl (6) of N-methyl-N-trimethylsilyltrifluoroacetamid (MSTFA; Macherey-Nagel, Düren, Germany), spiked with 60 µl/ml of an Alkane Standard Mixture C_{10}-C_{40} (Fluka, Vienna, Austria), were added and the samples were incubated for 30min at 37°C. GC-MS measurements were carried out on an Agilent 6890 gas chromatograph coupled to a LECO Pegasus 4D GCxGC-TOF mass spectrometer (LECO, USA). Injection volume was 1µl. In the GC step, the initial oven temperature was 70°C, which was held for 1min, followed by a 9°C/min temperature increase until the final temperature of 350°C was reached, which was held again for 8min. Metabolites were measured in splitless mode (1 and 6) and alternatively

609 also in split mode with a split ratio of 5 (6). In the MS step the data acquisition rate was set to 20
610 spectra/sec, the detector voltage to 1550V and the mass range to 40-600 m/z. Raw data were
611 processed with the LECO Chroma-TOF software (LECO, USA). Peak areas were normalized to the area
612 of the internal standard and to the fresh weight before statistical analysis. Outliers, as determined by
613 Grubb's test, were removed from the dataset. For Hierarchical clustering, log-2 transformed fold
614 change values were imported into MeV (MultiExperimentViewer, version 4.9.0, Saeed et al., 2003)
615 and clustering was done using the standard settings with gene tree optimization, Pearson
616 correlation, and average linkage clustering. For the PCA plot, normalized data were imported into R
617 (RStudio, version 0.98.507), missing values were replaced with the k nearest neighbor (knn) method
618 using the "impute.knn()" function and data were Z-transformed. PCA analysis was done using the
619 "prcomp()" function and scores for PC1 and PC2 were plotted against each other.
620
621 **Electrophoresis and Western blotting**
622 For 2D gels, proteins were extracted from 5-7 week-old soil-grown ox#3 plants which were grown in
623 short day. 4ml of 1x lambda phosphatase (λPP) buffer (NEB, Frankfurt am Main, Germany), including
624 cOmplete protease inhibitor (Roche, Vienna, Austria), were added to 2ml frozen and ground plant
625 material, followed by vortexing and centrifugation. 0, 30 or 50µg of λPP were added to 1.5ml of the
626 supernatant, followed by 15min incubation at 30°C. Proteins were extracted with phenol (Carl Roth,
627 Karlsruhe, Germany), precipitated with ammonium acetate and resuspended in 1x rehydration stock
628 solution (7M urea, 2M thiourea, 2% (w/v) CHAPS, 2% IPG buffer (GE Healthcare, Vienna, Austria),
629 2.8mg/ml DTT, Bromphenol blue). Protein extracts were then applied to 7cm Immobiline^{TM} DryStrips
630 (GE Healthcare, Vienna, Austria) over night and separated by isoelectric focusing on an IPGphor (GE
631 Healthcare, Vienna, Austria) according to the manufacturer's instructions. For second dimension
632 separation, the strip was incubated in SDS equilibration buffer (6M urea, 75mM TrisCl, 29.3%
633 glycerol, 2% SDS, Bromphenol blue, pH 8.8) with 10mg/ml DTT and then without DTT for 15min each,
634 followed by standard SDS PAGE and western blotting.

635 Phos-tag gel electrophoresis was done according to the manufacturer's instructions. Proteins were
636 separated on SDS PAGE gels containing 8% SDS, 25µM Phos-tag (WAKO, Neuss, Germany) and 50µM
637 $MnCl_2$ with an amperage of 15mA/gel for 1.25h. Before semi dry blotting, the gels were incubated in
638 transfer buffer containing 1mM EDTA, followed by washing with transfer buffer without EDTA.
639 Recombinantly expressed bZIP63-YFP was used as a size marker for the nonphosphorylated fusion
640 protein. For the expression, bZIP63 was amplified from cDNA (see table for primers) and cloned
641 NcoI/NotI into pTWIN (NEB, Frankfurt am Main, Germany) containing YFP, to create a c-terminal YFP
642 fusion. The protein was expressed in E. coli (ER2566 strain) and purified according to the
643 manufacturer's instructions. Total plant proteins were extracted with phenol. For light/extended
644 night comparison, rosettes of 5 week old plants were collected after 6h of light or extended night.
645 For +/- sucrose comparison, seedlings were first germinated and grown for one week in liquid ½
646 Gamborg medium containing 0.5% sucrose, followed by 1 week in medium without sucrose. For
647 treatment, at the onset of light 1% suc was added to half of the cultures and all cultures were kept in
648 the dark for 6 additional hours. For Phos-tag gels from kinase assays, the reactions were mixed with
649 2x Laemmli sample buffer and loaded on the gel.
650 Western blotting was done by semi dry transfer onto a PVDF membrane, antibody incubation, and
651 detection with an ECL kit following standard procedures. The following primary antibodies were
652 used: Anti-GFP (Roche, Vienna, Austria; or ChromoTek, Munich, Germany), Anti-AKIN10 (Agrisera,
653 Sweden), Anti-AMPKalpha-pT172 (Cell Signaling, Leiden, The Netherlands), Anti-Flag (Sigma-Aldrich,
654 Vienna, Austria), Anti-HA High Affinity (Roche, Vienna, Austria), Anti-HA (Santacruz, Heidelberg,
655 Germany), Anti-GAL4 DNA BD (Sigma-Aldrich, Vienna, Austria), polyclonal peptide antibodies against
656 bZIP63: peptide antibodies against an N-terminal (EKVFSDEEISGNHHWSVNGM) and a C-terminal
657 (SLEHLQKRIRSVGDQ) peptide were raised in rabbit and affinity purified (Davis biotechnology,
658 Regensburg, Germany). The bZIP63 antibodies were tested on protein extracts from wt, bZIP63 ko
659 and ox plants. While the antibodies recognized recombinant protein and bZIP63 in the ox extracts
660 well, they failed to detect endogenous levels of bZIP63, possibly due to the low abundance of the

protein (not shown). The following HRP-coupled secondary antibodies were used: Anti-mouse IgG, Anti-rabbit IgG, Anti-rat IgG (GE Healthcare, Vienna, Austria).

Immunoprecipitation of bZIP63-GFP

To identify in vivo phosphorylation sites on bZIP63, bZIP63-GFP was immunoprecipitated from ox#3 seedlings grown on ½ MS agar plates or leaves of mature soil-grown ox#3 plants, harvested at different time points in the light cycle and in extended night (see Figure 3 – figure supplement 2A for growth and harvesting conditions). In one experiment, leaves were infiltrated with H_2O containing 100µM of the proteasome inhibitor MG-132 (Calbiochem/Merck Millipore, Vienna, Austria) 6h before harvesting. Protein extracts were prepared by mixing frozen and ground plant material with an equal volume of cold extraction buffer (25mM TrisCl, 10mM $MgCl_2$, 15mM EDTA, 150mM NaCl, 1mM DTT, 1mM NaF, 0.5mM Na_3VO_4, 15mM β-glycerophosphate, 0.1% Tween20, Complete protease inhibitor, pH 7.5), followed by centrifugation. The supernatant was then incubated with protein A Sepharose CL-4B (GE Healthcare, Vienna, Austria), which had been pre-incubated for 2.5h in extraction buffer with Anti-GFP antibody (Roche, Vienna, Austria), or with GFP-Trap_A beads (ChromoTek, Munich, Germany) for 1h at 4°C. The beads were washed 2 – 3 times with extraction buffer and alternatively twice with wash buffer (50mM TrisCl, 250mM NaCl, 0.1% NP–40, 0.05% sodium deoxycholate, pH 7.5). Finally, the beads were resuspended in 1x Laemmli sample buffer, boiled for 5min at 95°C, and centrifuged. The supernatant was separated by SDS PAGE and bands were excised for LC-MS/MS analysis.

Identification of proteins and in vivo phosphorylation sites by LC-MS/MS

For the identification of phosphorylation sites, bZIP63-GFP was immunoprecipitated from leaves of ox#3 plants (see “Immunoprecipitation of bZIP63-GFP”). For the identification of kinases, root protein extracts were affinity purified with recombinant GST-bZIP63 (see Figure 3B for a scheme and the methods section “Kinase assays” for detailed description of the affinity purification).

687 Proteins were first separated by SDS PAGE. Bands of interest were then excised from Coomassie-
688 stained gels and gel sections were chopped, washed with 50mM ammonium bicarbonate (ABC, pH
689 8.5), and dried with acetonitrile (ACN). Disulfide bonds were reduced by incubating in 200µl of 10mM
690 DTT for 30min at 56°C. DTT was washed off and cysteines were alkylated by incubation with 100 µl of
691 54mM iodoacetamide for 20min at RT in the dark. Gel pieces were dried with ACN, then swollen in
692 10ng/µl trypsin (recombinant, proteomics grade, Roche, Vienna, Austria) in 50mM ABC and
693 incubated over night at 37°C. For higher sequence coverage of bZIP63 alternative proteases were
694 used: LysC (MS grade, WAKO, Neuss, Germany) at 37°C overnight, subtilisin (Sigma-Aldrich, Vienna,
695 Austria) at 37°C for 0.5 – 2h, chymotrypsin (sequencing grade, Roche, Vienna, Austria) at 25°C for 4
696 hours. Digestion was stopped by adding formic acid to a final concentration of approximately 1% and
697 peptides were extracted by sonication. Peptides were separated on an UltiMate 3000 HPLC system or
698 on a U3000 nano HPLC (both Dionex, Thermo Fisher Scientific). Digests were loaded on a trapping
699 column (PepMap C18, 5µm particle size, 300µm i.d. x 5mm, Thermo Fisher Scientific), equilibrated
700 with 0.1% trifluoroacetic acid (TFA), and separated on an analytical column (PepMap C18, 3µm,
701 75µm i.d. x 150mm, Thermo Fisher Scientific) by applying a 60 minutes linear gradient from 2.5% up
702 to 40% ACN with 0.1% formic acid, followed by a washing step with 80% ACN and 10%
703 trifluoroethanol (TFE) on the U3000 HPLC. The UltiMate 3000 HPLC was directly coupled to a linear
704 ion trap (LTQ, Thermo Fisher Scientific), which was operated in a data-dependent MS3 method for
705 the phosphorylation analysis. One full scan (m/z: 450-1600) was followed by maximal 4 MS/MS
706 scans. If in the MS/MS scan a fragment corresponding to a neutral loss from the precursor of 98, 49,
707 or 32 Th was observed among the top 8 peaks, a MS3 scan was triggered. Fragmentation energy was
708 set at 35%, Q-value at 0.25, and the activation time at 30ms. High resolution measurements were
709 acquired on an LTQ-Orbitrap Velos mass spectrometer (Thermo Fisher Scientific), equipped with a
710 nanoelectrospray ionization source (Proxeon, Thermo Fisher Scientific). The electrospray voltage was
711 set to 1500V. The mass spectrometer was operated in the data-dependent mode: 1 full scan (m/z:
712 350-1800, resolution 60000) with lock mass enabled was followed by maximal 12 MS/MS scans. The

lock mass was set at the signal of polydimethylcyclosiloxane at m/z 445.120025. Monoisotopic precursor selection was on, precursors with charge state 1 were excluded from fragmentation. The collision energy was set at 35%, Q-value at 0.25, and the activation time at 10ms. Fragmented ions were set onto an exclusion list for 60s. When ETD (electron transfer dissociation) was applied, the top 6 peaks from the full scan where fragmented with CID (collision-induced dissociation) and subsequently with ETD. For ETD, the energy parameters were as for the CID except the activation time was set to 80 or 120ms.

Data interpretation: Raw spectra for the kinase identification were interpreted by Mascot 2.2.04 (Matrix Science) using Mascot Daemon 2.2.2. Spectra were searched against the *Arabidopsis thaliana* entries in the nr-database with the following parameters: the peptide tolerance was set to 2Da, MS/MS tolerance was set to 0.8Da, carbamidomethylcysteine was set as a static modification, oxidation of Met as variable modification. Trypsin was selected as the protease allowing two missed cleavages. Mascot score cut-off was set to 30, except for the low abundance sample 1, where the cut-off was set to 20. For the phosphorylation analysis of purified bZIP63, either Mascot or Sequest (Proteome Discoverer 1.2; Thermo Scientific) were used. The search was extended to the phosphorylation of Ser, Thr, and Tyr. High resolution data were searched with 3ppm precursor mass tolerance. Proteolytic specificity was defined according to the digest. Results were manually validated including comparison of the fragmentation pattern and the relative retention of the nonphosphorylated counterpart. Site localization was checked by manual inspection at the spectrum level in the first place and was confirmed by the site-localization algorithm PhosphoRS (Taus et al., 2011).

Kinase assays

In vitro kinase assays were performed with GST-tagged recombinant proteins. The cDNA of *bZIP63.2*, *bZIP1*, *bZIP2*, *bZIP11*, *bZIP44.1*, *bZIP55*, *AKIN10.1/3*, and *AKIN11.1/2* was obtained by PCR (see table for primers) and cloned ApaI/NotI or NcoI/NotI into pGEX-4T. *SnAK2* was in pDEST15 (Crozet et al.,

2010). An inactive version (K/M) of *AKIN10* and non-phosphorylatable (S/A) versions of *bZIP63* were created by mutagenesis PCR using the primers listed in the primer table. The proteins were expressed in E. coli (ER2566 or BL21 strain), purified using Glutathione Sepharose 4B (GE Healthcare, Vienna, Austria) according to the manufacturer's instructions, and stored at -80°C in GST elution buffer containing 10 – 25% glycerol.

Kinase assays were performed by incubating the kinase and substrate for 20 – 30min in kinase reaction buffer (20mM Hepes, 20mM $MgCl_2$, 100µM EGTA, 1mM DTT, 50µM ATP, pH 7.5) at room temperature. For radioactive assays, 1µCi γ-^{32}P-labeled ATP (NEN/PerkinElmer, Waltham, MA, USA) was added in each reaction. The reactions were then separated by SDS PAGE and exposure on a Storage Phosphor Screen (GE Healthcare, Vienna, Austria) or Phos-tag gel electrophoresis and Western blotting, respectively.

For in-gel kinase assays, bZIP63 with an N-terminal 6xHis tag was used as a substrate. To construct the expression vector, bZIP63.2 was amplified from cDNA (see table of primers) and first cloned ApaI/NotI into pRSETa-QM (Invitrogen, Germany). From there the expression cassette was excised by SalI digest, followed by a fill in with DNA Polymerase I (Klenow fragment, NEB, Frankfurt am Main, Germany) and XbaI digest. The cassette was ligated with pTXB3 (NEB, Frankfurt am Main, Germany), which was first digested with BamHI, followed by a fill in and XbaI digest. The protein was expressed in E. coli (ER2566 strain) and purified over a HiTrap column (GE Healthcare, Vienna, Austria) according to the manufacturer's instructions. Plant protein extracts for the in-gel kinase assays were made from different plant material. For the identification of bZIP63 kinases, proteins were extracted either from roots of 8 week-old plants that were grown in hydroponic culture in short day and collected in the light phase (shown in Figure 4A and 4C), from root cell suspension culture, or from seedlings grown on ½ MS agar plates, which were harvested in the dark phase. 4 independent experiments were conducted. For specifications on the plant material used in each of the experiments and the kinases identified please refer to Figure 4 – source data 1. For the comparison of bZIP63 phosphorylation with wt and *akin10* plant extracts, roots and leaves of 2 week-old

765 seedlings grown in liquid culture in a 12hlight/12h dark cycle and collected after 4h of extended night
766 were used. Extraction was done by mixing the frozen and ground plant material with an equal
767 volume of cold protein extraction buffer (25mM TrisCl, 15mM EGTA, 10mM $MgCl_2$, 75mM NaCl, 1mM
768 NaF, 0.5mM $NaVO_3$, 15mM beta-glycerophosphate, 0.1% Tween20, 1mM DTT, Complete protease
769 inhibitor, pH 7.5), followed by centrifugation. Protein amounts were determined by Bradford assay.
770 For affinity purification of bZIP63-binding proteins, GST-tagged bZIP63 was expressed in E. coli and
771 the cell lysate of up to 1l culture in GST binding buffer (50mM TrisCl, 20mM $MgSO_4$, 2mM DTT, 5mM
772 EDTA, 0.5% Tween20, pH 8) was loaded on an equilibrated GSTrap FF column (GE Healthcare, Vienna,
773 Austria). The column was then washed with 5ml cold GST binding buffer and protein extraction
774 buffer, respectively, and 2 – 5ml of total root protein in cold protein extraction buffer were loaded.
775 Subsequently, proteins were eluted from the column by repeated washing with 5ml cold protein
776 extraction buffer with increasing salt concentrations, and concentrated with Amicon Ultra Centrifugal
777 Filter Units (Millipore). 8 – 20µg total protein extracts and up to 40µg affinity purified proteins were
778 loaded on standard SDS PAGE gels containing 1mg/ml substrate (6x His-bZIP63) in the separating gel
779 and run at 4°C with 20mA per gel. The gel was then incubated three times for 20min, respectively, at
780 room temperature in each of the following buffers: wash buffer I (50mM TrisCl, 20% isopropanol, pH
781 8), wash buffer II (50mM TrisCl, 1mM DTT, pH 8), and denaturation buffer (50mM TrisCl, 1mM DTT,
782 6M guanidinium HCl, pH 8). Subsequently, the gel was incubated in renaturation buffer (50mM
783 TrisCl, 0.05% Tween 20, pH 8) at 4°C for 12 – 18h. In this period, the buffer was exchanged 10 times
784 after at least 30min. After renaturation, the gel was incubated two times for 30min, respectively, in
785 kinase buffer (20mM HEPES, 20mM $MgCl_2$, 50µM $CaCl_2$ or 500µM EGTA, 1mM DTT, 0.05% Tween 20,
786 pH 7.5), followed by 30min incubation in kinase reaction solution (kinase buffer containing 50µM ATP
787 and 100µCi γ-^{32}P-labeled ATP). Finally, the gel was washed two times for 15min, respectively, in 5%
788 TCA and several times in 5% TCA containing 1% sodium pyrophosphate, until the wash solution was
789 only weakly radioactive. The dried gels were exposed on a Storage Phosphor Screen and the signal
790 was recorded on a Typhoon 8600 (GE Healthcare, Vienna, Austria).

Y2H assay

AKIN10.1/3, *AKIN11.1/2*, *AKINβ1*, *AKINβ2*, *SNF4*, and *bZIP63.2* were amplified from cDNA (see table for primers) and cloned ApaI/NotI or NcoI/NotI into pBTM117 and *bZIP63.2* was cloned into pACTIIJ to generate N-terminal fusions with the LexA-BD and the GAL4-AD, respectively. The yeast strain L40 (MATα *his*Δ*200 trp1-900 leu2-3.112 ade*2 LYS2::(*lexA op*)$_4$HIS3 URA3::(*lexA op*)$_8$lacZ Gal4 gal80) was transformed with empty pACTIIJ or *bZIP63.2*-containing pACTIIJ in combination with different pBTM117 vectors. Freshly grown L40 was mixed gently with 1ml transformation mix (800µl 50% PEG 3600, 100µl 2M LiAc, 100µl 1M DTT, 10µl bacterial RNA (10µg/µl)), to get a cloudy suspension. 2.5µg of each plasmid were added to 125µl transformation mix, followed by 20min incubation at 30°C and 44°C, respectively, addition of 1ml H2O, and 1min centrifugation at 3500g. The cells were resuspended in a small volume and plated on SD medium without Leu and Trp to select for successful transformation. Single colonies were inoculated in SD medium without Leu and Trp and proteins were extracted from 2ml of an over-night culture. The yeast cells were resuspended in 200µl enzyme lysis buffer (25mM TrisCl, 20mM NaCl, 8mM $MgCl_2$, 5mM DTT, 0.1% NP-40, pH 7.5), 200µl glass beads (0.4 – 0.6mm diameter) were added, the cells were frozen in N_2, thawed, and broken by vigorous shaking on a Vibrax at 4°C for 20min. The supernatant after 10min centrifugation was transferred to a fresh tube and kept on ice. The protein concentration of the extract was determined by Bradford assay. The GUS activity was determined by mixing 50µl of the extract with 650µl Z-buffer (60mM Na_2HPO_4, 40mM NaH_2PO_4, 10mM KCl, 10mM $MgSO_4$, 0.25% beta mercaptoethanol) and 100µl ONPG (4mg/ml), and incubating for up to 10min at room temperature. The reaction was stopped by adding 400µl 1M Na_2CO_3 and the extinction at 420nm was measured on a photometer. The GUS activity in U/mg protein was calculated as follows: (A420 x 24 x 1000)/(45 x incubation time [min] x protein concentration [mg/ml])

Bimolecular fluorescence complementation (BiFC) and multi-color BiFC

For BiFC and multi-color BiFC interaction studies in *Nicotiana tabacum*, *bZIP63.2*, *AKIN10.1/3*, *AKIN11.1/2* and *SNF4* were cloned into modified pBIN19 vectors, containing either the N- or C-terminal moieties of the split CFP system as N-terminal fusions as described in Waadt et al. (2008) (see Figure 4D for scheme). To generate BiFC plasmids for ApaI/NotI and NcoI/NotI cloning, CPK3, harboring XbaI, NcoI, and ApaI (for plasmids with MCS (multi cloning site) 1) or ApaI and NcoI (for plasmids with MCS 2) in the terminus and NotI and SmaI in the C-terminus was generated by PCR from cDNA (see table for primers). It was then cloned XbaI/SmaI or ApaI/SmaI into the different BiFC casettes in pUC19 from Waadt et al. (2008). The cassettes were then cloned into pBIN19 with HindIII/EcoRI and CPK3 was exchanged for other genes using ApaI and NotI. Agrobacterium tumefaciens (AGL1 strain) was transformed with the resulting plasmids by electroporation and further used for transient transformation of tobacco leaf epidermis. For transformation, 5ml agrobacterium overnight cultures were filled to 50ml with fresh LB medium containing 50µg/ml Kanamycin and 10µg/ml Gentamicin and grown for 4h at 30°C. The cells were pelleted by centrifugation at 3500g, resuspended in LB containing 150µM acetosyringone, and grown for another 2h. The cultures were then pelleted again and resuspended in 5% sucrose solution to reach a final OD600 of 2. For co-infiltration, equal volumes of agrobacteria suspensions, containing the respective constructs, were mixed and infiltrated into the leaves of 5 week-old plants. 48h after infiltration equally sized leaf sections were analyzed for their CFP fluorescence signal with an LSM510 confocal laser scanning microscope (Zeiss) and the corresponding ZEN software (Zeiss). The same settings were used for each construct to allow comparison of the signal intensities. To verify that the fusion proteins were expressed and to determine the relative amount of each interaction partner, proteins were extracted from the leaf sections used for microscopy and subjected to Western blot analysis with antibodies against the Flag (N-terminal CFP moiety) and HA (C-terminal CFP moiety) epitopes.

Multi-color BiFC was done as described in Waadt et al. (2008) with some modifications. bZIP11 fused to the N-terminal moiety of CFP (CFP-N), bZIP1 fused to the N-terminal moiety of VENUS (VENUS-N),

842 and bZIP63 (wt or S29/294/300A) fused to the C-terminal moiety of CFP (CFP-C) were expressed from
843 one plasmid to have co-expression at equal amounts in all transformed cells (for a scheme of the
844 construct see Figure 9A). To generate the construct, bZIP1 and bZIP11 were first amplified from cDNA
845 by PCR (see table for primers) and cloned ApaI/NotI into pBIN19 containing a c-terminal fusion of
846 CFP-C and CFP-N, respectively (plasmids described above). From there, 35S::bZIP1 was cloned
847 HindIII/NotI into pUC19 containing CPK3 with a c-terminal VENUS-N fusion (described above) to
848 exchange the shorter 35S primer in the VENUS construct. Then, the two cassettes including the 35S
849 promoter, bZIP1 or 11 and the VENUS-N or CFP-N tag were amplified by PCR introducing KpnI/HindII
850 in the front and BamHI in the back of the bZIP1 cassette and BamHI in the front and HindIII in the
851 back of the bZIP11 cassette (see table for primers). The PCR products were ligated into pCRBlunt
852 (Invitrogen, Germany) and the bZIP1 cassette was then cloned KpnI/BamHI in front of the bZIP11
853 cassette. Finally, the combined cassette with bZIP1 and 11 was cloned HindII into pBIN19 containing
854 bZIP63 wt or S29/294/300A (mutated by PCR) with an n-terminal CFP-C fusion. AKIN10 was amplified
855 from cDNA by PCR (see table for primers) and cloned ApaI/NotI into pBIN19 containing a c-terminal
856 mCherry tag. Agrobacterium tumefaciens (AGL1 strain) was transformed with the resulting plasmids
857 by electroporation and further used for transient transformation of tobacco (*Nicotiana tabacum*) leaf
858 epidermis as described above. 48h after infiltration equally sized leaf sections were analyzed for their
859 VENUS, CFP, and mCherry fluorescence signal with a TCS SP5 DM-6000 confocal laser scanning
860 microscope (Leica) and the corresponding Leica software. CFP, VENUS, and mCherry were excited
861 with 458nm (Ar laser), 514nm (Ar laser), and 574nm (white light laser), respectively. The fluorescence
862 was detected at 461-495nm, 520-550nm, and 600-615nm, respectively. To avoid bleed-through of
863 the CFP signal into the VENUS channel CFP and VENUS were excited and detected separately.
864 Pictures were taken with a 20x air objective and the same settings for both combinations (wt bZIP63
865 and S29/294/300A). The pinhole was set to 1.5. To determine the relative VENUS/CFP signal ratio,
866 images were processed in the LasX software from Leica. Nuclei showing a CFP/VENUS as well as
867 mCherry signal were selected and the signal intensity was determined with the histogram tool. For

each nucleus a ratio of the background corrected pixel sum from VENUS and CFP was built. All values for one leaf were divided by the median of the ratio from the bZIP63 S29/294/300A construct to allow comparison between experiments. In total, six leaves from two infiltrations were analyzed with similar results.

Virus-induced gene silencing (VIGS)

Two week-old GY9 plants were infiltrated (*akin10/11*) or not (control) with an *AKIN10-AKIN11* silencing construct according to the method described by Burch-Smith et al. (2006). For the *AKIN10-AKIN11* construct two gene-specific fragments corresponding to *AKIN10* and *AKIN11* were cloned in tandem into the TRV-based vector pYL156a. First, a 480 bp *AKIN10* fragment was amplified from cDNA using the *AKIN10 VIGS* primers (see table for primers) and cloned into the pYL156/pTRV2 vector using EcoRI/KpnI. A 503-bp *AKIN11* fragment (Baena-Gonzalez et al., 2007) was thereafter amplified from cDNA using the *AKIN11 VIGS* primers (see primer list) and cloned into the pYL156/pTRV2 vector harboring the KIN10 fragment using XhoI/KpnI. Two weeks after infiltration the *AKIN10-AKIN11* knock-down plants displayed visible growth defects and anthocyanin accumulation. Silencing of AKIN10 and AKIN11 in these plants was confirmed by western blotting with an antibody against phosphorylated AMPK alpha (Anti-AMPKalpha-pT172) before use in Phos-tag gels (see Figure 5 – figure supplement 7). The VIGS experiments were repeated 4 times and 3 biological replicates were analyzed in each experiment with consistent results.

Protoplast transformation for P2H and promoter activation assays

Protoplast were obtained from 3 week-old soil-grown wt Arabidopsis plants and transformed according to the guide method (Yoo et al., 2007) with small modifications. Leaves were harvested 1h after onset of the light phase, cut into tiny stripes, and digested for 30min under vacuum and 3h at atmospheric pressure, respectively, with enzyme solution (1.25% (w/v) Cellulase R-10, 0.3% Macerozyme R-10, 400mM mannitol, 20mM KCl, 10mM $CaCl_2$, 20mM MES, pH 5.7). The protoplast

894 suspension was filtered on a metal net to remove leaf debris and washed twice with 10ml of W5
895 solution (2mM MES, 154mM NaCl, 125mM $CaCl_2$, 5mM KCl, pH 5.7). Protoplasts were resuspended in
896 10ml of W5, incubated on ice for at least 1h and subsequently resuspended to a final concentration
897 of 1 x 105 cells/ml in MMg buffer (4mM MES, 400mM mannitol, 15mM $MgCl_2$, pH 5.7). Protoplasts
898 were then co-transformed with 10µg each of up to three effector plasmids, 7µg of a reporter
899 plasmid, and 3µg of a *35S::NAN* transfection control reporter plasmid (Kirby and Kavanagh, 2002) for
900 normalization. For P2H assays, the effector plasmids were pHBTL containing *bZIP63.2*, *bZIP1*, or
901 *bZIP11* with an N-terminal GAL4-AD or GAL4-BD fusion (described in detail in Ehlert et al., 2006) and
902 alternatively pHBTL containing *AKIN10.1/3*. The reporter plasmid contained *GAL-UAS$_4$::GUS* (beta
903 galactosidase) (Ehlert et al., 2006). For promoter activation assays, effector plasmids were pHBTL
904 containing HA-tagged *bZIP63.2* or *AKIN10.1/3*. pBT10 containing *proASN1::GUS* or *proProDH::GUS*
905 (Dietrich et al., 2011) was used as a reporter plasmid. For transformation, 200µl of the protoplast
906 suspension were gently mixed with the DNA and 220µl of PEG (40% PEG 4000, 200mM mannitol,
907 100mM $CaCl_2$) were added, followed by gentle mixing, and 10min incubation at room temperature.
908 The protoplasts were then washed by addition of 800µl W5 and 1min centrifugation at 300g. The
909 supernatant was removed and the protoplasts were incubated for 16h in 200µl of WI solution (4mM
910 MES, 500mM mannitol, 20mM KCl, pH 5.7) in the growth chamber in order to not affect their diurnal
911 circle. GUS and NAN enzyme assays were performed according to Kirby and Kavanagh (2002) and the
912 relative activity of GUS and calculated as GUS/NAN. The expression of the effector constructs was
913 confirmed by Western blot analysis.
914
915 **Sequence alignment of bZIP63 homologues**
916 Homologues of bZIP63 in 8 plant species were identified by blasting the protein sequence of bZIP63.2
917 on the Phytozome webpage (http://phytozome.net). The protein sequences were aligned with
918 ClustalΩ (http://www.ebi.ac.uk/Tools/msa/clustalo/) using the default settings and the Clustal
919 output file was imported into GeneDoc (http://www.psc.edu/biomed/genedoc) for visualization and

minor adjustments of the alignment. The identity matrix for the alignment was calculated using the PID3 method in the SIAS webmask (http://imed.med.ucm.es/Tools/sias.html).

Gene identifiers of the *bZIP63* homologues (numbers are the Phytozome10 references): *Medicago truncatula* (Medtr7g115120), *Glycine max* (Glyma.10G162100), *Populus trichocarpa* (Potri.013G040700), *Vitis vinifera* (GSVIVG0102179000), *Zea mays* (GRMZM2G007063), *Oryza sativa* (LOC_Os03g58250), *Selaginella moellendorffii* (270282), *Physcomitrella patens* (Phpat.009G02690)

RT-qPCR

RNA was extracted with phenol from total rosettes of 4.5 week-old soil-grown plants at the indicated time points. 500µl RNA extraction buffer (1% SDS, 10mM EDTA, 200mM NaAc, pH 5.2) and 500µl acidic phenol (pH 4, Carl Roth, Karlsruhe, Germany) were added to 100mg frozen and ground plant material, followed by 1min vortexing and 10min centrifugation. The aqueous phase was extracted twice with an equal volume of PCI (Phenol:Chloroform:Isoamylalcohol (25:24:21), Carl Roth, Karlsruhe, Germany) by vortexing for 30sec and 2min centrifugation, and twice with chloroform. Then, the RNA was precipitated by adding ⅓ volume 10M LiCl and incubating at 4°C for at least 2h, followed by 15min centrifugation at 4°C. The pellet was washed once with 2.5M LiCl and then with 70% EtOH, dried and resuspended in 50µl RNAse free H_2O. 6.5µg RNA were treated with 2u of RQ1 DNAse (Promega, Mannheim, Germany), according to the manufacturer's instructions and precipitated again for at least 2h with ⅓ volume of 10M LiCl to remove the DNAse from the solution. The solution was then centrifuged for 15min, washed once with 70% EtOH, dried and resuspended in RNAse free H_2O. 1.5µg RNA were reverse transcribed using M-MLV RT [H-] Point Mutant (Promega, Mannheim, Germany) according to the manufacturer's instructions and diluted 1:4 with RNAse free H2O. 2µl of cDNA (15ng/µl) or H_2O (for the no template control) were added to 18µl of a PCR reaction mix containing 0.25u DreamTaq polymerase (Thermo Scientific, Vienna, Austria), 1x Dream Taq buffer, additional 3mM $MgCl_2$, 100µM dNTPs, 400nM of each primer, and 0.4x SYBR Green I nucleic acid gel stain (Sigma-Aldrich, Vienna, Austria). The qPCR was performed on a Mastercycler ep

realplex2 (Eppendorf) in white 96-well twin.tec real-time PCR plates (Eppendorf, Vienna, Austria) with the following program: 1 cycle with 3min at 95°C, followed by 40 cycles with 20sec at 95°C, 20sec at 59/60°C, and 12sec at 72°C. 2-3 technical replicates were used. A 20min melting curve was added in the end. For data evaluation, raw data were imported into LinRegPCR (version 2014.02, Ramakers et al., 2003), where the PCR efficiency was checked and the N0 (staring concentration of cDNA) was calculated with a common baseline setting for each primer pair. Samples excluded by LinReqPCR were not used. In case only two technical replicates were used, samples for which the dCq between the two technical replicates was bigger than 0.5 were also excluded from the calculations. The mean N0 of the technical replicates was calculated for each sample and primer pair. The resulting mean N0 of the test genes was then normalized by dividing by the mean N0 of the reference genes. For qPCR of *AKIN10*, *AKIN11* (Figure 5 – figure supplement 1D); *bZIP63*, *bZIP1*, *bZIP11* (Figure 5 – figure supplement 3); *ASN1*, *DIN10*, and *ProDH* (Figure 7G) *TBP2* (Tata binding protein 2) was used as a reference gene. For pPCR of *bZIP63*, (Figure 1 – figure supplement 1D and 1E, Figure 7 – figure supplement 1A); *CAB2*, *SEN1*, *SAG103*, and *YLS3* (Figure 1 – figure supplement 3B); *ASN1*, *ProDH*, *BCAT2*, *AA-TP family protein*, and *DIN10* (Figure 5 – figure supplement 2C) the geometric mean of the values for *TBP2* and *MHF15* (Thioredoxin superfamily protein) were used. The normalized N0 values were then used to calculate the mean and SD. Outliers were determined with the Grubb's test and removed.

Statistical tests

Statistical tests were performed in excel or R. Equality of variances was tested with Levene's test. This was followed by unpaired t-tests or multivariate statistics. In case of equal variance ANOVA followed by Bonferroni or TukeyHSD corrected pairwise comparison was chosen. In case of unequal variance Welch corrected ANOVA was applied, followed by Games Howell test of all samples or pairwise comparison of samples with equal variance.

Gene identifiers of *Arabidopsis thaliana* genes

bZIP63 (At5g28770), *bZIP1* (At5g49450), *bZIP11* (At4g34590), *bZIP2* (At2g18160), *bZIP44* (At1g75390), *bZIP53* (At3g62420), *AKIN10/SnRK1.1* (At3g01090), *AKIN11/SnRK1.2* (At3g29160), *AKINβ1* (At5g21170), *AKINβ2* (At4g16360), *SNF4/AKINβγ* (At1g09020), *SnAK2/GRIK1* (At3g45240), *ASN1/DIN6* (At3g47340), *DIN10* (At5g20250), *ProDH/ERD5* (At3g30775), *BCAT2* (AT1G10070), *AA-TP* (amino acid transporter) *family protein* (AT2G40420), *TBP2* (At1g55520), *MHF15* (At5g06430), *CAB2* (At1g29920), *SEN1/DIN1* (At4g35770), *SAG103* (At1g10140), *YLS3* (At2g44290).

Primer table

Gene	forward primer	reverse primer
Primers for cloning		
genomic *bZIP63*	GGTACCAAAACTATAAATTTCTTGTAGGACAGTG	TTGCGGCCGCCCTGATCCCCAACGCTTCGAATACG
bZIP63.2	GGGCCCATGGAAAAAGTTTTCTCCGACGAAGAAATCTCC	TTGCGGCCGCCCTGATCCCCAACGCTTCGAATACG
AKIN10.1+3	GGGCCCATGGATGGATCAGGCACAGGCAGTA	GCGGCCGCAGAGGACTCGGAGCTGAGCAA
AKIN11.1+2	GGGCCCATGGATCATTCATCAAATAG	GCGGCCGCAGATCACACGAAGCTCTGTAA
SNF4	GGGCCCATGTTTGGTTCTACATTGGA	GCGGCCGCAAAGACCGAGCAGGAATTGGAA
AKINβ1.1	GGGCCCATGGGAAATGCGAACGGCAAA	GCGGCCGCACCGTGTGAGCGGTTTGTAG
AKINβ2.1+2	GGGCCCATGTCTGCTGCTTCTGATGGT	GCGGCCGCACCTCTGCAGGGATTTGTAG
bZIP1	CGATGGGCCCCATGGCAAACGCAGAGAAG	CGATGCGGCCGCTGTCTTAAAGGACG
bZIP2	AAAACCATGGCGTCATCTAGCAGCAC	TGCGGCCGCTATACATATTGATATCATTAG
bZIP11	TAGGGCCCATGGAATCGTCGTCGTCGGGAA	TGGCGGCCGCAATACATTAAAGCATCAGAAG
bZIP44.1	CAGGGCCCATGAATAATAAAACTG	CTGCGGCCGCAACAGTTGAAAACATC
bZIP53	AAAACCATGGGGTCGTTGCAAATGCAAAC	TGCGGCCGCTGCAATCAAACATATCAGCAG
AKIN10 VIGS	GGAATTCACTTTTTCAGCTCAGAAAATTTTG	GGGGTACCCCCTCGAGCCACTCCTGATATTATCTGCTG
AKIN11 VIGS	CCTCGAGGTTTCTGTATATTTCTTCGCTC	GGGGTACCCAGTACTCTACACCAGATATTATC
BiFC MCS1	TCTAGAGGGCCCATGGGCCACAGACACAG	CCCGGGGCGGCCGCACATTCTGCGTC
BiFC MCS2	AAAAGGATCCGGGCCCATGGGCCACAGACACAGCAAGTCCAAATCCTCCG	CCCGGGGCGGCCGCACATTCTGCGTC
multi-color BiFC bZIP1	TCGGTACCAAGCTTAGCTTGCATGCCTGCAGG	CAGGATCCAGCTGGCGAAAGGGGGATGTGCTG
multi-color BiFC bZIP11	CAGGATCCTTAGCTTGCATGCCTGCAGGTCC	CTAGGCCTAAGCTTCGCTATTACGCCAGCTGGCGAAAGG
Mutagenesis		
bZIP63S29A	CGTCGTTGAATCGCTCGGCCGCCGAATGGGCATTCAATC	ACGTCATTCCATTAACCGACCAGTG
bZIP63S59A	GTGTGGTGTTTCCGTCTCCGCTCCTCCTAATGTTCCTG	CACACGCCGTCGTAGATTCTCCGTCGTC
bZIP63S102A	GATACTTCTGGTAGAGCTGACAATGGTGGAGC	GTATCCTGAGGTTTGATGAAAGTTC

bZIP63S160A	CTGATTCTCTATTAGCTAGCATCCTTTTAACG	ATCAGCTAGACGGTCCAGAAGAAG
bZIP63S261A	CAGAGACATCAAATGCTCCAGACACTACAAG	CTTGTAGTGTCTGGAGCATTTGATGTCTCTG
bZIP63S294A	GAACAGAACAGCTGCCATGCGTAGAGTTGAG	TGTTCATCTTGCACCCTATCAAGGC
bZIP63S294/300A	GAACAGAACAGCTGCCATGCGTAGAGTTGAGGCCTTGGAACATCTGCAG	TGTTCATCTTGCACCCTATCAAGGC
AKIN10K48M	GGTTGCTATCATGATCCTCAATCGTCG	GCAACCTTATGTCCTGTCAATGC
qPCR		
bZIP63	GAAGAAATCTCCGGTAACCATCAC	GATTCTCCGTCGTCTGCAGC
bZIP1	AACGCGGGTCTTAGATCGGAGAAG	TCAGCGTTAAACTCGTCGTAGCAA
bZIP11	TCGTCAGGATCGGAGGAGAGT	GATCGTCTAGGAGCTTTTGTTTCTTC
CAB2	TCAATCTTTTGAATTCGAGTGAGA	TCCACCACAAACACAAACCTAC
SEN1	CAGAGTCGGATCAGGAATGG	ATTATGATTTCATCGTGTTTCC
SAG103	AGCTCGAGTGCTGGGATG	CGGATTCACAGATCCTTCCT
YLS3	GACATCACTAAGTGCCCTGCT	ACTGTTTCGTTCAGACCTTTAGC
AKIN10	ACTGGATTTGCAGAGAGTACAAGGTCC	TCAGAGGACTCGGAGCTGAGCA
AKIN11	GCTCGTAACTTTTTCCAGCAGA	TTCAGGTCTCTATGGACAACCA
ASN1	GTCGCAAGATCAAGGCTC	TGAAGTCTTTGTCAAGGAAAGG
DIN10	GCTTGTATTGCCTGATGGA	ATCTTTAGCAAGCTGACACC
ProDH	CGCCAGTCCACGACACAATTCA	CGAATCAGCGTTATGTGTTGCG
BCAT2	AAGGTTATCAGGTAGTAGAGAAGG	TTCCTGATATGTGATAGTGCC
AA-TP family protein	GTTCTTGGGATCAACTTCTACAG	AACCATTTACATTCCGTAGGAC
TBP2	TGCAAGAAAGTATGCTCGG	ACATGAGCCTACAATGTTCTG
MHF15	GTTTCCTGAGCTTCTCCAC	TGGTCGCTTCATCTTGAG
characterization of plant lines (PCR)		
bZIP63	TTGCGGCCGCCCTGATCCCCAACGCTTCGAATACG	AACCATGGATAATCACACAGCTAAAGACATTGG
bzip63 RB	TGGCGAATGAGACCTCAATTGCGAGCTTT	
bzip63 LB	CATTTTATAATAACGCTGCGGACATCTAC	
AKIN10	CCAGCATAATAGAGAACGAAGC	GTCCGGTTTAGTATTCAGAGG
akin10 LB	ATATTGACCATCATACTCATTGC	

Author contributions

AM, LP, BW, DA, AS, CW, TK, and CV performed experimental research and data analysis with substantial input from TN, JVC, JH, EBG, CC, and WW. AM, LP, BW, WDL and MT designed the experiments. AM and MT wrote the manuscript.

Acknowledgements

We thank Lena Fragner (University of Vienna) for help with the metabolomics measurements and Klaus Harter (University of Tübingen) and Sjef Smeekens (Utrecht University) for critical comments on the manuscript. We further thank the Core Facility Cell Imaging and Ultrastructure Research

(CIUS, University of Vienna) for providing access and support to the Leica confocal laser scanning microscope. This work was funded by the FP7 Marie Curie ITN MERIT (GA 264474) (LP, AS, TN), the Austrian Science Fund (FWF) projects AP19825 (AM, BW, MT) and AP23435 (AM, MT), the Deutsche Forschungsgemeinschaft (DFG) project HA2146/8-2 (CC), and the Fundação para a Ciência e a Tecnologia projects PTDC/BIA-PLA/3937/2012 and UID/Multi/04551/2013 (EBG).

List of supporting material

Figure 1 – figure supplement 1. Molecular characterization of the *bzip63* line and expression of bZIP63 in the ko and ox lines

Figure 1 – figure supplement 2. Phenotype of *bZIP63* mutants in dark-induced senescence

Figure 1 – figure supplement 3. Expression of senescence marker genes during prolonged darkness

Figure 1 – figure supplement 4. Effect of sugar on bZIP63 mutants in light

Figure 1 – source data 1. ImageJ macro for determination of leaf area and green leaf area

Figure 2 – figure supplement 1. Metabolic changes in bZIP63 ko and ox plants

Figure 2 – source data 1. Excel table of relative metabolite levels in *bZIP63* mutants and p-values from T-tests

Figure 3 – figure supplement 1. Comparison of Phos-tag western blots from different figures.

Figure 3 – figure supplement 2. Overview over identified phospho-peptides of bZIP63

Figure 4 – figure supplement 1. Auto-phosphorylation from the protein extracts is negligible in in-gel kinase assays

Figure 4 – figure supplement 2. Overview over the kinases identified by LC-MS/MS after affinity purification with bZIP63

Figure 4 – source data 1. Excel table containing a detailed overview over the identified kinases and analyzed samples as well as all peptides found for the kinase subunit

Figure 5 – figure supplement 1. Molecular characterization of the *akin10* line

Figure 5 – figure supplement 2. Phenotype and gene expression of selected AKIN10 target genes in the *akin10* line

Figure 5 – figure supplement 3. Expression of bZIPs in the *akin10* line

Figure 5 – figure supplement 4. SnAK2 increases the kinase activity of AKIN10 and AKIN11 but does not phosphorylate bZIP63

Figure 5 – figure supplement 5. AKINβ1 and AKINβ2 don not interact with bZIP63

Figure 5 – figure supplement 6. Altered sugar-dependent in vivo phosphorylation of bZIP63 in seedlings

Figure 5 – figure supplement 7. *AKIN10/AKIN11* VIGS plants

Figure 6 – figure supplement 1. AKIN10 phosphorylates bZIP63 but not GST

Figure 6 – figure supplement 2. AKIN10 phosphorylates S29, S294, and S300 on bZIP63

Figure 6 – figure supplement 3. The AKIN10 target sites and S160 in the bZIP domain hare highly conserved

Figure 6 – figure supplement 4. Expression of bZIP63 and AKIN10 in the promoter activation assays

Figure 6 – source data 1. Sequences of the bZIP63 homologues

Figure 7 – figure supplement 1. Characterization of the *bzip63* complementation lines

Figure 7 – figure supplement 2. Complementation of the dark-induced senescence phenotype of *bzip63*

Figure 7 – source data 1. Excel table containing the relative metabolite levels of the complementation lines and the PCA loadings

Figure 8 – figure supplement 1. Western blots and controls for the protoplast two-hybrid (P2H) assays

Figure 8 – figure supplement 2. SnAK2 does not phosphorylate bZIP63 or the S1 class bZIPs

References

Araújo WL, Tohge T, Ishizaki K, Leaver CJ, Fernie AR. 2011. Protein degradation - an alternative respiratory substrate for stressed plants. *Trends Plant Sci*. **16:** 489-98. doi: 10.1016/j.tplants.

Baena-Gonzalez E, Rolland F, Thevelein JM, Sheen J. 2007. A central integrator of transcription networks in plant stress and energy signalling. *Nature* **448**: 938-42. doi: 10.1038/nature06069

Baena-Gonzalez E, Sheen J. 2008. Convergent energy and stress signaling. *Trends in Plant Science* **13**: 474-482. doi: 10.1016/j.tibs.2008.02.002

Bayer RG, Kostler T, Jain A, Stael S, Ebersberger I, Teige M. 2014. Higher plant proteins of cyanobacterial origin - are they or are they not preferentially targeted to chloroplasts? *Molecular plant*. pii: ssu095. doi: 10.1093/mp/ssu095

Buchanan-Wollaston V, Page T, Harrison E, Breeze E, Lim PO, Nam HG, Lin JF, Wu SH, Swidzinski J, Ishizaki K, Leaver CJ. 2005. Comparative transcriptome analysis reveals significant differences in gene expression and signalling pathways between developmental and dark/starvation-induced senescence in Arabidopsis. *The Plant Journal* **42**:567-585. doi: 10.1111/j.1365-313X.2005.02399.x

Correa LG, Riano-Pachon DM, Schrago CG, dos Santos RV, Mueller-Roeber B, Vincentz M. 2008. The role of bZIP transcription factors in green plant evolution: adaptive features emerging from four founder genes. *PloS One* **3**: e2944. doi: 10.1371/journal.pone.0002944

Crozet P, Jammes F, Valot B, Ambard-Bretteville F, Nessler S, Hodges M, Vidal J, Thomas M. 2010. Cross-phosphorylation between Arabidopsis thaliana sucrose nonfermenting 1-related protein kinase 1 (AtSnRK1) and its activating kinase (AtSnAK) determines their catalytic activities. *Journal of Biological Chemistry* **285**: 12071-12077. doi: 10.1074/jbc.M109.079194

Deppmann CD, Alvania RS, Taparowsky EJ. 2006. Cross-species annotation of basic leucine zipper factor interactions: Insight into the evolution of closed interaction networks. *Molecular Biology and Evolution* **23**: 1480-92. doi: 10.1093/molbev/msl022

Dietrich K, Weltmeier F, Ehlert A, Weiste C, Stahl M, Harter K, Droege-Laser W. 2011. Heterodimers of the Arabidopsis transcription factors bZIP1 and bZIP53 reprogram amino acid metabolism during low energy stress. *The Plant Cell* **23**: 381-95. doi: 10.1105/tpc.110.075390

Ehlert A, Weltmeier F, Wang X, Mayer CS, Smeekens S, Vicente-Carbajosa J, Droege-Laser W. 2006. Two-hybrid protein-protein interaction analysis in Arabidopsis protoplasts: establishment of a

1071 heterodimerization map of group C and group S bZIP transcription factors. *The Plant Journal* **46**: 890-
1072 900. doi: 10.1111/j.1365-313X.2006.02731.x

1073 Emanuelle S, Hossain MI, Moller IE, Pedersen HL, van de Meene AM, Doblin MS, Koay A, Oakhill JS,
1074 Scott JW, Willats WG, Kemp BE, Bacic A, Gooley PR, Stapleton DI. 2015. SnRK1 from Arabidopsis
1075 thaliana is an atypical AMPK. *Plant Journal* **82:** 183-92. doi: 10.1111/tpj.12813

1076 Furihata T, Maruyama K, Fujita Y, Umezawa T, Yoshida R, Shinozaki K, Yamaguchi-Shinozaki K. 2006.
1077 Abscisic acid-dependent multisite phosphorylation regulates the activity of a transcription activator
1078 AREB1. *Proceedings of the National Academy of Sciences USA* **103**: 1988-93. doi:
1079 10.1073/pnas.0505667103

1080 Guo S, Vanderford NL, Stein R. 2010. Phosphorylation within the MafA N terminus regulates C-
1081 terminal dimerization and DNA binding. *The Journal of Biological Chemistry* **285***:* 12655-61. doi:
1082 10.1074/jbc.M110.105759

1083 Hanson J, Hanssen M, Wiese A, Hendriks MM, Smeekens S. 2008. The sucrose regulated transcription
1084 factor bZIP11 affects amino acid metabolism by regulating the expression of ASPARAGINE
1085 SYNTHETASE1 and PROLINE DEHYDROGENASE2. *The Plant Journal* **53**: 935-49. doi: 10.1111/j.1365-
1086 313X.2007.03385.x

1087 Hardie DG. 2007. AMP-activated/SNF1 protein kinases: conserved guardians of cellular energy.
1088 *Nature reviews Molecular Cell Biology* **8**: 774-85. doi: 10.1038/nrm2249

1089 Hardie DG, Ross FA, Hawley SA. 2012. AMPK: a nutrient and energy sensor that maintains energy
1090 homeostasis. *Nature reviews Molecular Cell Biology* **13**: 251-62. doi: 10.1038/nrm3311

1091 Harthill J, Meek SE, Morrice N, Peggie MW, Borch J, Wong BHC, MacKintosh C. 2006. Phosphorylation
1092 and 14-3-3 binding of Arabidopsis trehalose-phosphate synthase 5 in response to 2-deoxyglucose.
1093 The Plant Journal 47: 211-223. doi: 10.1111/j.1365-313X.2006.02780.x

1094 Hedbacker K, Carlson M. 2008. SNF1/AMPK pathways in yeast. *Frontiers in Bioscience* **13**: 2408-20

1095 Holmberg CI, Tran SE, Eriksson JE, Sistonen L. 2002. Multisite phosphorylation provides sophisticated
1096 regulation of transcription factors. *Trends in Biochemical Sciences* **27**: 619-27. doi: 10.1016/S0968-
1097 0004(02)02207-7

1098 Huang J Z, Huber S C. 2001. Phosphorylation of synthetic peptides by a CDPK and plant SNF1-related
1099 protein kinase. Influence of proline and basic amino acid residues at selected positions. *Plant and Cell*
1100 *Physiol*ogy. **42**: 1079-1087. doi: 10.1093/pcp/pce137

1101 Jakoby M, Weisshaar B, Droege-Laser W, Vicente-Carbajosa J, Tiedemann J, Kroj T, Parcy F. 2002.
1102 bZIP transcription factors in Arabidopsis. *Trends in Plant Science* **7**: 106-11. doi: 10.1016/S1360-
1103 1385(01)02223-3

1104 Kang SG, Price J, Lin PC, Hong JC, Jang JC. 2010. The arabidopsis bZIP1 transcription factor is involved
1105 in sugar signaling, protein networking, and DNA binding. *Molecular Plant* **3**: 361-73. doi:
1106 10.1093/mp/ssp115

1107 Kim JW, Tang QQ, Li X, Lane MD. 2007. Effect of phosphorylation and S-S bond-induced dimerization
1108 on DNA binding and transcriptional activation by C/EBPbeta. *Proceedings of the National Academy of*
1109 *Sciences USA* **104**: 1800-4. doi: 10.1073/pnas.0611137104

1110 Kirby J, Kavanagh TA. 2002. NAN fusions: a synthetic sialidase reporter gene as a sensitive and
1111 versatile partner for GUS. *The Plant Journal* **32**: 391-400. doi: 10.1046/j.1365-313X.2002.01422.x

1112 Kinoshita E, Kinoshita-Kikuta E, Takiyama K, Koike T. 2006. Phosphate-binding tag, a new tool to
1113 visualize phosphorylated proteins. *Mol Cell Proteomics* **5**: 749-57. doi: 10.1074/mcp.T500024-
1114 MCP200

1115 Kirchler T, Briesemeister S, Singer M, Schutze K, Keinath M, Kohlbacher O, Vicente-Carbajosa J, Teige
1116 M, Harter K, Chaban C. 2010. The role of phosphorylatable serine residues in the DNA-binding
1117 domain of Arabidopsis bZIP transcription factors. *European Journal of Cell Biology* **89**: 175-83. doi:
1118 10.1016/j.ejcb.2009.11.023

1119 Kleinboelting N, Huep G, Kloetgen A, Viehoever P, Weisshaar B. 2012. GABI-Kat SimpleSearch: new
1120 features of the Arabidopsis thaliana T-DNA mutant database. *Nucleic Acids Research* **40**: D1211-
1121 D1215. doi: 10.1093/nar/gkr1047

1122 Kulma A, Villadsen D, Campbell DG, Meek SEM, Harthill JE, Nielsen TH, MacKintosh C. 2004.
1123 Phosphorylation and 14-3-3 binding of Arabidopsis 6-phosphofructo-2-kinase/fructose-2,6-
1124 bisphosphatase. *The Plant Journal* **37**: 654-667. doi: 10.1111/j.1365-313X.2003.01992.x

1125 Kunz S, Pesquet E, Kleczkowski LA. 2014. Functional dissection of sugar signals affecting gene
1126 expression in Arabidopsis thaliana. *PloS One* **9**: e100312. doi: 10.1371/journal.pone.0100312

Lee S, Shuman JD, Guszczynski T, Sakchaisri K, Sebastian T, Copeland TD, Miller M, Cohen MS, Taunton J, Smart RC, Xiao Z, Yu LR, Veenstra TD, Johnson PF. 2010. RSK-mediated phosphorylation in the C/EBP leucine zipper regulates DNA binding, dimerization, and growth arrest activity. *Molecular and Cellular Biology* **30**: 2621-35. doi: 10.1128/MCB.00782-09

Ma J. 2012. Reprogramming of metabolism by the Arabidopsis thaliana bZIP11 transcription factor. PhD thesis, Utrecht University.

Ma J, Hanssen M, Lundgren K, Hernandez L, Delatte T, Ehlert A, Liu CM, Schluepmann H, Droege-Laser W, Moritz T, Smeekens S, Hanson J. 2011. The sucrose-regulated Arabidopsis transcription factor bZIP11 reprograms metabolism and regulates trehalose metabolism. *The New Phytologist* **191**: 733-45. doi: 10.1111/j.1469-8137.2011.03735.x

Matiolli CC, Tomaz JP, Duarte GT, Prado FM, Del Bem LE, Silveira AB, Gauer L, Correa LG, Drumond RD, Viana AJ, Di Mascio P, Meyer C, Vincentz M. 2011. The Arabidopsis bZIP gene AtbZIP63 is a sensitive integrator of transient abscisic acid and glucose signals. *Plant Physiology* **157**: 692-705. doi: 10.1104/pp.111.181743

Mayr B, Montminy M. 2001. Transcriptional regulation by the phosphorylation-dependent factor CREB. *Nature reviews Molecular Cell Biology* **2**: 599-609. doi: 10.1038/35085068

McGee SL, Hargreaves M. 2008. AMPK and transcriptional regulation. *Frontiers in Bioscience* **13**: 3022-33. doi: 10.2741/2907

Motohashi H, O'Connor T, Katsuoka F, Engel JD, Yamamoto M. 2002. Integration and diversity of the regulatory network composed of Maf and CNC families of transcription factors. *Gene* **294**: 1-12. doi: 10.1016/S0378-1119(02)00788-6

Naegele T, Mair A, Sun X, Fragner L, Teige M, Weckwerth W. 2014. Solving the differential biochemical Jacobian from metabolomics covariance data. *PLoS One* **9**: e92299. doi: 10.1371/journal.pone.0092299

Nukarinen E, Nägele T, Pedrotti L, Mair A, Teige M, Baena-Gonzalez E, Dröge-Laser W, Weckwerth W. 2015. Dynamic phosphoproteomics reveals the antagonistic control of SnRK1 on TOR signaling. Submitted for publication.

Oh SA, Lee SY, Chung IK, Lee CH, Nam HG. 1996. A senescence-associated gene of Arabidopsis thaliana is distinctively regulated during natural and artificially induced leaf senescence. *Plant Molecular Biology* **30**: 739-754. doi: 10.1007/BF00019008

1157 Para A, Li Y, Marshall-Colón A, Varala K, Francoeur NJ, Moran TM, Edwards MB, Hackley C, Bargmann
1158 BO, Birnbaum KD, McCombie WR, Krouk G, Coruzzi GM. 2014. Hit-and-run transcriptional control by
1159 bZIP1 mediates rapid nutrient signaling in Arabidopsis. *Proc Natl Acad Sci U S A* **111:** 10371-6. doi:
1160 10.1073/pnas.1404657111

1161 Polge C, Thomas M. 2007. SNF1/AMPK/SnRK1 kinases, global regulators at the heart of energy
1162 control? *Trends in Plant Science* **12**: 20-8. doi: 10.1016/j.tplants.2006.11.005

1163 Porra RJ, Tompson WA, Kriedemann PE. 1989. Determination of accurate extinction coefficients and
1164 simultaneous equations for assaying chlorophylls a and b extracted with four different solvents:
1165 verification of the concentration of chlorophyll standards by atomic absorption spectroscopy.
1166 *Biochimica et Biophysica Acta* **975**: 384-394. doi: 10.1016/S0005-2728(89)80347-0

1167 Reinke AW, Baek J, Ashenberg O, Keating AE. 2013. Networks of bZIP protein-protein interactions
1168 diversified over a billion years of evolution. *Science* **340**: 730-4. doi: 10.1126/science.1233465

1169 Rodrigues-Pousada C, Menezes RA, Pimentel C. 2010. The Yap family and its role in stress response.
1170 *Yeast* **27**: 245-58. doi: 10.1002/yea.1752

1171 Ramakers C, Ruijter JM, Deprez RH, Moorman AF. 2003. Assumption-free analysis of quantitative
1172 real-time polymerase chain reaction (PCR) data. *Neuroscience letters* **339**: 62-6. doi: 10.1016/S0304-
1173 3940(02)01423-4

1174 Saeed AI, Sharov V, White J, Li J, Liang W, Bhagabati N, Braisted J, Klapa M, Currier T, Thiagarajan M*,*
1175 *et al.* 2003. TM4: a free, open-source system for microarray data management and analysis.
1176 *BioTechniques* **34**: 374-8.

1177 Schindelin J, Arganda-Carreras I, Frise E, Kaynig V, Longair M, Pietzsch T, Preibisch S, Rueden C,
1178 Saalfeld S, Schmid B*, et al.* 2012. Fiji: an open-source platform for biological-image analysis. *Nature*
1179 *Methods* **9**: 676-82. doi: 10.1038/nmeth.2019

1180 Schuetze K, Harter K, Chaban C. 2008. Post-translational regulation of plant bZIP factors. *Trends in*
1181 *Plant Science* **13**: 247-55. doi: 10.1016/j.tplants.2008.03.002

1182 Sugden C, Donaghy P, Halford NG, Hardie DG. 1999. Two SNF1-Related Protein Kinases from Spinach
1183 Leaf Phosphorylate and Inactivate 3-Hydroxy-3-Methylglutaryl-Coenzyme A Reductase, Nitrate
1184 Reductase, and Sucrose Phosphate Synthase in Vitro. *Plant Physiology* **120**: 257-274. doi:
1185 10.1104/pp.120.1.257

1186 Sussman MR, Amasino RM, Young JC, Krysan PJ, Austin-Phillips S. 2000. The Arabidopsis knockout
1187 facility at the University of Wisconsin-Madison. *Plant Physiology* **124**: 1465-7. doi:
1188 10.1104/pp.124.4.1465

1189 Szabados L, Savouré A. 2010. Proline: a multifunctional amino acid. *Trends Plant Sci.* **15:** 89-97. doi:
1190 10.1016/j.tplants

1191 Szal B, Podgórska A. 2012. The role of mitochondria in leaf nitrogen metabolism. *Plant Cell Environ*.
1192 **35:** 1756-68. doi: 10.1111/j.

1193 Taus T, Kocher T, Pichler P, Paschke C, Schmidt A, Henrich C, Mechtler K. 2011. Universal and
1194 confident phosphorylation site localization using phosphoRS. *Journal of Proteome Research* **10**: 5354-
1195 62. doi: 10.1021/pr200611n

1196 Tome F, Naegele T, Adamo M, Garg A, Marco-Llorca C, Nukarinen E, Pedrotti L, Peviani A, Simeunovic
1197 A, Tatkiewicz A, Tomar M, Gamm M. 2014. The low energy signaling network. *Frontiers in plant*
1198 *science* **5**: 353. doi: 10.3389/fpls.2014.00353

1199 Tsukada J, Yoshida Y, Kominato Y, Auron PE. 2011. The CCAAT/enhancer (C/EBP) family of basic-
1200 leucine zipper (bZIP) transcription factors is a multifaceted highly-regulated system for gene
1201 regulation. *Cytokine* **54**: 6-19. doi: 10.1016/j.cyto.2010.12.019

1202 Umezawa T, Sugiyama N, Takahashi F, Anderson JC, Ishihama Y, Peck SC, Shinozaki K. 2013. Genetics
1203 and phosphoproteomics reveal a protein phosphorylation network in the abscisic acid signaling
1204 pathway in Arabidopsis thaliana. *Science Signaling* **6**: rs8. doi: 10.1126/scisignal.2003509

1205 Usadel B, Blasing OE, Gibon Y, Retzlaff K, Hohne M, Gunther M, Stitt M. 2008. Global transcript levels
1206 respond to small changes of the carbon status during progressive exhaustion of carbohydrates in
1207 Arabidopsis rosettes. *Plant Physiology* **146**: 1834-61. doi: 10.1104/pp.107.115592

1208 van der Graaff E, Schwacke R, Schneider A, Desimone M, Flügge UI, Kunze R. 2006. Transcription
1209 Analysis of Arabidopsis Membrane Transporters and Hormone Pathways during Developmental and
1210 Induced Leaf Senescence. *Plant Physiology* **141**:776-92. doi:10.1104/pp.106.079293

1211 Veerabagu M, Kirchler T, Elgass K, Stadelhofer B, Stahl M, Harter K, Mira-Rodado V, Chaban C. 2014.
1212 The Interaction of the Arabidopsis Response Regulator ARR18 with bZIP63 Mediates the Regulation
1213 of PROLINE DEHYDROGENASE Expression. *Molecular Plant* **7**: 1560-77. doi: 10.1093/mp/ssu074

1214 Waadt R, Schmidt LK, Lohse M, Hashimoto K, Bock R, Kudla J. 2008. Multicolor bimolecular
1215 fluorescence complementation reveals simultaneous formation of alternative CBL/CIPK complexes in
1216 planta. *The Plant Journal* **56**: 505-16. doi: 10.1111/j.1365-313X.2008.03612.x

1217 Walter M, Chaban C, Schutze K, Batistic O, Weckermann K, Nake C, Blazevic D, Grefen C, Schumacher
1218 K, Oecking C, Harter K, Kudla J. 2004. Visualization of protein interactions in living plant cells using
1219 bimolecular fluorescence complementation. *The Plant Journal* **40**: 428-38. doi: 10.1111/j.1365-
1220 313X.2004.02219.x

1221 Weiste C, Dröge-Laser W. 2014. The Arabidopsis transcription factor bZIP11 activates auxin-mediated
1222 transcription by recruiting the histone acetylation machinery. *Nat Commun*. **5:** 3883. doi:
1223 10.1038/ncomms4883.

1224 Yoo SD, Cho YH, Sheen J. 2007. Arabidopsis mesophyll protoplasts: a versatile cell system for
1225 transient gene expression analysis. *Nature Protocols* **2**: 1565-72. doi: 10.1038/nprot.2007.199

1226 Yoshida S, Ito M, Watanabe A. 2001. Isolation and RNA Gel Blot Analysis of Genes that Could Serve as
1227 Potential Molecular Markers for Leaf Senescence in Arabidopsis thaliana. *Plant Cell Physiology*
1228 **42**:170-178. doi: 10.1093/pcp/pce021

1229

Figures Legends and tables

Figure 1. *bZIP63* mutants have a phenotype in dark-induced senescence

(A) and **(B)** Dark-induced senescence phenotype of 4.5 week-old soil grown plants. Comparison of a *bzip63* line in the Wassilewskya (Ws-2), and two bZIP63 ox lines in the Columbia (Col-0) background, after nine days in darkness. **(A)** Representative leaf series. **(B)** Box-and-whiskers plot of the total green leaf area of eight biological replicates as determined with ImageJ. See Figure 1 – figure supplement 1 for molecular characterization of the bZIP63 mutant lines, Figure 1 – figure supplement 2 for a scheme of the determination of the green leaf area, quantitative chlorophyll measurements, controls and green area of individual leaves, Figure1 – source data 1 for the used ImageJ macro, and Figure 1 - figure supplement 3 for expression of senescence marker genes in wt and *bzip63*. **(C)** and **(D)** Sugar rescue of the dark-induced senescence phenotype. Seedlings were grown for 12 days on ½ MS agar containing 0.5% sucrose transferred to ½ MS agar containing 0% or 2% glucose and grown for another six days before incubation in the dark for seven days. **(A)** Representative seedlings. **(B)** Box-and whiskers plot of the chlorophyll content of 8 seedlings per line and condition. See Figure 1 – figure supplement 4 for pictures and chlorophyll content of seedlings before dark incubation.
P-values from T-tests between mutants and wt < 0.05, < 0.01, and < 0.001 are indicated by *, **, and ***, respectively.

Figure 2. *bZIP63* mutants have an altered primary metabolism

Metabolic phenotype of five week-old soil grown plants after 6h light (L) and extended night (E). Log-2 fold changes of metabolite levels in ko and ox compared to their respective wt, displayed on a simplified map of the central primary metabolism. Values are means of five biological replicates. P-values from T-tests between mutants and wt < 0.05, <0.01, and < 0.001 are indicated by *, ** and ***, respectively. For more details including mean values and SD see Figure 2 – figure supplement 1 and Figure 2 – source data 1.

Figure 3. bZIP63 is phosphorylated at multiple sites in an energy-dependent manner in vivo

(A) 2D gel western blots (αGFP) of lambda phosphatase (λPP)-treated protein extracts from adult soil-grown plants expressing bZIP63-GFP (ox#3). **(B)** Phos-tag gel western blots showing the in vivo phosphorylation state of bZIP63 in seedlings after 6h extended night in the presence (+) or absence (–) of 1% sucrose and in five week-old soil-grown plants after 6h light (L) or extended night (EN). Plants either expressed 35S::bZIP63-GFP (ox#3) or a genomic fragment of bZIP63 (GY11) with a YFP-tag. Recombinant bZIP63-YFP was used as an nonphosphorylated control. Numbered arrowheads on the right mark the position of each observed bZIP63 band for easy reference with other figures (see Figure 3 – figure supplement 1 for a comparative image of all Phos-tag western blots). For more information on the genomic line see Figure 7 and Figure 7 – figure supplement 1. **(C)** Identification of in vivo phosphorylation sites by immunoprecipitation (IP) and tandem mass spectrometry (MS/MS). An exemplary western blot of the IP is shown. The scheme at the bottom shows the positions of the identified in vivo phosphorylation sites and the total sequence coverage reached with each proteolytic enzyme (grey bars). Asterisks mark the identification of a phospho-site. For more information on samples and (phospho-) peptides see Figure 2 – figure supplement 2.

IEF, isoelectric focusing; CBB, coomassie brilliant blue; BD, basic domain; ZIP, leucine zipper; LTQ, linear ion trap quadrupole; chym., chymotrypsin

Figure 4. Several different kinases can phosphorylate bZIP63

(A) In-gel kinase assay with a root protein extract from hydroponically grown wild type plant and bZIP63 as substrate. Arrows indicate the positions of potential bZIP63 kinases. **(B)** Scheme of the kinase identification process. **(C)** In-gel kinase assay with samples from affinity purification of a root protein extract with bZIP63 and bZIP63 as a substrate (left) and a list of catalytic and regulatory (*) kinase subunits identified with high confidence (right). The list also contains the gene identifier (AGI), molecular weight (MW), and number of samples in which the protein was found. For controls and a

list of all identified kinases and kinase peptides see Figure 4 – figure supplement 1 and 2 and Figure 4 – source data 1.

CBB, Coomassie brilliant blue

Figure 5. The SnRK1 kinase AKIN10 phosphorylates bZIP63 and interacts with bZIP63 in vivo

(A) In-gel kinase assay with protein extracts from wt and *akin10* plants and bZIP63 as a substrate (top), western blot against AKIN10 (αAKIN10, middle), and Coomassie brilliant blue stain (CBB, bottom). Asterisks mark the position of AKIN10. For characterization of the akin10 line see Figure 5 – figure supplement 1-3. **(B)** In vitro kinase assay with recombinant AKIN10/AKIN11 and bZIP63 as a substrate. See also Figure 5 – figure supplement 4 for kinase assays including the SnRK1 upstream kinase SnAK2. **(C)** and **(D)** Interaction of SnRK1 subunits with bZIP63. Homo-dimerization of bZIP63 was used as a positive control. **(C)** Yeast two-hybrid (Y2H) assay with auto-activation in grey and interaction with bZIP63 in blue. Bars represent means ± SD of eight biological replicates. For Y2H with SnK1 β1 and β2 see Figure 5 – figure supplement 6. **(D)** Laser scanning microscopy images of bimolecular fluorescence complementation (BiFC) in transiently transformed N. tabacum leaves (top). Arrowheads indicate the position of the nucleus. Size bar = 20µm. Expression of the fusion proteins was verified by western blots (αHA, αFlag, bottom). **(E)** Phos-tag gel western blots showing the in vivo phosphorylation state of bZIP63 in 4-5 week-old soil grown plants after 6h light (L) or extended night (EN) in the presence and absence of AKIN10 alone or both AKIN10 and AKIN11. Plants overexpressing bZIP63-YFP in the *akin10* line were compared to plants overexpressing bZIP63-GFP in the wt background (ox#3) (left). Additionally, AKIN10 and AKIN11 were knocked down (*akin10/11*) by virus-induced gene silencing (VIGS) in plants expressing genomic bZIP63 with a YFP-tag (GY9 line). See Figure 5 – figure supplement 7 for images and a western blots of the VIGS plants. Recombinant bZIP63-YFP was used as a nonphosphorylated control. Numbered arrowheads on the right mark the position of each observed bZIP63 band for easy reference with other figures (see Figure 3 – figure

supplement 1 for a comparative image of all Phos-tag western blots). A comparison of the phosphorylation state of bZIP63 in seedlings can be found in Figure 5 – figure supplement 6.

Figure 6. AKIN10 targets three highly conserved and functionally important serine residues in bZIP63

(A) In vitro kinase assay of wt and S/A mutants of GST-tagged bZIP63 with AKIN10. Positions of full length (FL) and N-terminal fragments of bZIP63 are marked by black arrows. The scheme on the right shows the position of the in vivo phosphorylation sites and the in vitro target sites of AKIN10 (red asterisk) on bZIP63. See Figure 6 – figure supplement 1 and 2 for controls and Phos-tag gel of kinase assays, respectively. **(B)** Conservation of phosphorylation sites in bZIP63. Sequences of bZIP63 homologues from eight species were aligned with ClustalΩ. The scheme on top indicates the positions of the in vivo phosphorylation and AKIN10 target sites on bZIP63. The histogram below shows the sequence identity (red/black) and similarity (grey) to A. thaliana bZIP63. Red bars represent the in vivo phosphorylation sites. Below, the alignment of the sequence surrounding the AKIN10 target sites and the SnRK1 consensus motif (Huang and Huber, 2001) are shown. The grey/black shading indicates the degree of conservation, phosphorylation sites are in red. For alignment of non-AKIN10 target sites and full sequence alignment see Figure 6 – figure supplement 3, for sequences in fasta format see Figure 6 – source data 1. **(C)** Promoter activation assays in protoplasts with an ASN1/ProDH promoter-driven GUS reporter. Activation by bZIP63 wt and S/A mutants without (grey) or with (blue) co-transformation of AKIN10 is shown. Bars are means ± SD of 4 biological replicates, given in % of the activity of wt bZIP63 with AKIN10. Horizontal dashed lines indicate the signal in the control without bZIP63. Letters indicate significant differences as determined by ANOVA and pairwise T-testing ($P < 0.05$). See Figure 6 – figure supplement 4 for a western blot control.

CBB, Coomassie brilliant blue.

Figure 7. The *bzip63* phenotype can be complemented by wt bZIP63, but not by bZIP63 harboring S/A mutantions of the AKIN10 target sites

(A) Genomic complementation constructs. Exons are green, introns black. See Figure 7 – figure supplement 1 for characterization of the complementation lines. **(B)** Phos-tag gel western blots (αGFP) showing the in vivo phosphorylation state of bZIP63 in the complementation lines after 6h light (L) or extended night (EN) in five week-old soil-grown plants. Recombinant bZIP63-YFP was used as nonphosphorylated control. Numbered arrowheads on the right mark the position of each observed bZIP63 band for easy reference with other figures (see Figure 3 – figure supplement 1 for a comparative image of all Phos-tag western blots). **(C)** and **(D)** Dark-induced senescence phenotype of 4.5 week-old soil-grown plants after nine days in darkness. **(C)** Leaves 3 – 7 of one representative plant per line. **(D)** Box-and-whiskers plot of the total green leaf area of eight biological replicates. Letters indicate significant differences as determined by ANOVA and pairwise T-testing ($P < 0.05$). See Figure 7 – figure supplement 2 for untreated plants and green leaf area of individual leaves. **(E)** and **(F)** Metabolite profile. **(E)** Hierarchical clustering of log-2 fold changes of metabolite concentrations compared to wt. Values are means of five biological replicates. **(F)** Principal component analysis (PCA). PC1 is plotted against PC2. The proportion of variance in % is indicated. The red line surrounds *bzip63* and GAY samples, the green line wt, GY, and ox#3 samples. For relative metabolite concentrations and PCA loading see Figure 7 – source data 1. **(G)** Relative expression of potential bZIP63 target genes in five week-old plants during early extended night as determined by RT-qPCR. Values are means ± SD of four biological replicates and are given as fold change compared to Ws-2 at 0h (left) or 4h (right). P-values from T-tests between mutants and wt < 0.05, <0.01, and < 0.001 are indicated by *, ** and ***, respectively. Letters indicate significant differences as determined by ANOVA and pairwise T-testing ($P < 0.05$).

CBB, Coomassie brilliant blue

Figure 8. AKIN10-mediated phosphorylation of bZIP63 promotes its dimerization

(A) and **(B)** Protoplast two-hybrid (P2H) assays. **(A)** Interaction of bZIP63 fused to the Gal4-AD (activation domain) with bZIP63, bZIP1, and bZIP11 fused to the Gal4-BD (binding domain) without and with co-transformation of AKIN10. Bars represent the mean normalized GUS activity ± SD of 3-4 biological replicates. P-values from T-tests < 0.05 and < 0.01 are indicated by * and **, respectively. **(B)** Interaction of AD-bZIP63 (left) or AD-bZIP11 (right) with wt and S/A mutants of BD-bZIP63 without and with co-transformation of AKIN10. Values are given in % of the signal with wt bZIP63 and AKIN10. Letters indicate significant differences as determined by ANOVA and pairwise T-testing (P < 0.05). For western blots for (A) and (B) see Figure 8 – figure supplement 1. **(C)** In vitro kinase assay of bZIP63, 1, 2, 11, 44, and 53 with AKIN10 and the SnRK1 upstream kinase SnAK2. For a kinase assay with the bZIPs and alone SnAK2 see Figure 8 – figure supplement 2. **(D)**. Phos-tag gel western blots (αGFP) showing the in vivo phosphorylation state of S29 in bZIP63 after 6h light (L) or extended night (EN). Five week-old soil-grown plants of two genomic *bzip63* complementation lines harboring different S/A mutations were used. In line GAY14 (left) none of the AKIN10 target sites (S29/294/300) can be phosphorylated, while in the S294/300A (right) line S29 can still be phosphorylated. Numbered arrowheads on the right mark the position of each observed bZIP63 band for easy reference with other figures (see Figure 3 – figure supplement 1 for a comparative image of all Phos-tag western blots). The likely phosphorylation state of the bands in the western blot is shown on the right. X stands for one of the non-mutated serines (59, 102, 160, or 261).

CBB, Coomassie brilliant blue

Figure 9 – Phosphorylation of bZIP63 shifts its dimerization preferences

(A) Multi-color bimolecular fluorescence complementation (BiFC) in transiently transformed N. tabacum leaves to test the effect of bZIP63 phosphorylation on its dimerization preference. A cassette containing bZIP63 (wt or S29/294/300A), bZIP11, and bZIP1 – tagged with the C-terminal moiety of CFP and the N-terminal moieties of CFP and VENUS, respectively – was co-transformed

with mCherry-tagged AKIN10. CFP (bZIP63-11) and VENUS (bZIP63-1) fluorescence was detected on a confocal laser scanning microscope and quantified for nuclei showing co-expression of AKIN10. Top: scheme of the multi-color BiFC construct and principle. Bottom center: representative microscopy pictures. Size bar = 50µm. Bottom right: Box-and-whiskers plot of the VENUS/CFP ratio of 115-118 nuclei, normalized to the median of the S29/294/300A bZIP63 construct. T-test p-value was < 0.001, as indicated by ***. **(B)** Model of the regulation of bZIP63 dimerization and activity by AKIN10. Energy deprivation triggers activation of AKIN10, which phosphorylates S29 on bZIP63. This leads to increased formation of specific bZIP63 dimers and altered expression of dimer specific genes.

Supplemental data

Figure 1 – figure supplement 1. Molecular characterization of the *bzip63* line and expression of bZIP63 in the ko and ox lines

(A) Scheme of the genomic locus (top) and the protein (bottom) of bZIP63. UTRs and exons are shown in grey and green, respectively. The position of the T-DNA in the first exon, as well as the position of primers used for PCR and RT-qPCR are indicated. The position of the T-DNA insertion was determined by sequencing of the PCR product in **(C)**. **(B)** PCR on genomic DNA using primers fw and rv to show the homozygous T-DNA insertion in the *bzip63* line. **(C)** PCR on genomic DNA from *bzip63* plants using primers fw, rv, LB, and RB to determine the localization and orientation of the T-DNA insertion. **(D)** and **(E)** Expression of *bZIP63* in wt, bZIP63 ko and ox plants. RT-qPCR of bZIP63 in five week-old plants after 6h of light (L) or extended night (EN) using primers fwq and rvq. Bars represent means ± SD of 5 biological replicates and are given as fold change to Ws-2 in L. **(F)** Pictures of five week-old wt and mutant plants grown in a 12h light/12h dark cycle.

Figure 1 – figure supplement 2. Phenotype of *bZIP63* mutants in dark-induced senescence

Dark-induced senescence phenotype of 4.5 week-old soil-grown plants. Comparison of a *bzip63* line in the Wassilewskya (Ws-2) and two bZIP63 ox lines in the Columbia (Col-0) background. **(A)** Scheme of the workflow to determine the green leaf area. A detailed description and the ImageJ macro can be found in the methods section and in Figure 1 – source data 1. **(B)** Total chlorophyll (chl) content in µg/mg freshweight (FW) of plants before and after 9 days in darkness. Bars represent the mean ± SD of six biological replicates. **(C)** Representative leaf series of plants before dark treatment. **(D)** Barplot of the total green leaf area of the rosette before darkness. Values are the mean ± SD of four biological replicates. **(E)** Dark-induced senescence timecourse. **(F)** Dotplot of the green leaf area of individual leaves after nine days in darkness.

P-values from T-tests between mutants wt < 0.05, <0.01, and < 0.001 are indicated by *, ** and ***, respectively.

Figure 1 – figure supplement 3. Expression of senescence marker genes during prolonged darkness

Chlorophyll content **(A)** and expression of senescence marker genes **(B)** in 4.5 week-old soil-grown wt and *bzip63* plants after 0-4 days of darkness. Bars represent the mean ± SD of three biological replicates. Letters indicate significant differences as determined by ANOVA and pairwise T-testing ($P < 0.05$). **(A)** Total rosettes were harvested at the indicated time points and the chlorophyll content in µg/mg FW was determined. **(B)** From the same plants, expression of the photosynthetic marker gene *CAB2* (CHLOROPHYLL A/B-BINDING PROTEIN 2) and three senescence marker genes (Dietrich et al., 2011) was determined by RT-qPCR. The expression is shown relative to wt at day 0 (before dark incubation). *SEN1* (SENESCENCE 1) and *SAG103* (SENESCENCE-ASSOCIATED GENE 103) are known to be strongly induced by dark-induced senescence, while YLS3 (YELLOW-LEAF-SPECIFIC 3) is induced by natural, but not by dark-induced senescence (Oh et al., 1996; van der Graaff et al., 2006, Yoshida et al., 2001).

Figure 1 – figure supplement 4. Effect of sugar on bZIP63 mutants in light

Controls for the sugar rescue of the dark-induced senescence phenotype shown in Figure 1C and 1D. Seedlings were grown for 12 days on ½ MS agar containing 0.5% sucrose transferred to ½ MS agar containing 0% or 2% glucose and grown for another six days in a 12h light/ 12h dark cycle. **(A)** Representative seedlings. **(B)** Box-and whiskers plot of the chlorophyll content of eight seedlings. T-tests revealed no significant differences between chlorophyll content in wt and mutants.

Figure 1 – source data 1. ImageJ macro for determination of leaf area and green leaf area

Figure 2 – figure supplement 1. Metabolic changes in *bZIP63* ko and ox plants

Table of the metabolite levels in *bzip63* and ox#3 compared to their respective wt shown in Figure 2. Values are the log-2 transformed means of five biological replicates. P-values from T-tests between mutants and wt < 0.05, <0.01, and < 0.001 are indicated by *, ** and ***, respectively. The color

gradient indicates increased (red) or decreased (blue) metabolite levels in the mutant. For relative changes between mutant and wt including the SD and p-values from T-tests see Figure 2 – source data 1.

Figure 2 – source data 1. Excel table of relative metabolite levels in *bZIP63* mutants and p-values from T-tests

Table of relative metabolite levels in Ws-2, *bzip63*, Col-0 and ox#3 after 6h in light or extended night, which were used to calculate the log2-fold changes shown in Figures 1C and see Figure 1 – figure supplement 2. Mean values and SD of five biological replicates are given as fold changes to the corresponding wt. P-values from T-tests between wt and mutant are listed.

Figure 3 – figure supplement 1. Comparison of Phos-tag western blots from different figures.

For better comparison of Phos-tag western blots (αGFP) shown in different figures of this manuscript, all Phos-tag western blots were aligned here. In case more than one image of the same lines and conditions exists, only one is shown. The bands were labeled with numbers from 1 to 8, where 1 is the presumably non-phosphorylated state and 8 is the highest phosphorylated form. The two semicircles to the right of each blot indicate the presence of a band at this position in each of the two lanes, with the shade corresponding to the intensity of the band (light grey for weak bands, dark for strong bands). The figures and figures supplements (S) in which the blots are shown are given below.

Figure 3 – figure supplement 2. Overview over identified phospho-peptides of bZIP63

(A) Sample overview, summarizing for each of the five independent experiments: plant material, growth conditions, the number of samples digested with each proteolytic enzyme, and the identified phospho-sites (Y). Experiments 1 to 3 were measured with a linear ion trap quadrupole (LTQ), experiments 4 and 5 with an LTQ-Oribtrap (OT). **(B)** Phospho-peptide identification frequencies for

the proteolytic enzymes. The barplot shows, for each proteolytic enzyme, the number of samples in which an in vivo phosphorylation-site was covered (black or red) or not covered (grey), and how often a phospho-peptide was identified (red). **(C)** Graph showing the total protein coverage from all experiments, as well as the protein coverage that was achieved with each of the four proteolytic enzymes in % and as a sequence. Parts of the sequence that were covered and not covered are shown in black and light grey, respectively. Identified phospho-serines are red. Below the coverage, all identified phospho-peptides are listed and the instrument used for identification is specified (LTQ or OT). The numbers on top indicate the position in the protein sequence. The scheme below indicates the position of the conserved bZIP domain (green), including the basic domain (dark green), and the N- and C-terminal extensions (yellow).

L, light; EN, extended night; D, dark; suc, sucrose; T, trypsin; C, chymotrypsin; L, LysC; S, subtilisin; NLS, nuclear localization signal

Figure 4 – figure supplement 1. Auto-phosphorylation from the protein extracts is negligible in in-gel kinase assays

In-gel kinase assay with samples from affinity purification of a root protein extract from hydroponically grown plants with bZIP63. Comparison of a gel with bZIP63 as a substrate (top, see also Figure 4C) and a gel without substrate (middle). A Coomassie brilliant blue (CBB) stained gel is shown at the bottom.

Figure 4 – figure supplement 2. Overview over the kinases identified by LC-MS/MS after affinity purification with bZIP63

References for Figure 4 – figure supplement 2

Bayer RG, Stael S, Rocha AG, Mair A, Vothknecht UC, Teige M. 2012. Chloroplast-localized protein kinases: a step forward towards a complete inventory. *Journal of Experimental Botany* **63**: 1713-23. doi: 10.1093/jxb/err377

Benetka W, Mehlmer N, Maurer-Stroh S, Sammer M, Koranda M, Neumuller R, Betschinger J, Knoblich JA, Teige M, Eisenhaber F. 2008. Experimental testing of predicted myristoylation targets involved in asymmetric cell division and calcium-dependent signalling. *Cell Cycle* **7**: 3709-19. doi: 10.4161/cc.7.23.7176

Berendzen KW, Bohmer M, Wallmeroth N, Peter S, Vesic M, Zhou Y, Tiesler FK, Schleifenbaum F, Harter K. 2012. Screening for in planta protein-protein interactions combining bimolecular fluorescence complementation with flow cytometry. *Plant Methods* **8**: 25. doi: 10.1186/1746-4811-8-25

Bitrian M, Roodbarkelari F, Horvath M, Koncz C. 2011. BAC-recombineering for studying plant gene regulation: developmental control and cellular localization of SnRK1 kinase subunits. *The Plant Journal* **65**: 829-42. doi: 10.1111/j.1365-313X.2010.04462.x

Boruc J, Mylle E, Duda M, De Clercq R, Rombauts S, Geelen D, Hilson P, Inze D, Van Damme D,.Russinova E. 2010. Systematic localization of the Arabidopsis core cell cycle proteins reveals novel cell division complexes. *Plant Physiology* **152**: 553-65. doi: 10.1104/pp.109.148643

Boudsocq M, Willmann MR, McCormack M, Lee H, Shan L, He P, Bush J, Cheng SH, Sheen J. 2010. Differential innate immune signalling via Ca(2+) sensor protein kinases. *Nature* **464**: 418-22. doi: 10.1038/nature08794

Dammann C, Ichida A, Hong B, Romanowsky SM, Hrabak EM, Harmon AC, Pickard BG, Harper JF. 2003. Subcellular targeting of nine calcium-dependent protein kinase isoforms from Arabidopsis. *Plant Physiology* **132**: 1840-48. doi: 10.1104/pp.103.020008

Dong CH, Rivarola M, Resnick JS, Maggin BD, Chang C. 2008. Subcellular co-localization of Arabidopsis RTE1 and ETR1 supports a regulatory role for RTE1 in ETR1 ethylene signaling. *The Plant Journal* **53**: 275-86. doi: 10.1111/j.1365-313X.2007.03339.x

Fragoso S, Espindola L, Paez-Valencia J, Gamboa A, Camacho Y, Martinez-Barajas E, Coello P. 2009. SnRK1 isoforms AKIN10 and AKIN11 are differentially regulated in Arabidopsis plants under phosphate starvation. *Plant Physiology* **149**: 1906-16. doi: 10.1104/pp.108.133298

Gissot L, Polge C, Jossier M, Girin T, Bouly JP, Kreis M, Thomas M. 2006. AKINbetagamma contributes to SnRK1 heterotrimeric complexes and interacts with two proteins implicated in plant pathogen resistance through its KIS/GBD sequence. *Plant Physiology* **142**: 931-44. doi: 10.1104/pp.106.087718

Kitsios G, Alexiou KG, Bush M, Shaw P, Doonan JH. 2008. A cyclin-dependent protein kinase, CDKC2, colocalizes with and modulates the distribution of spliceosomal components in Arabidopsis. *The Plant Journal* **54**: 220-35. doi: 10.1111/j.1365-313X.2008.03414.x

Koroleva OA, Tomlinson ML, Leader D, Shaw P, Doonan JH. 2005. High-throughput protein localization in Arabidopsis using Agrobacterium-mediated transient expression of GFP-ORF fusions. *The Plant Journal* **41**: 162-74. doi: 10.1111/j.1365-313X.2004.02281.x

Lee JY, Taoka K, Yoo BC, Ben-Nissan G, Kim DJ, Lucas WJ. 2005. Plasmodesmal-associated protein kinase in tobacco and Arabidopsis recognizes a subset of non-cell-autonomous proteins. *The Plant Cell* **17**: 2817-31. doi: 10.1105/tpc.105.034330

Mehlmer N, Wurzinger B, Stael S, Hofmann-Rodrigues D, Csaszar E, Pfister B, Bayer R, Teige M. 2010. The Ca(2+) -dependent protein kinase CPK3 is required for MAPK-independent salt-stress acclimation in Arabidopsis. *The Plant Journal* **63**: 484-98. doi: 10.1111/j.1365-313X.2010.04257.x

Padmanaban S, Chanroj S, Kwak JM, Li X, Ward JM, Sze H. 2007. Participation of endomembrane cation/H+ exchanger AtCHX20 in osmoregulation of guard cells. *Plant Physiology* **144**: 82-93. doi: 10.1104/pp.106.092155

Park HJ, Ding L, Dai M, Lin R, Wang H. 2008. Multisite phosphorylation of Arabidopsis HFR1 by casein kinase II and a plausible role in regulating its degradation rate. *The Journal of biological chemistry* **283**: 23264-73. doi: 10.1074/jbc.M801720200

Perales M, Portoles S, Mas P. 2006. The proteasome-dependent degradation of CKB4 is regulated by the Arabidopsis biological clock. *The Plant Journal* **46**: 849-60. doi: 10.1111/j.1365-313X.2006.02744.x

Pierre M, Traverso JA, Boisson B, Domenichini S, Bouchez D, Giglione C, Meinnel T. 2007. N-myristoylation regulates the SnRK1 pathway in Arabidopsis. *The Plant Cell* **19**: 2804-21. doi: 10.1105/tpc.107.051870

Rodriguez Milla MA, Uno Y, Chang IF, Townsend J, Maher EA, Quilici D, Cushman JC. 2006. A novel yeast two-hybrid approach to identify CDPK substrates: characterization of the interaction between AtCPK11 and AtDi19, a nuclear zinc finger protein. *FEBS Letters* **580**: 904-11. doi: 10.1016/j.febslet.2006.01.013

Salinas P, Fuentes D, Vidal E, Jordana X, Echeverria M, Holuigue L. 2006. An extensive survey of CK2 alpha and beta subunits in Arabidopsis: multiple isoforms exhibit differential subcellular localization. *Plant Cell Physiology* **47**: 1295-1308. doi: 10.1093/pcp/pcj100

Zhu SY, Yu XC, Wang XJ, Zhao R, Li Y, Fan RC, Shang Y, Du SY, Wang XF, Wu FQ, Xu YH, Zhang XY, Zhang DP. 2007. Two calcium-dependent protein kinases, CPK4 and CPK11, regulate abscisic acid signal transduction in Arabidopsis. *The Plant Cell* **19**: 3019-36. doi: 10.1105/tpc.107.050666

Figure 4 – source data 1. Excel table containing a detailed overview over the identified kinases and analyzed samples as well as all peptides found for the kinase subunit

The tab "kinase overview" contains a table showing in which samples each kinase subunit was identified, including the number of peptides, proteotypic peptides, MASCOT (Matrix Science) score, and expected molecular weight. The other tabs list all peptides found for the kinase subunits in each sample and state whether the peptide is proteotypic (Y) or not.

Figure 5 – figure supplement 1. Molecular characterization of the *akin10* line

(A) Scheme of the genomic locus and protein of *AKIN10* (top) and *IMS2* (bottom). For the genomic locus, UTRs and exons are shown in grey and green, respectively. For *AKIN10* an alternative first exon for splicing form 2 (sf2) is shown in light green. The confirmed (*AKIN10*) and annotated but not detected (*ISM2*) T-DNA insertion sites are indicated, as well as the binding sites of primers used for PCRs in (B-D). For the AKIN10 protein, the positions of the kinase catalytic domain (KD), the ubiquitin-associated domain (UBA), the kinase-associated domain (KA), as well as the binding sites for antibodies against AKIN10 and AMPK-pT172 used in (E) are shown. The AMPK-pT172 antibody recognizes the phosphorylated T in the T-loop of both AKIN10 and AKIN11. The position of K48, which was mutated in the inactive AKIN10 version used in this manuscript, is shown as well. **(B)** PCR on genomic DNA from wt and *akin10* plants to confirm the T-DNA insertion in *AKIN10* and homozygosity of the plant lines. **(C)** PCR on genomic DNA from wt and *akin10* plants did not confirm the second T-DNA insertion in the *akin10* line in the *IMS2* gene. **(D)** Expression of *AKIN10* and *AKIN11* in rosette leaves of five week-old wt and *akin10* plants after 6h of light (L) and extended night (EN) as determined by RT-qPCR. Bars represent the means ± SD of four biological replicates and are normalized to wt in L. Letters indicate significant differences as determined by ANOVA and pairwise T-testing ($P < 0.05$). **(E)** Western blots detecting AKIN10 (αAKIN10) and AKIN10 and 11 phosphorylated in the T-loop (αAMPK-pT172) in wt and *akin10* plants. Proteins were extracted from

mature soil-grown plants after 6h of light or extended night (left) or from two week-old seedlings treated with 6h of extended darkness in the presence (+) or absence (-) of 1% sucrose (suc; right). CBB, Coomassie Brilliant Blue

Figure 5 – figure supplement 2. Phenotype and gene expression of selected AKIN10 target genes in the *akin10* line

(A) No obvious difference in growth could be observed between wt and *akin10* plants grown for seven weeks under short day conditions. The number of leaves, fresh weight (FW), dry weight (DW) and the water content (FW/DW) were determined. Bars represent the means ± SD of 20 biological replicates. **(B)** Mild flowering phenotype of *akin10*. Wt and *akin10* plants were grown under short day conditions and the number of leaves at time of bolting was determined. Bars represent the means ± SD of 14 (wt) and 11 (*akin10*) biological replicates. **(C)** Expression of selected AKIN10 target genes (Baena-Gonzalez et al., 2007) involved in amino acid metabolism (*ASN1*, *ProDH*, *BCAT2* (BRANCHED-CHAIN AMINO ACID TRANSAMINASE 2), *AA-TP family protein* (amino acid transporter family protein)) and sugar metabolism (*DIN10*) after 6h of light (L) and extended night (E) as determined by RT-qPCR. Bars represent the means ± SD of three biological replicates.
P-values from T-tests between mutants and wt < 0.05, <0.01, and < 0.001 are indicated by *, ** and ***, respectively.

Figure 5 – figure supplement 3. Expression of bZIPs in the *akin10* line

Expression of *bZIP63*, *bZIP1*, and *bZIP11* in rosette leaves of five week-old wt and *akin10* plants after 6h of light (L) and extended night (EN) as determined by RT-qPCR. Bars represent the means ± SD of four biological replicates and are normalized to wt in L. P-values from T-tests between mutants and wt < 0.05, <0.01, and < 0.001 are indicated by *, ** and ***, respectively.

Figure 5 – figure supplement 4. SnAK2 increases the kinase activity of AKIN10 and AKIN11 but does not phosphorylate bZIP63

(A) In vitro kinase assay with recombinant AKIN10 or AKIN11 and bZIP63 as a substrate in the presence of SnAK2. **(B)** Phos-tag gel western blot of an in vitro kinase assay with inactive AKIN10 (AKIN10 K/M), active AKIN10, or AKIN11 and bZIP63 as a substrate in the presence of SnAK2. An antibody recognizing the C-terminus of bZIP63 (αbZIP63) was used (see Figure 5 - figure supplement 1). **(C)** In vitro kinase assay with AKIN10 and/or SnAK2 and bZIP63 as a substrate showing the activity of AKIN10 in the presence or absence of SnAK2. The signal intensity from the bZIP63 phosphorylation is given in % of the strongest signal.

CBB, Coomassie brilliant blue

Figure 5 – figure supplement 5. AKINβ1 and AKINβ2 don not interact with bZIP63

Yeast two-hybrid (Y2H) assay showing of AKINβ1 and AKINβ2 with bZIP63. Homo-dimerization of bZIP63 was used as a positive control. Auto-activation of BD-fusion proteins is shown in grey, interaction with bZIP63 in blue. Bars represent means ± SD of eight biological replicates.

Figure 5 – figure supplement 6. Altered sugar-dependent in vivo phosphorylation of bZIP63 in seedlings

Phos-tag gel western (αGFP) blots showing the in vivo phosphorylation state of bZIP63 in plants overexpressing bZIP63-GFP/YFP in the wt or *akin10* background. Proteins were extracted from seedling cultures after 6h extended night in the presence (+) or absence (–) of 1% sucrose. Recombinant bZIP63-YFP was used as nonphosphorylated control. Numbered arrowheads on the right mark the position of each observed bZIP63 band for easy reference with other figures (see Figure 3 – figure supplement 1 for a comparative image of all Phos-tag western blots). 8 indicates the hyper-phosphorylated form of bZIP63. CBB, Coomassie brilliant blue

Figure 5 – figure supplement 7. *AKIN10/AKIN11* VIGS plants

AKIN10 and *AKIN11* were knocked down in plants expressing a genomic fragment of bZIP63 with a c-terminal YFP tag (GY9 line) using VIGS. Two week-old plants were infiltrated with the VIGS construct (*akin10/11*, right) or not (control, left) and two weeks later plants showed a clear phenotype and a strong reduction in AKIN10 and AKIN11 protein amount. **(A)** Pictures of representative plants showing stunted growth of *akin10/11* plants, as well as increased anthocyanin accumulation, leaf wilting and early senescence. **(B)** Western blot of control and *akin10/11* leaf extracts with an antibody against the phosphorylated T-loop of AMPK (αAMPK-pT172), recognizing both AKIN10 and AKIN11. Samples marked with an asterisk were used for the Phos-tag gels shown in Figure 5 E. CBB, Coomassie brilliant blue

Figure 6 – figure supplement 1. AKIN10 phosphorylates bZIP63 but not GST

(A) In vitro kinase assay with recombinant AKIN10 and GST-tagged bZIP63 or GST as a substrate. Positions of full length (FL) and N-terminal fragments of bZIP63 are marked by black arrows. The scheme on the right shows the position of the in vivo phosphorylation sites and the in vitro target sites of AKIN10 (red asterisk) in GST-bZIP63, as well as the approximate length of the N-terminal fragments. **(B)** Western blot (αbZIP63-N and -C) of GST-tagged bZIP63, used as substrate for the kinase assays. The scheme on the right indicates the binding sites of the two antibodies on bZIP63 and the approximate length of the detected fragments.

CBB, Coomassie brilliant blue

Figure 6 – figure supplement 2. AKIN10 phosphorylates S29, S294, and S300 on bZIP63

Phos-tag gel western blot (αbZIP63-C) of an in vitro kinase assay with active (wt) and inactive (K/M) AKIN10 and wt and S/A mutants of GST-tagged bZIP63 as substrate. The scheme on the bottom shows which of the three AKIN10 target sites can be phosphorylated (P) or are mutated (X). The scheme on the right indicates the likely phosphorylated sites for each band.

Figure 6 – figure supplement 3. The AKIN10 target sites and S160 in the bZIP domain hare highly conserved

(A) and **(B)** Sequence conservation of bZIP63. Sequences of bZIP63 homologues from eight species were aligned with ClustalΩ. **(A)** Conservation of non-AKIN10 target sites. The scheme on top indicates the positions of the in vivo phosphorylation and AKIN10 target sites on bZIP63. The histogram below shows the sequence identity (red/black) and similarity (grey) to A. thaliana bZIP63 in each position. Red bars represent the in vivo phosphorylation sites. Below, an alignment of the sequences surrounding the phosphorylation sites not targeted by AKIN10 is depicted. The grey/black shading indicates the degree of conservation, phosphorylation sites are in red. **(B)** Full sequence alignment. Species names are abbreviated. The grey/black shading indicates the degree of conservation. Red arrows indicate the positions of the in vivo phosphorylation sites. Numbers on top indicate the position in the alignment, numbers on the right indicate the position in each sequence. A consensus sequence is given below the alignment. The sequence identity matrix is at the bottom right.

Figure 6 – figure supplement 4. Expression of bZIP63 and AKIN10 in the promoter activation assays

Exemplary western blot (αHA) of protoplasts co-transformed with *AKIN10* and wt or S/A mutants of *bZIP63*. CBB, Coomassie brilliant blue

Figure 6 – source data 1. Sequences of the bZIP63 homologues

Text file containing the sequences of the bZIP63 homologes used for ClustalΩ alignment in Figure 5B and Figure 5 – figure supplement 3 in fasta format.

Figure 7 – figure supplement 1. Characterization of the *bzip63* complementation lines

(A) and **(B)** Expression of bZIP63 in different plant lines. **(A)** RT-qPCR of *bZIP63* in five week-old plants after 6h of light (L) or extended night (EN). Bars represent means ± SD of five biological replicates and are given as fold change to Ws-2 in L. The 6h L samples were also used for the metabolic profiling

shown in Figures 6E and F and Figure 6 – source data 1. **(B)** Western blot (αGFP) detecting YFP-tagged bZIP63 in transgenic plant lines after 6h of L and EN. **(C)** Epifluorescence microscopy images of soil-grown seedlings of the GY9 and GAY14 lines showing expression of bZIP63-YFP. From top to bottom: leaf epidermis, leaf veins, roots, lateral root tips. Scale bar is 20µm. **(D)** Phos-tag gel western blots (αGFP) showing the in vivo phosphorylation state of bZIP63 in the complementation lines. Proteins were extracted from seedling cultures after 6h extended night in the presence (+) or absence (–) of 1% sucrose. Recombinant bZIP63-YFP was used as an nonphosphorylated control. Numbered arrowheads on the right mark the position of each observed bZIP63 band for easy reference with other figures (see Figure 3 – figure supplement 1 for a comparative image of all Phos-tag western blots).

CBB, Coomassie brilliant blue

Figure 7 – figure supplement 2. Complementation of the dark-induced senescence phenotype of *bzip63*

(A) Representative leaf series of 4.5 week-old plants before and after nine days in darkness. **(B)** Barplot of the total green leaf area of the rosette before darkness. Values are the mean ± SD of four biological replicates. **(C)** Dotplot of the green leaf area of individual leaves after nine days in darkness. Values are the mean ± SD of eight biological replicates. The insertion at the right side shows the values from leaves 3 – 7 as a barplot (framed by dotted line). Letters indicate significant differences as determined by ANOVA and pairwise T-testing ($P < 0.05$). The p-values of the F-test for each leaf are given.

Figure 7 – source data 1. Excel table containing the relative metabolite levels of the complementation lines and the PCA loadings

The tab “metabolites normalized to wt” contains the relative metabolite levels, which were used to calculate the fold changes shown in Figure 7E, as well as P-values from statistical tests. Values are the

mean ± SD of five biological replicates given as fold change to the corresponding wt. The tab "PCA - variance and loadings" contains the SD, proportion of variance, and loadings of all principal components from the PCA analysis shown in Figure 7F.

Figure 8 – figure supplement 1. Western blots and controls for the protoplast two-hybrid (P2H) assays

(A) Western blot showing the expression of AD (activation domain)-bZIPs and AKIN10 (αHA) and BD (DNA binding domain)-bZIP63 (αBD) in the P2H assay in Figure 8A. **(B)** Exemplary western blot showing the expression of BD-bZIP63 in the P2H assays in Figure 8B.

CBB, Coomassie brilliant blue

Figure 8 – figure supplement 2. SnAK2 does not phosphorylate bZIP63 or the S1 class bZIPs

In vitro kinase assay of bZIP63, 1, 2, 11, 44, and 53 with SnAK2.

CBB, Coomassie brilliant blue

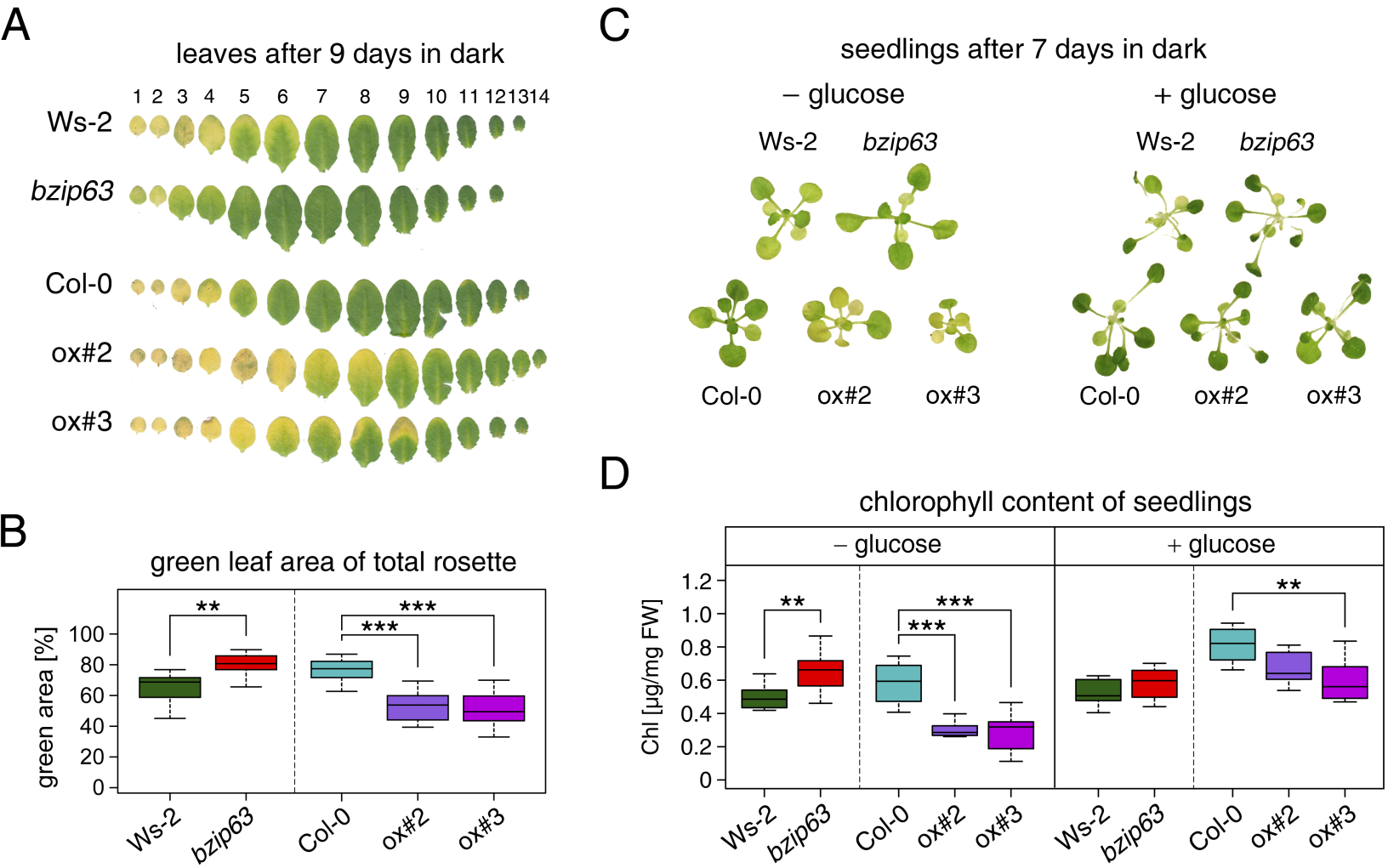
A
leaves after 9 days in dark
1 2 3 4 5 6 7 8 9 10 11 12 13 14
Ws-2
bzip63
Col-0
ox#2
ox#3
C
seedlings after 7 days in dark
– glucose
+ glucose
Ws-2
bzip63
Col-0
ox#2
ox#3
B
green leaf area of total rosette
green area [%]
0
20
40
60
80
100
**
***
***
Ws-2
bzip63
Col-0
ox#2
ox#3
D
chlorophyll content of seedlings
– glucose
+ glucose
Chl [µg/mg FW]
0
0.2
0.4
0.6
0.8
1.0
1.2
**
***
***
**
Ws-2
bzip63
Col-0
ox#2
ox#3

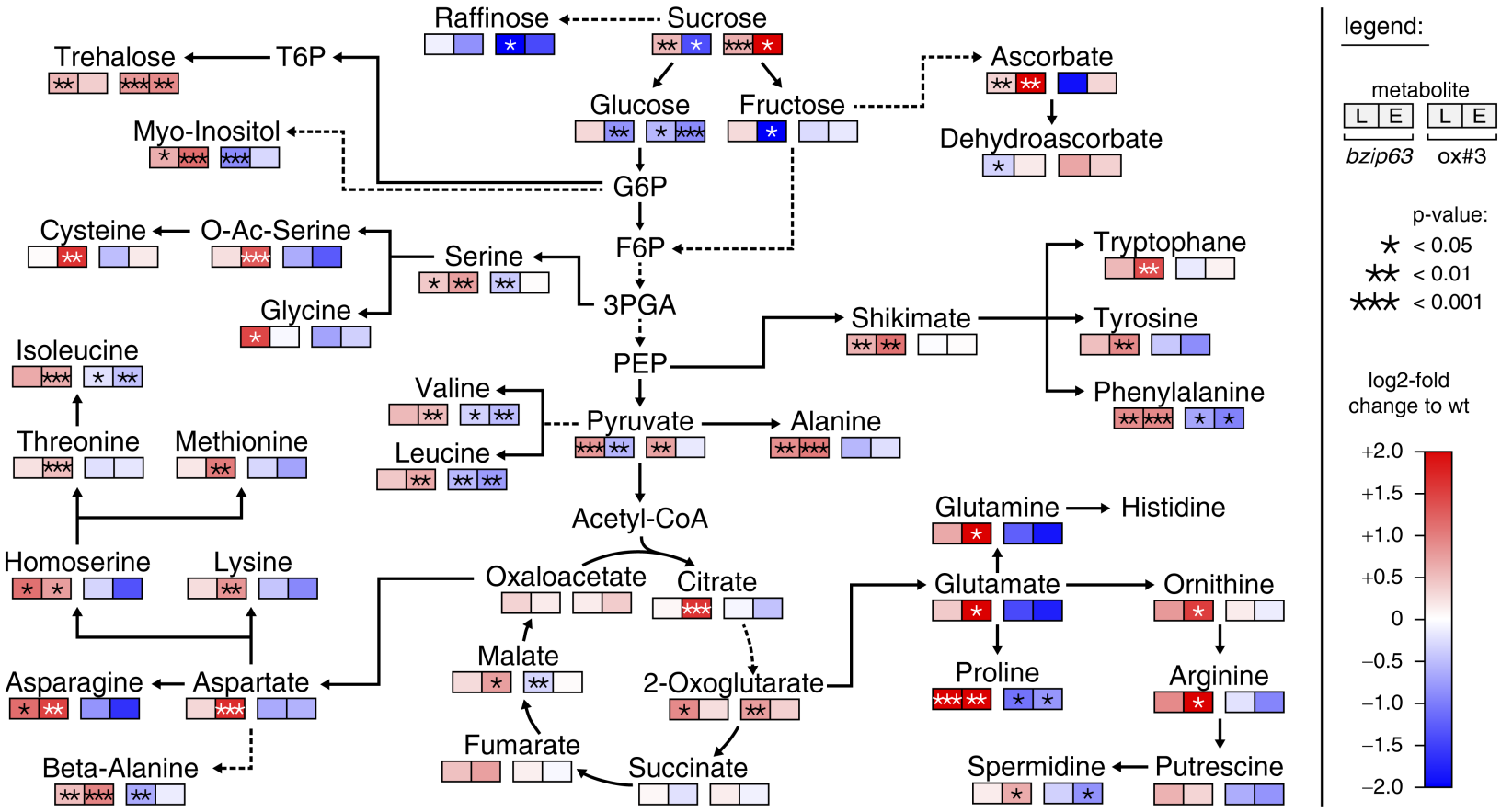
Raffinose
Sucrose
Trehalose
T6P
Ascorbate
Glucose
Fructose
Myo-Inositol
Dehydroascorbate
G6P
Cysteine
O-Ac-Serine
F6P
Serine
Tryptophane
Glycine
3PGA
Shikimate
Tyrosine
Isoleucine
PEP
Valine
Pyruvate
Alanine
Phenylalanine
Threonine
Methionine
Leucine
Acetyl-CoA
Glutamine
Histidine
Homoserine
Lysine
Oxaloacetate
Citrate
Glutamate
Ornithine
Malate
Proline
Arginine
Asparagine
Aspartate
2-Oxoglutarate
Fumarate
Succinate
Spermidine
Putrescine
Beta-Alanine
legend:
metabolite
L E
L E
bzip63
ox#3
p-value:
* < 0.05
** < 0.01
*** < 0.001
log2-fold change to wt
+2.0
+1.5
+1.0
+0.5
0
−0.5
−1.0
−1.5
−2.0

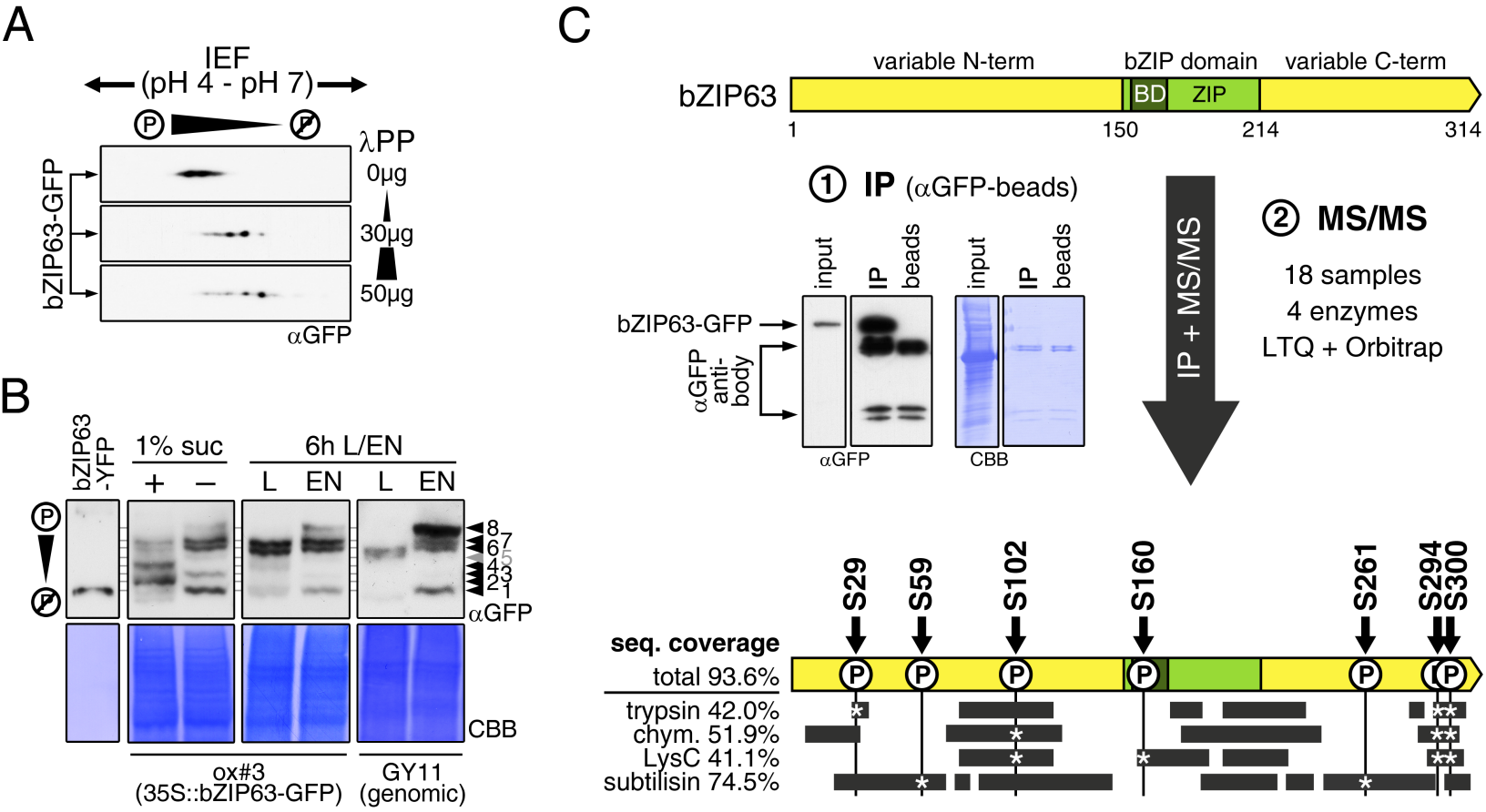
A
IEF
(pH 4 - pH 7)
λPP
0µg
30µg
50µg
bZIP63-GFP
αGFP
B
bZIP63
-YFP
1% suc
6h L/EN
+
–
L
EN
L
EN
8
7
6
5
4
3
2
1
αGFP
CBB
ox#3
(35S::bZIP63-GFP)
GY11
(genomic)
C
bZIP63
variable N-term
bZIP domain
variable C-term
BD
ZIP
1
150
214
314
① IP (αGFP-beads)
input
IP
beads
input
IP
beads
bZIP63-GFP
αGFP anti-body
αGFP
CBB
IP + MS/MS
② MS/MS
18 samples
4 enzymes
LTQ + Orbitrap
S29
S59
S102
S160
S261
S294
S300
seq. coverage
total 93.6%
trypsin 42.0%
chym. 51.9%
LysC 41.1%
subtilisin 74.5%

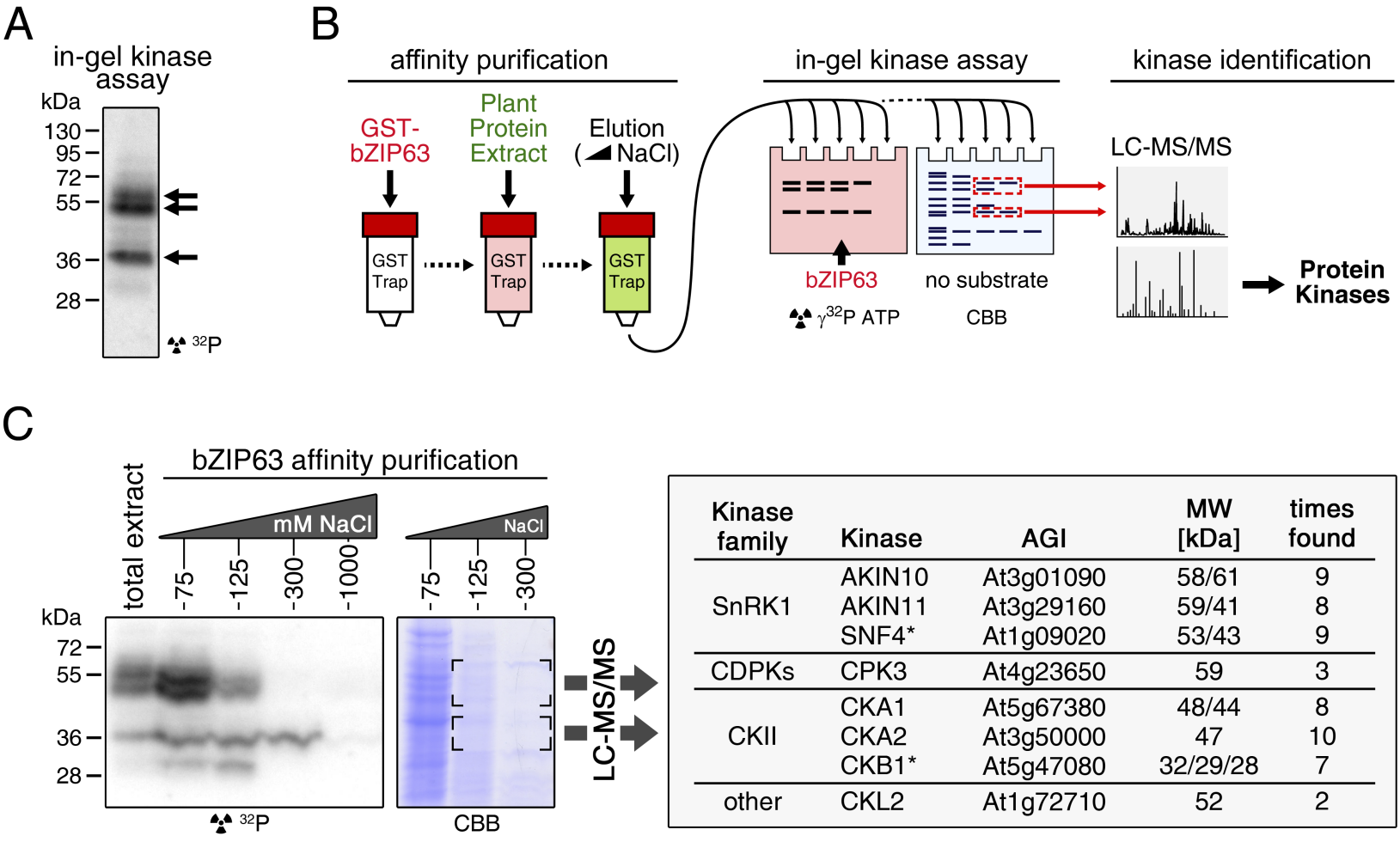

Kinase family	Kinase	AGI	MW [kDa]	times found
SnRK1	AKIN10	At3g01090	58/61	9
	AKIN11	At3g29160	59/41	8
	SNF4*	At1g09020	53/43	9
CDPKs	CPK3	At4g23650	59	3
CKII	CKA1	At5g67380	48/44	8
	CKA2	At3g50000	47	10
	CKB1*	At5g47080	32/29/28	7
other	CKL2	At1g72710	52	2

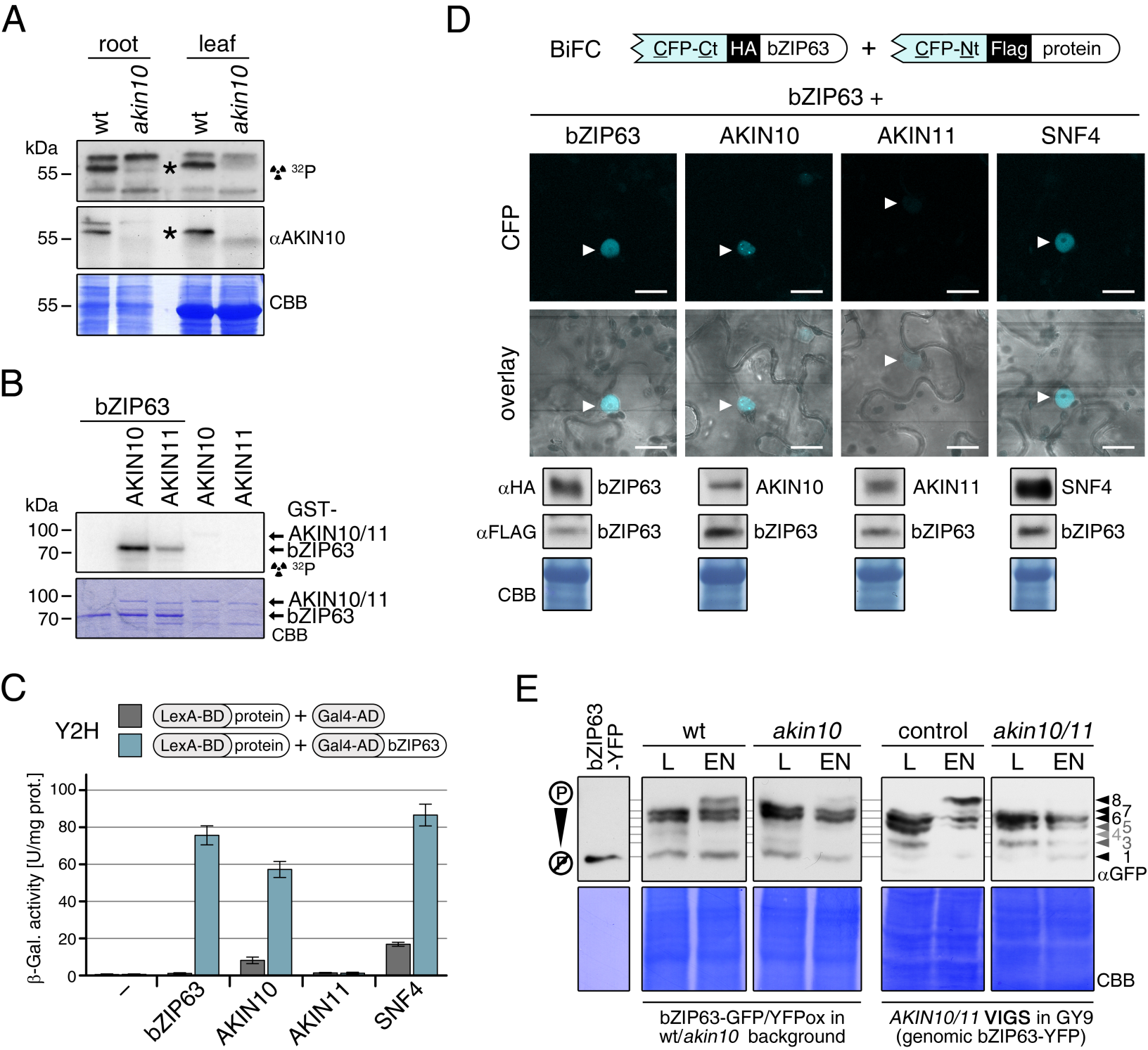
A
root
leaf
wt
akin10
wt
akin10
kDa
55
32P
αAKIN10
CBB
B
bZIP63
AKIN10
AKIN11
AKIN10
AKIN11
kDa
100
70
GST-
AKIN10/11
bZIP63
32P
CBB
C
Y2H
LexA-BD protein + Gal4-AD
LexA-BD protein + Gal4-AD bZIP63
β-Gal. activity [U/mg prot.]
0
20
40
60
80
100
–
bZIP63
AKIN10
AKIN11
SNF4
D
BiFC
CFP-Ct HA bZIP63 + CFP-Nt Flag protein
bZIP63 +
bZIP63
AKIN10
AKIN11
SNF4
CFP
overlay
αHA
αFLAG
CBB
E
bZIP63 -YFP
wt
akin10
control
akin10/11
L
EN
αGFP
CBB
bZIP63-GFP/YFPox in wt/akin10 background
AKIN10/11 VIGS in GY9 (genomic bZIP63-YFP)

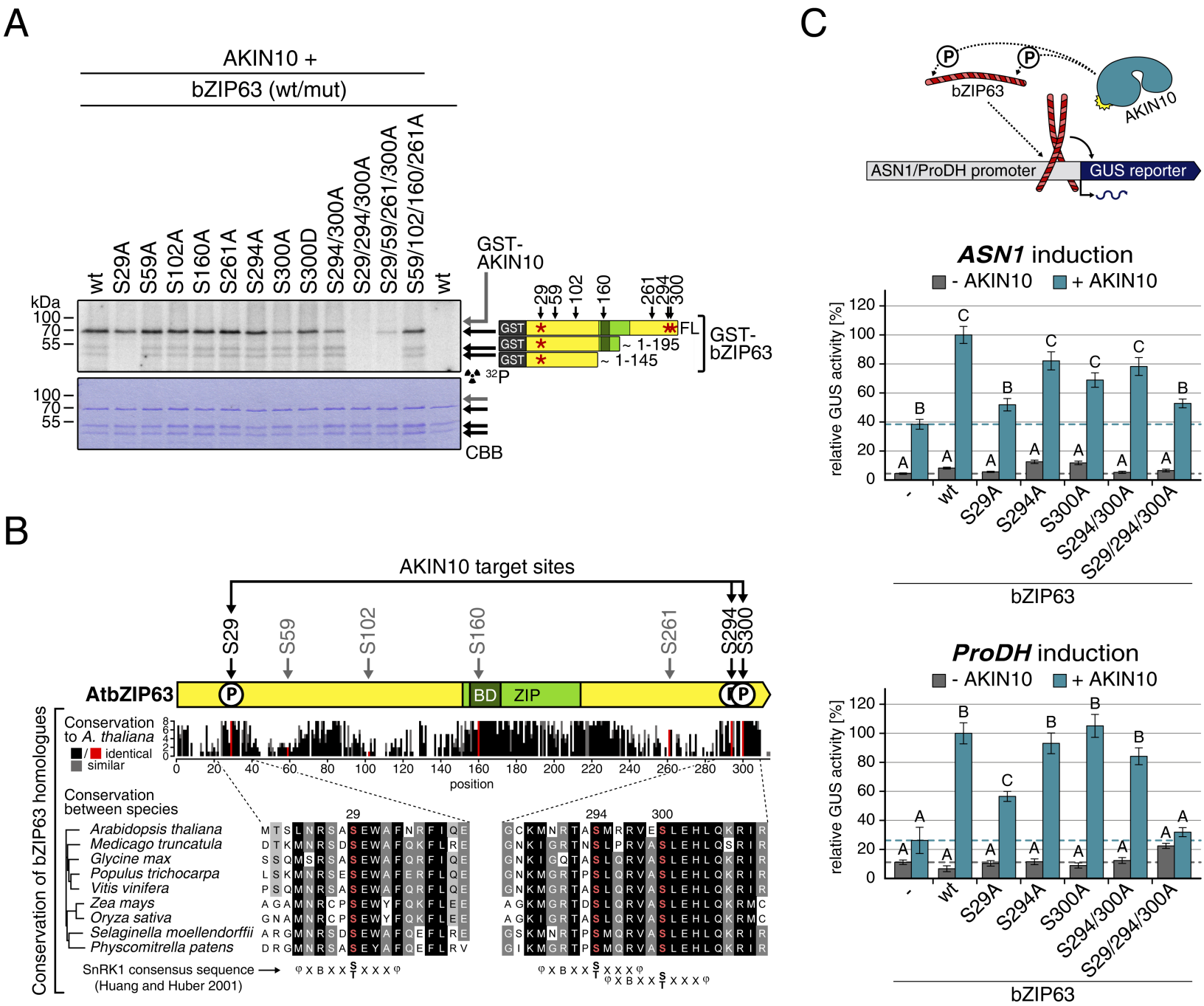
A
AKIN10 +
bZIP63 (wt/mut)
wt
S29A
S59A
S102A
S160A
S261A
S294A
S300A
S300D
S294/300A
S29/294/300A
S29/59/261/300A
S59/102/160/261A
wt
kDa
100
70
55
GST-AKIN10
29
59
102
160
261
294
300
GST
FL
~ 1-195
~ 1-145
GST-bZIP63
32P
CBB
B
AKIN10 target sites
S29
S59
S102
S160
S261
S294
S300
AtbZIP63
P
BD
ZIP
Conservation to A. thaliana
identical
similar
position
Conservation between species
Conservation of bZIP63 homologues
Arabidopsis thaliana
Medicago truncatula
Glycine max
Populus trichocarpa
Vitis vinifera
Zea mays
Oryza sativa
Selaginella moellendorffii
Physcomitrella patens
SnRK1 consensus sequence
(Huang and Huber 2001)
C
bZIP63
AKIN10
ASN1/ProDH promoter
GUS reporter
ASN1 induction
- AKIN10
+ AKIN10
relative GUS activity [%]
bZIP63
ProDH induction

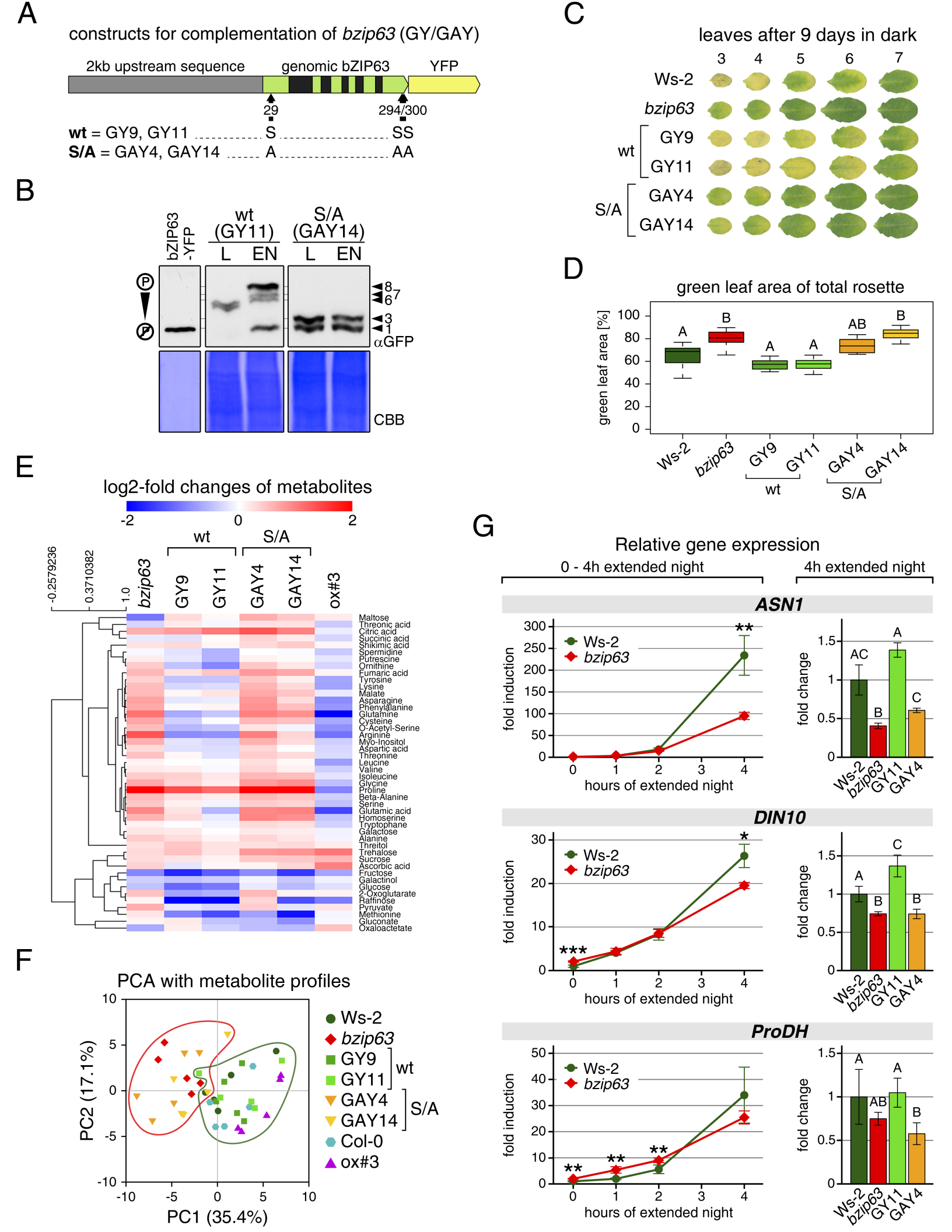
A
constructs for complementation of bzip63 (GY/GAY)
2kb upstream sequence
genomic bZIP63
YFP
29
294/300
wt = GY9, GY11 ..... S ..... SS
S/A = GAY4, GAY14 ..... A ..... AA
B
bZIP63 -YFP
wt (GY11)
S/A (GAY14)
L EN L EN
P
P
8
6
7
3
1
αGFP
CBB
C
leaves after 9 days in dark
3 4 5 6 7
Ws-2
bzip63
wt
GY9
GY11
S/A
GAY4
GAY14
D
green leaf area of total rosette
green leaf area [%]
100 80 60 40 20 0
A B A A AB B
Ws-2 bzip63 GY9 GY11 GAY4 GAY14
wt
S/A
E
log2-fold changes of metabolites
-2 0 2
wt S/A
-0.2579236
0.3710382
1.0
bzip63 GY9 GY11 GAY4 GAY14 ox#3
Maltose
Threonic acid
Citric acid
Succinic acid
Shikimic acid
Spermidine
Putrescine
Ornithine
Fumaric acid
Tyrosine
Lysine
Malate
Asparagine
Phenylalanine
Glutamine
Cysteine
O-Acetyl-Serine
Arginine
Myo-Inositol
Aspartic acid
Threonine
Leucine
Valine
Isoleucine
Glycine
Proline
Beta-Alanine
Serine
Glutamic acid
Homoserine
Tryptophane
Galactose
Alanine
Threitol
Trehalose
Sucrose
Ascorbic acid
Fructose
Galactinol
Glucose
2-Oxoglutarate
Raffinose
Pyruvate
Methionine
Gluconate
Oxaloactetate
F
PCA with metabolite profiles
PC2 (17.1%)
PC1 (35.4%)
10 5 0 -5 -10
-10 -5 0 5 10
Ws-2
bzip63
GY9
GY11
wt
GAY4
GAY14
S/A
Col-0
ox#3
G
Relative gene expression
0 - 4h extended night
4h extended night
ASN1
DIN10
ProDH
Ws-2
bzip63
fold induction
hours of extended night
fold change
AC B A C
Ws-2 bzip63 GY11 GAY4

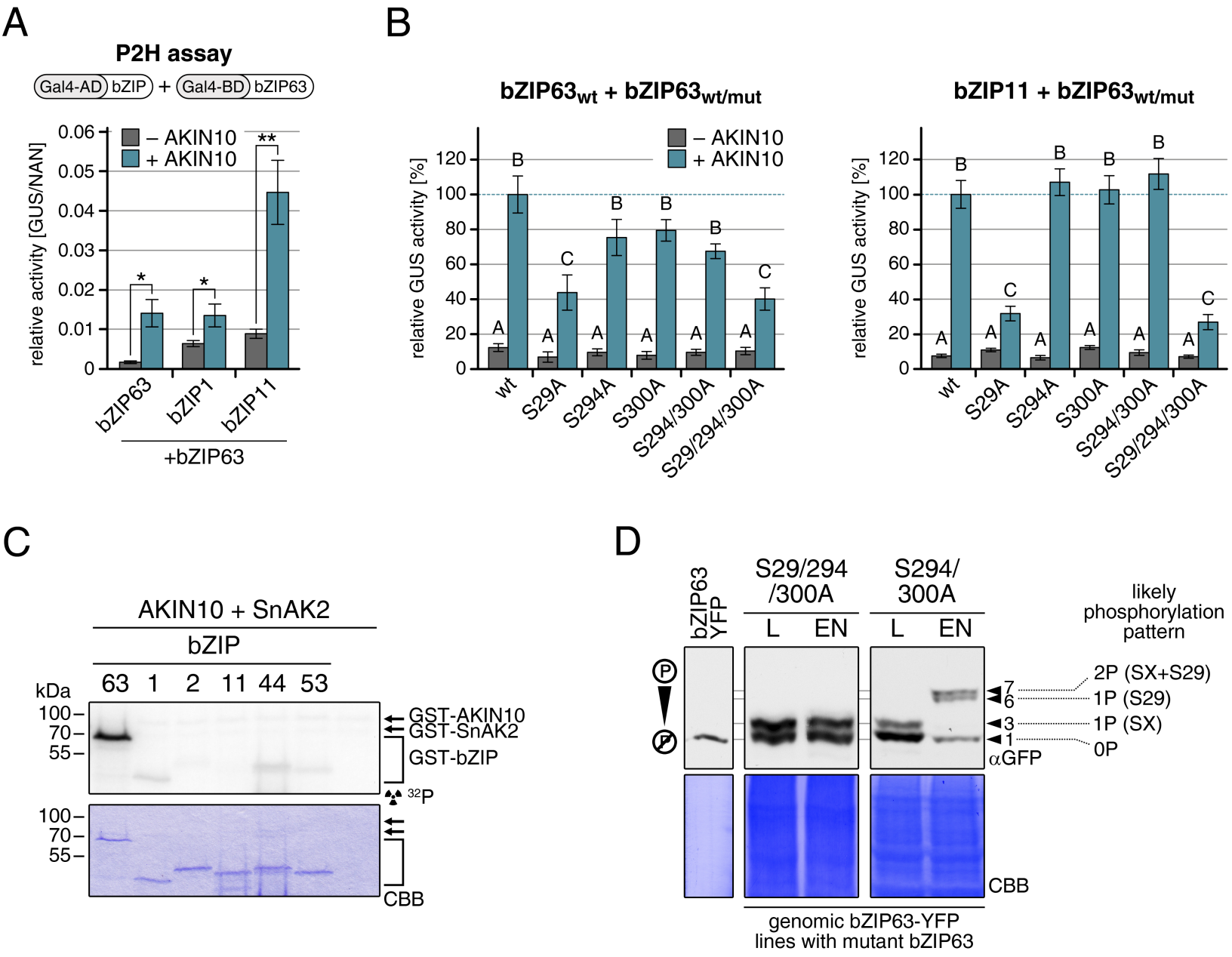
A
P2H assay
Gal4-AD bZIP + Gal4-BD bZIP63
relative activity [GUS/NAN]
– AKIN10
+ AKIN10
bZIP63
bZIP1
bZIP11
+bZIP63
B
bZIP63wt + bZIP63wt/mut
bZIP11 + bZIP63wt/mut
relative GUS activity [%]
wt
S29A
S294A
S300A
S294/300A
S29/294/300A
C
AKIN10 + SnAK2
bZIP
63 1 2 11 44 53
kDa
GST-AKIN10
GST-SnAK2
GST-bZIP
32P
CBB
D
bZIP63 YFP
S29/294 /300A
S294/ 300A
L EN
likely phosphorylation pattern
2P (SX+S29)
1P (S29)
1P (SX)
0P
αGFP
CBB
genomic bZIP63-YFP lines with mutant bZIP63

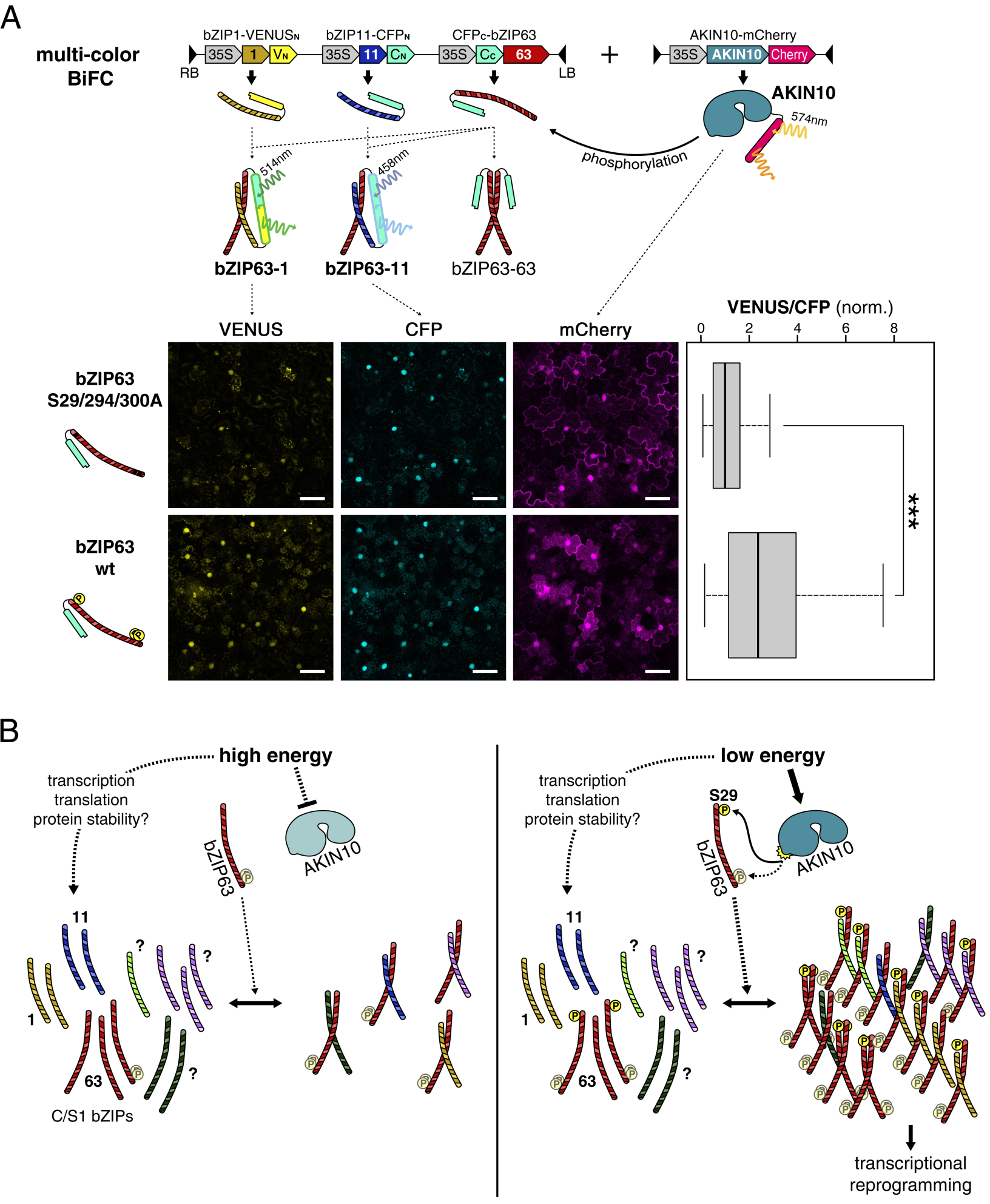
A
multi-color BiFC
bZIP1-VENUSN
bZIP11-CFPN
CFPc-bZIP63
AKIN10-mCherry
35S
1
VN
11
CN
Cc
63
AKIN10
Cherry
RB
LB
AKIN10
574nm
phosphorylation
514nm
458nm
bZIP63-1
bZIP63-11
bZIP63-63
VENUS
CFP
mCherry
VENUS/CFP (norm.)
0
2
4
6
8
***
bZIP63 S29/294/300A
bZIP63 wt
B
high energy
low energy
transcription
translation
protein stability?
bZIP63
AKIN10
S29
11
1
63
?
C/S1 bZIPs
transcriptional reprogramming

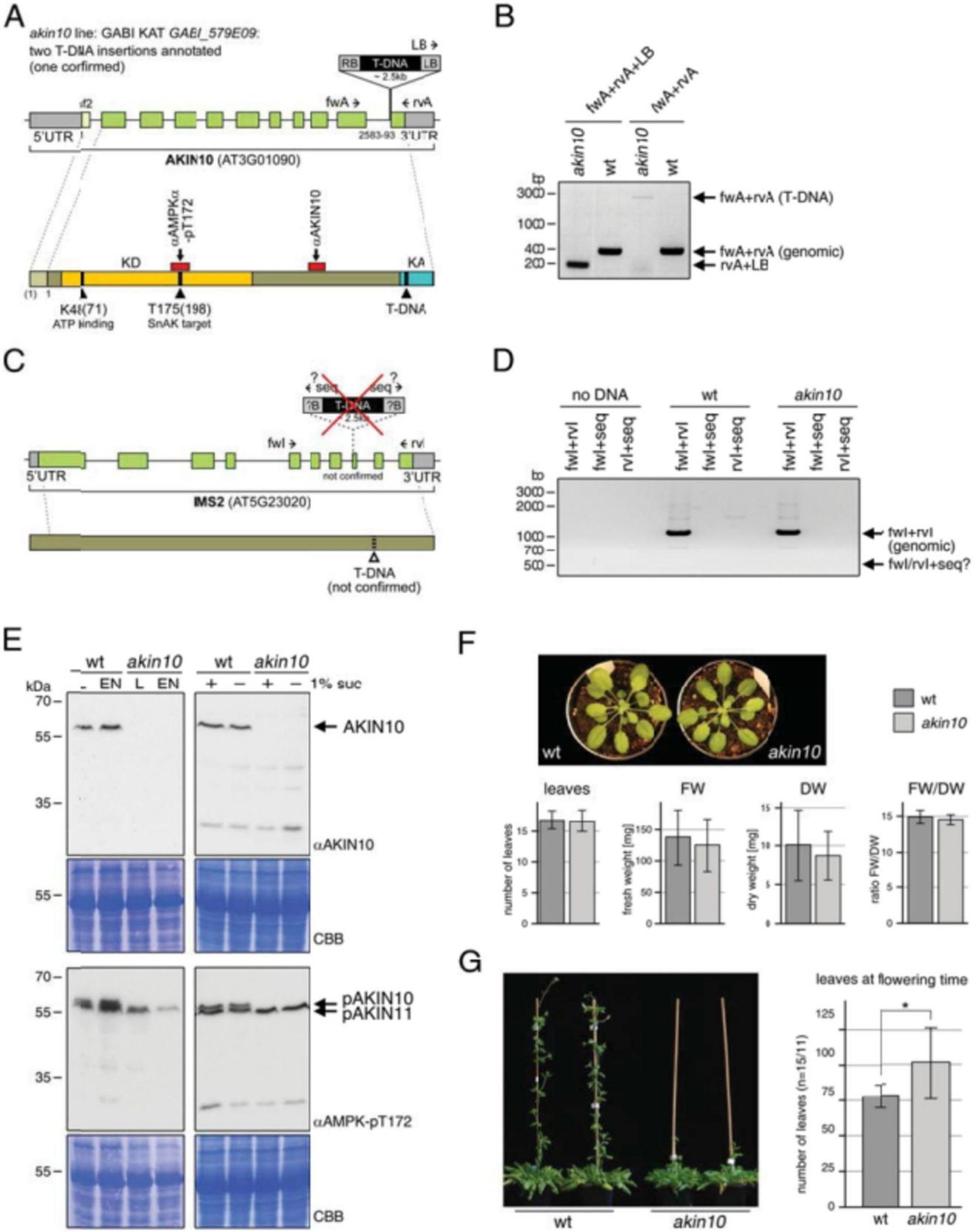
A
akin10 line: GABI KAT GAEI_579E09:
two T-DNA insertions annotated
(one corfirmed)
LB
RB T-DNA LB
~ 2.5kb
fwA
rvA
5'UTR
2583-93 3'UTR
AKIN10 (AT3G01090)
αAMPKα -pT172
αAKIN10
KD
KA
(1) 1
K48(71) ATP binding
T175(198) SnAK target
T-DNA
B
fwA+rvA+LB
fwA+rvA
akin10
wt
akin10
wt
bp
3000
1000
400
200
fwA+rvA (T-DNA)
fwA+rvA (genomic)
rvA+LB
C
?
seq
seq
?
?B T-DNA ?B
2.5kb
fwI
rvI
5'UTR
not confirmed
3'UTR
IMS2 (AT5G23020)
T-DNA
(not confirmed)
D
no DNA
wt
akin10
fwI+rvI
fwI+seq
rvI+seq
bp
3000
2000
1000
700
500
fwI+rvI (genomic)
fwI/rvI+seq?
E
wt
akin10
wt
akin10
kDa
-
EN
L
EN
+
–
+
–
1% suc
70
55
35
AKIN10
αAKIN10
CBB
pAKIN10
pAKIN11
αAMPK-pT172
F
wt
akin10
leaves
FW
DW
FW/DW
number of leaves
fresh weight [mg]
dry weight [mg]
ratio FW/DW
G
wt
akin10
leaves at flowering time
number of leaves (n=15/11)
*

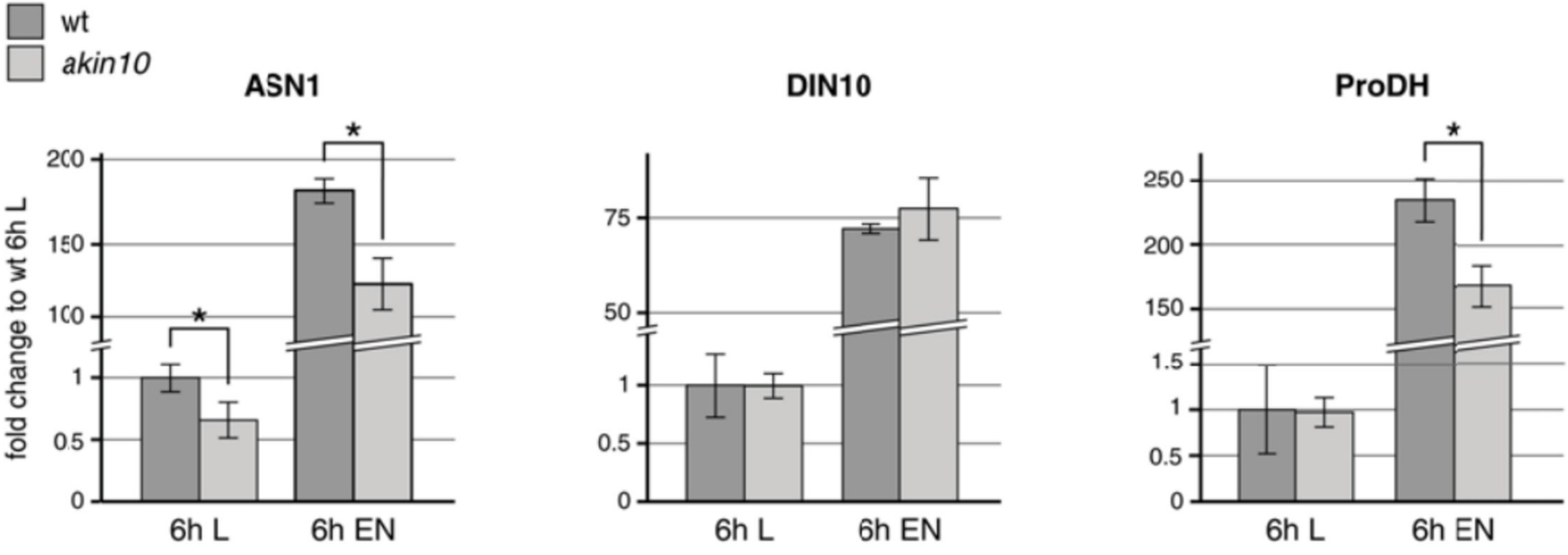
wt
akin10
ASN1
DIN10
ProDH
fold change to wt 6h L
200
150
100
1
0.5
0
75
50
250
1.5
*
6h L
6h EN

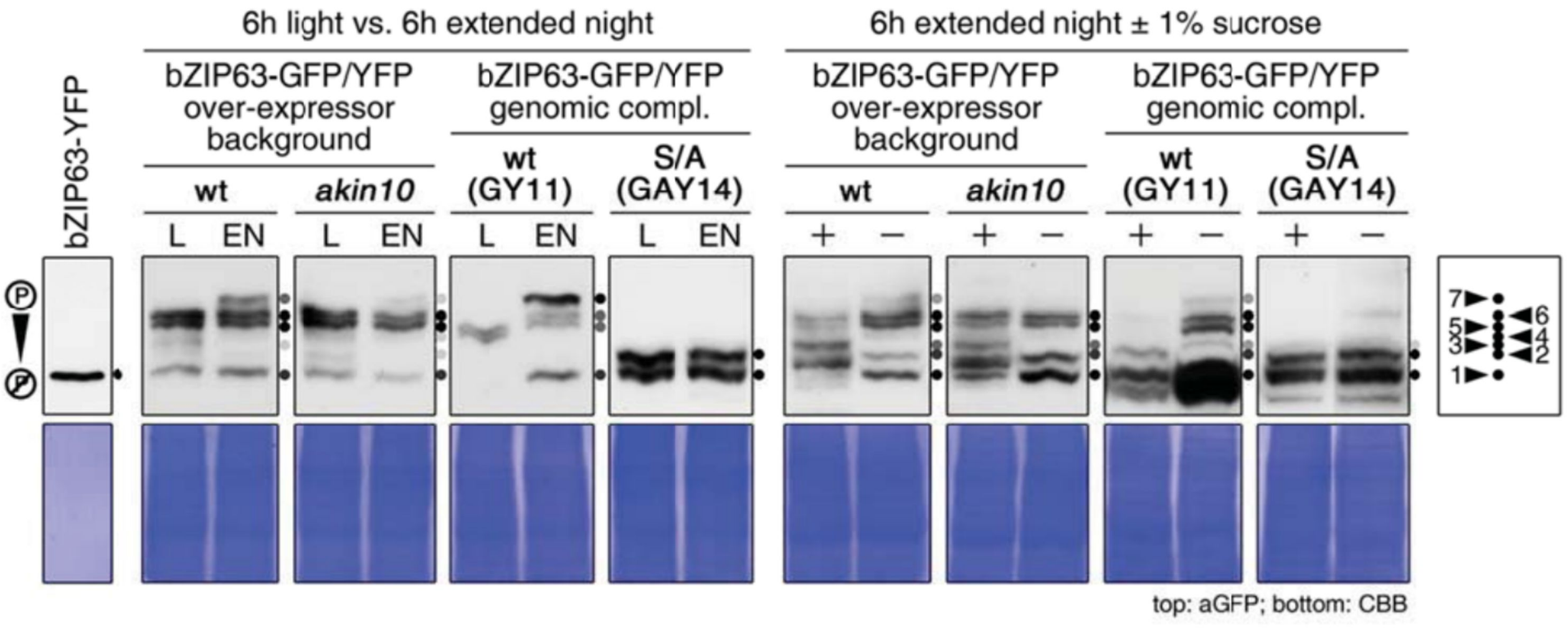
6h light vs. 6h extended night
6h extended night ± 1% sucrose
bZIP63-YFP
bZIP63-GFP/YFP over-expressor background
bZIP63-GFP/YFP genomic compl.
wt
akin10
wt (GY11)
S/A (GAY14)
L
EN
+
−
P
7
6
5
4
3
2
1
top: aGFP; bottom: CBB